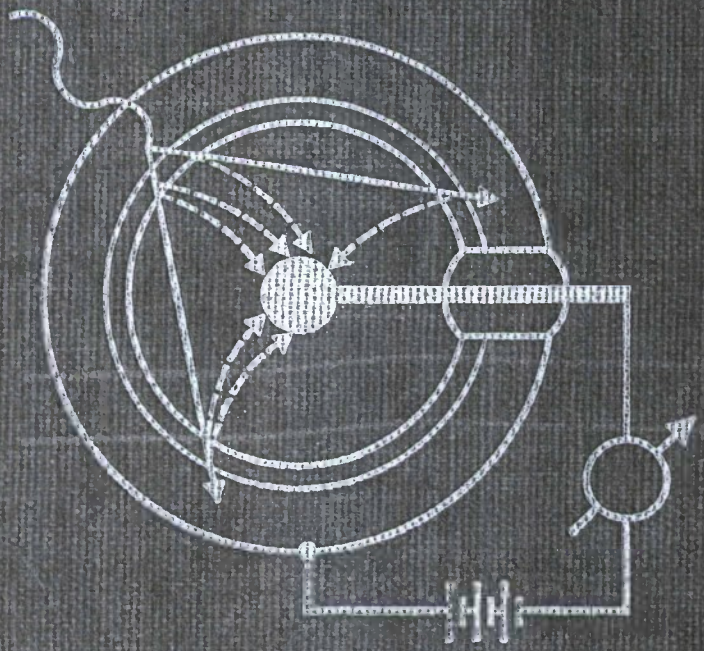
ECOM
ARD-3
c.2

A MONOGRAPH ON HIGH INTENSITY RADIATION DOSIMETRY WITH SEMIRAD

LOAN COPY: RETURN TO
AFWL (WLIL-2)
KIRTLAND AFB, N MEX

NUMBER 3
THE UNITED STATES ARMY
RESEARCH AND
DEVELOPMENT
SERIES



AD-653037

THE UNITED STATES ARMY RESEARCH AND DEVELOPMENT SERIES

Number 3

A MONOGRAPH ON HIGH-INTENSITY RADIATION DOSIMETRY WITH SEMIRAD

20081216 346

A NOTEWORTHY CONTRIBUTION TO R&D

When the Army Research and Development Monograph Series was initiated, the stated intent was to limit these publications to comprehensive reports reflecting accurately the state-of-the-art in areas of scientific research having broad potential application to requirements of the civilian as well as the military scientific community.

The Chief of Research and Development at that time, Lieutenant General Arthur G. Trudeau, since retired, stated in part: "Having drawn heavily from the intellectual efforts of others, the United States Army wishes to reciprocate by adding to the reservoir upon which all mankind may rely for the continued betterment of society."

Indications from many parts of the world are that the first two books in the Army R&D Monograph Series have served effectively the purpose for which they are intended. The first, *Radiation Preservation of Food*, published in August 1957, is still recognized as the most comprehensive report of its kind ever made available to the world scientific community. Its enlightening and stimulating impact generated worldwide interest in use of nuclear energy for the peaceful purpose of serving nutritional needs of untold millions.

Similarly, *A Monograph of the Chaetomiaceae*, distributed in March 1963, has occasioned requests for copies from scientists in many nations. It has been acclaimed as the most authoritative and comprehensive document on cellulose-destroying fungi currently available to the scientific community.

Long and intensive effort is reflected in this, the third Army R&D monograph. It has been heralded by reviewing authorities in the U.S. Atomic Energy Commission and the nuclear science community as an important contribution to the advancement of knowledge in measurement of high-intensity radiation dosimetry. The Army is pleased to include the work of Dr. Stanley Kronenberg of the U.S. Army Electronics Command in the monograph series.

A. W. BETTS
Lieutenant General, USA
Chief of Research and Development.
United States Army

FOREWORD

The effects of nuclear radiation on military materiel are complex and profound. The understanding of these effects is important in order to design materiel effectively to meet future combat needs. Determination of the intensity of the various components of the radiation is a prerequisite to a scientific approach to this problem. Previous studies in the area had led to measuring devices which worked well at low levels of radiation but which would saturate at high level, or which had slow response time and would not resolve short pulses of radiation. Interpretation of experimental data was compounded by the contributions of different components and differences between immediate and long-term effects.

Our organization is charged with the furnishing of equipment to the combat troops which will function effectively in all battle environments, including a nuclear environment. It became apparent that one of the key requirements for further advance of understanding in this field was a measuring system which could determine the radiation dose rate as a function of time. The successful achievement of secondary-electron mixed radiation dosimetry (SEMIRAD) has expedited our understanding of the damaging effects of nuclear radiation on military materiel, especially electronic components and systems.

The work reported here has been underway for many years. Many of the key discussions have been published in well-known technical journals. However, no consolidated, comprehensive treatment has previously been available for the scientist working in this field. This book will fill the need for such a ready reference book and should meet the numerous requests from interested scientists.

F. S. Besson, Jr.
General, USA
Commanding General,
Army Materiel Command.

HIGH-INTENSITY RADIATION DOSIMETRY WITH SEMIRAD

(Secondary-Electron Mixed-Radiation Dosimeters)

Stanley Kronenberg



U.S. Army Electronics Command
FORT MONMOUTH, NEW JERSEY
September 1966

CONTENTS

Chapter	Title	Page
	Preface	1
1	Principles of SEMIRAD Radiation Detectors	3
2	SEMIRAD Vacuum Considerations	7
3	SEMIRAD Dose-Rate Limitations	11
4	SEMIRAD Sensitivity	13
5	SEMIRAD Energy Dependence	21
6	Emission of Secondary Electrons by High-Energy Particles	29
7	SEMIRAD Pulse Amplification and Cable Connection	43
8	Calibration of SEMIRAD	51
9	Instruments with Wide Sensitivity Range	53
10	Measurement of Fast-Neutron Fluxes in an Environment of Fast Neutrons and Gamma Rays	59
11	Construction of SEMIRAD Diodes and Diode-Type Dosimeters	65
12	Pulsed Radiation Rate Measurements with SEMIRAD	75
	References	93

PREFACE

This work is the outgrowth of work in nuclear radiation dosimetry at laboratories of the U.S. Army Electronics Command, Fort Monmouth, New Jersey. As a result of the evaluation of nuclear tests in 1955 and 1957 (References 51 and 52), it was apparent that further instrumentation research was mandatory.

In pulsed-radiation studies, our primary interest is in fast and slow neutrons, gamma rays, and X-rays, because these particles have a considerable range and a high penetrating power. A number of different types of devices that produce pulsed radiation were developed, mainly for the purpose of radiation effects study and for laboratory simulation of nuclear-weapons environments.

Some of these devices are Godiva-type fast reactors (e.g., Godiva II at Los Alamos Scientific Laboratory, Los Alamos, New Mexico), linear accelerators (LINAC, e.g., Rensselaer Polytechnic Institute, Troy, New York), slow pulsed reactors (TRIGA, e.g., General Atomics, San Diego, California), pulsed X-ray machines (Sandia Corporation, Albuquerque, New Mexico), nuclear rocket-propulsion prototypes (Project KIWI), and controlled fusion plasma machines (Stellarator, Princeton University, Princeton, New Jersey).

Of prime importance in the study of the radiation environment and its effects is the availability of reliable measurement methods. It is required that separate measurements of fast and/or slow neutrons and of gammas be made. The total dose, as well as the dose rate as a function of time, should also be measured separately. The most commonly used total-dose measurements are: film dosimetry, ion-chamber dosimeters, phosphate glass dosimeters for gammas, and threshold dosimetry for fast or slow neutrons.

Several devices are available for the measurement of gamma and neutron dose rates, and one can choose them depending on the expected environment. Before selecting the dose-rate-measuring device, one must consider two factors: first, the device must not saturate at the highest expected dose rate; second, it must be able to follow the expected changes in dose rate as a function of time.

Among the available dose-rate meters, those that record single particles cannot be used, because they saturate at about 10^6 counts per second ($\sim 10^{-2}$ rads per second). This value is far below the rates we are concerned with. Instruments that fall into this category are: the Geiger counter, the Long counter, the Hurst counter, and the photomultiplier-scintillator-crystal system designed to measure single scintillations. On the other hand, the ion chamber, if designed for high rates, is a very useful instrument. A typical ion chamber saturates at a dose rate of 3×10^3 rads per second and has a time response in the range of microseconds. Thus, in the case of a pulse of moderate dose rate, wherein the fine structure of less than a microsecond is not required (e.g., a Triga pulse), the ion chamber is the easiest and most efficient instrument to use.

For pulses involving much higher intensities, the combination of a photocell and a scintillating crystal is usable. The results from such a system do not show saturation up to very high dose rates. The only saturation is caused by the space charge limitation of the photocell and the response time is very fast. Some effects, however, discussed later in this monograph, make the readout unreliable for a short time after the phosphor is bombarded with radiation. The reading is reliable while the intensity is increasing with time, but in some cases deviations are noticeable when the pulse is on its way down. This effect may be due to damage in the photosurface of the photocell or in the crystal; however, the actual explanation is unknown.

Similar considerations apply to solid-state devices used for high-intensity dose-rate measurements. We know that these devices suffer radiation damage. When a silicon diode is irradiated with fast neutrons, for example, the dislocations produced by the neutron collisions change the lifetime of the current carriers. This effect is used to measure total dose. When the crystal is used as a dose-rate meter, however, its sensitivity changes as the radiation pulse progresses with time. Therefore, when using a solid-state device as a dose-rate meter, one has to consider the total dose delivered during the pulse.

This monograph describes the SEMIRAD technique of making pulsed radiation measurements. SEMIRAD devices are superior in many ways to the instruments mentioned above and make it possible to: (1) distinguish between the neutron and the gamma contributions in a mixed-radiation environment; (2) obtain

true pulse shapes even at the highest obtainable radiation intensities; and (3) follow the shape of the radiation pulse within nanoseconds. This instrumentation is applicable only for high-intensity radiation environments; its use at low dose rates is not recommended because of its low sensitivity.

This monograph is designed to assist scientists who are primarily interested in areas other than pulsed radiation research but use high-intensity radiation pulses in their work. Chapters 1, 2, and 7 through 12 will be of special interest to these scientists. Chapters 3 through 6 go deeper into the characteristics and principles of SEMIRAD devices and are written mainly for those who are working on high-intensity radiation dosimetry. In addition, the SEMIRAD technique has been successfully applied to the measurement of total doses delivered at high intensities; this topic also is treated herein.

ACKNOWLEDGEMENTS

Over a period of years, many scientists and engineers of the U.S. Army Electronics Command (USAECOM), Air Force Weapons Laboratories, U.S. Navy, Defense Atomic Support Agency, U.S. Atomic Energy Commission, Nuclear Defense Laboratory and many other U.S. Government agencies, as well as industry, have contributed to the development of SEMIRAD dosimetry. In particular, the following scientists personally did a great amount of work on this project:

Dr. Wolfgang Ramm
Mr. Basil Markow
Mr. Michael J. Basso
Mr. Kristian L. Nilson
Mr. Harry J. Van Gorden
Mr. William P. Lonnie
Mr. Robert L. Pfeffer
Mr. Daren Luke
Dr. John Malik
Mr. John A. Schweitzer
Mr. Charles M. LoCascio
Mr. Ockle Johnson
Mr. Isidore A. Balton
Mr. Harry L. Berkowitz
T/Sergeant Alyan R. Hill
1st Lt. Karl Baum
1st Lt. Willard J. Ekman

The author is deeply indebted to them, and especially to Mr. Harry Murphy, Jr., Air Force Weapons Laboratory, Kirtland Air Force Base, New Mexico, who cooperated on all phases of this research; also, to Mr. Normand Stulman, U.S. Army Materiel Command Headquarters, Washington, D.C., whose assistance in selecting and editing material, as well as in numerous other ways, contributed invaluably to this publication.

CHAPTER 1

PRINCIPLES OF SEMIRAD RADIATION DETECTORS

Ion-Chamber Detectors. When a system consisting of two electrodes in a gas with an applied electric field between them is irradiated with X- or gamma rays, a current will flow between the two conductors. This current is the result of the radiation-induced ionization of the gas and is proportional to the radiation intensity. Measurements of the current as a function of time and of its integral give values proportional to the dose rate (radiation intensity) and to the total dose, respectively.

Although the direct action of the X-rays, gammas, or neutrons on the gas does produce some ionization, the bulk of the ions is formed by the passage through the gas of Compton electrons, photoelectrons, and recoil particles ejected from the ion-chamber wall by the incident radiation (Figure 1.1A). Unless precautions are taken to irradiate only the gas, the response of ion-chamber detectors is found to be proportional to the radiation energy absorbed per unit mass of the wall material. An adjustment in the absorbing characteristics of the wall material produces a change in the radiation-sensitivity characteristics of this material.

For an ion chamber to be sensitive to neutrons, its wall must have a coating that reacts with neutrons. If the reaction product is a charged high-energy particle, the latter produces ions in the gas and the ion current is proportional to the neutron flux. For the measurement of fast neutrons, the wall may be coated with a material containing hydrogen. Then some of the recoil protons produced by the (n, p) elastic scattering in the wall escape inside the chamber and produce ionization. A wall coating of a fissionable material with high fission cross section for fast neutrons (e.g., U^{238}) may also be used, and in this case, the ionizing particles are the fission fragments. For detection of slow neutrons, one can use a layer of boron, where α particles are produced, or a layer of U^{235} (Figure 1.1B).

From this description, we would expect that, for constant radiation environment and other parameters, the sensitivity of a small-size ion chamber should decrease with decreasing gas pressure. High-energy particles traversing the sensitive volume produce fewer ion pairs if the gas pressure is lowered so the ionization current would be expected to vanish for very small pressures. On the contrary, the ion-chamber current decreases with pressure only to a certain point and then, upon

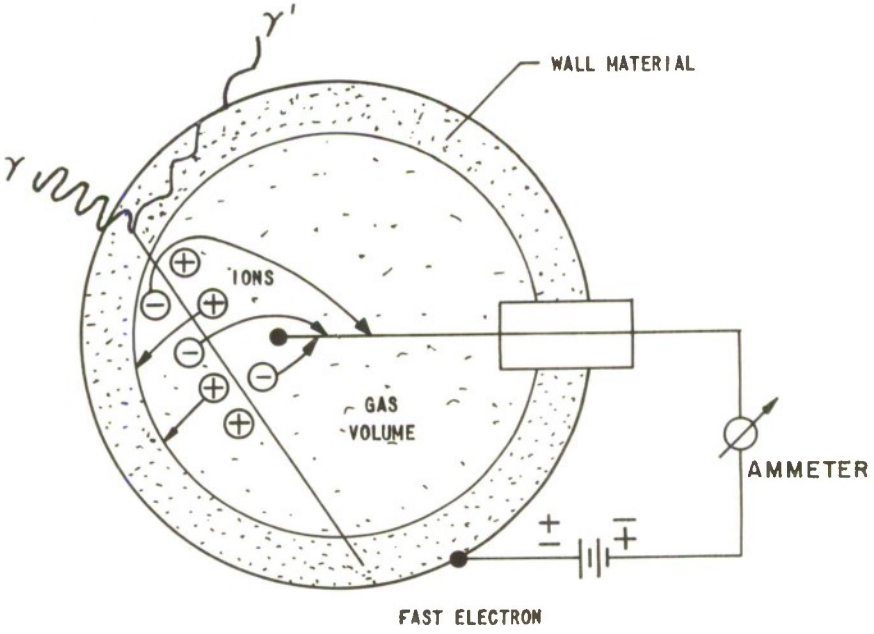


FIGURE 1.1A. *Ion-chamber performance (gamma radiation).*

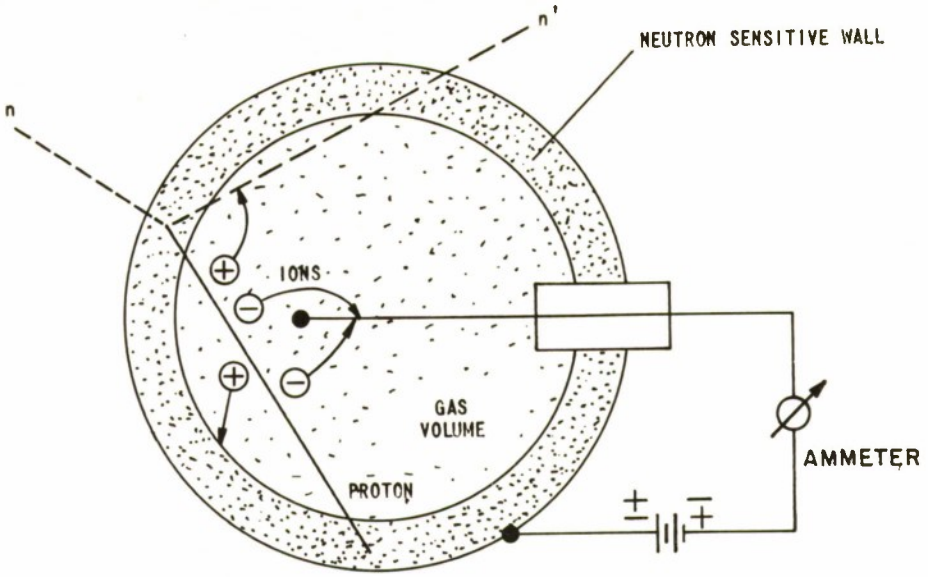


FIGURE 1.1B. *Ion-chamber performance (fast-neutron radiation).*

further evacuation, increases to an equilibrium point and remains constant.

This effect is due to low-energy secondary electrons emitted from the wall as a result of high-energy particle bombardment. At pressures above a certain level these secondaries cannot escape from the wall and thus cannot contribute to the ionization current. At the pressure where a minimum sensitivity of the chamber is observed ($\sim 2.10^{-3}$ mm Hg in Figure 1.2), sufficient concentration of gas molecules is present to lower the contribution of secondary electrons to the current, but the gas concentration is too low for ionization by the high-energy particles. A measurement of such a response curve as a function of air pressure is shown in Figure 1.2 for a chamber 2.5 cm in diameter and 7.5 cm long.

SEMIRAD Detectors (Reference 50). SEMIRAD have the same general appearance as do ion chambers; however, unlike ion chambers, SEMIRAD are evacuated to a very low pressure. As a consequence, little or no ionization is produced in SEMIRAD, and the entire response is due to secondary electrons.

When the wall of a SEMIRAD is irradiated with X-rays, gamma rays, or neutrons, a number of particles are ejected. In the case of X- and gamma rays, these particles are photoelectrons and Compton electrons; and for gamma energies above 1.05 Mev, these particles include both positrons and electrons from pair production. In the case of fast neutrons, the ejected particles are mainly protons with energies averaging one-half those of the neutrons in an instrument with walls of hydrogenous material. When these ejected particles pass through the surface of the SEMIRAD chamber wall, they cause secondary-electron emission. Secondary electrons are also emitted when the high-energy Compton and photoelectrons or protons reenter the opposite wall of the chamber (Figure 1.3A). If a positively charged electrode with an applied voltage higher than the energy of the secondary electrons is placed within the chamber, the secondary electrons are swept up, and the total charge collected is proportional to the radiation dose received.

As is true of the ion chamber, SEMIRAD can be made sensitive to neutrons by variation of the material of the chamber walls (Figure 1.3B). As in the case of ion chambers, the neutron sensitivity of SEMIRAD can be enhanced if we increase the amount of hydrogen contained in the wall material, or if we coat the inside of the surface with a fissionable material, boron or any other material with high cross section for slow- or fast-neutron reactions. Detection of a mixed (gamma and neutron) radiation dose can thus be accomplished with two SEMIRAD, one with nonhydrogenous, and one with hydrogenous walls.

Since the energy of the secondary electrons is not very high (most are below 50 ev), only a moderate voltage need be applied to ensure complete collec-

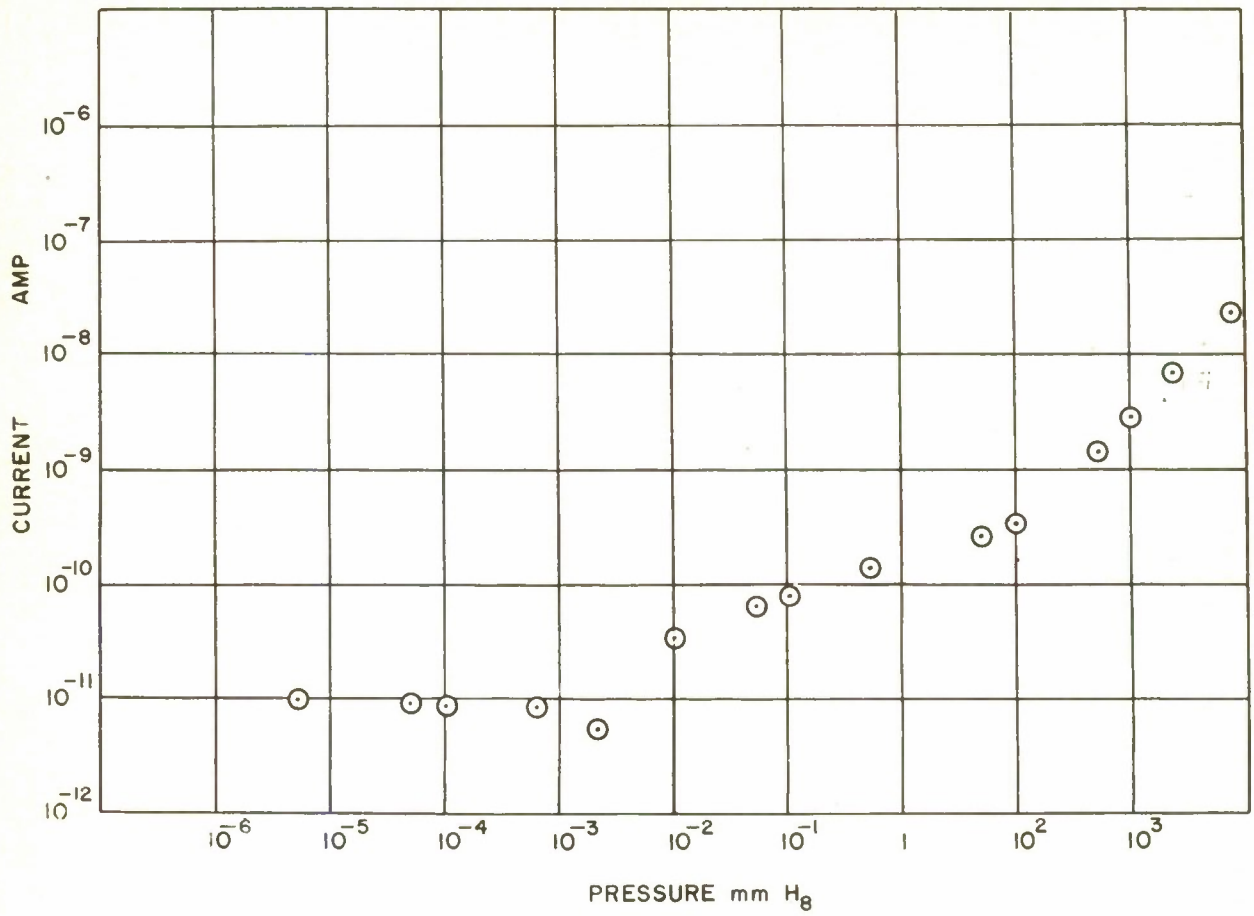


FIGURE 1.2. *Sensitivity of an ion chamber as a function of the gas pressure. (Dose rate: 1.1 rads/sec; maximum X-ray energy: 250 kv; 1.1-mm cadmium filter; applied voltage on the chamber: 300 v.) Sensitivity below 10^{-3} mm Hg. is approximately 9×10^{-12} a/rad/sec.*

tion. The primary particles (electrons and protons) are not collected because their energy is much too high to be affected by the collecting potential.

Since SEMIRAD operation depends not on the collection of positive and negative gas ions, but on the collection of electrons alone, recombination effects do not occur, and therefore SEMIRAD do not saturate due to charge recombination at high dose rates. This nonsaturation is perhaps SEMIRAD's most outstanding feature. Furthermore, since the secondary electrons are collected rapidly because of the small inertia of electrons as compared with ions, the response time of SEMIRAD is approximately one millionth that of ion-chamber dosimeters. In general the time necessary to collect electrons in a two-electrode system is given by the nonrelativistic expression:

$$t = \sqrt{\frac{d^2 m}{2ev}} \tag{1.1}$$

where d is the distance between the electrodes, v the applied voltage and e and m electron charge and mass, respectively ($t \sim 5.3 \times 10^{-10}$ seconds for $d = 1$ cm and $v = 1000$ v). In general, these times are shorter than the time resolution of the electronic equipment necessary to transmit, amplify, and record the pulse, and this equipment, therefore, sets the limit for time resolution.

The SEMIRAD is capable of measuring the fluxes and total doses of high-energy electrons. For this purpose, we must use an instrument with a wall sufficiently thin to permit the electrons to enter the evacuated chamber and to prevent the gamma radiation, which may be present in the environment, from interacting with the wall material, producing electrons, and so contributing to the instrument output.

The thickness of the wall depends on the Z of the wall material and on the energy of the electrons

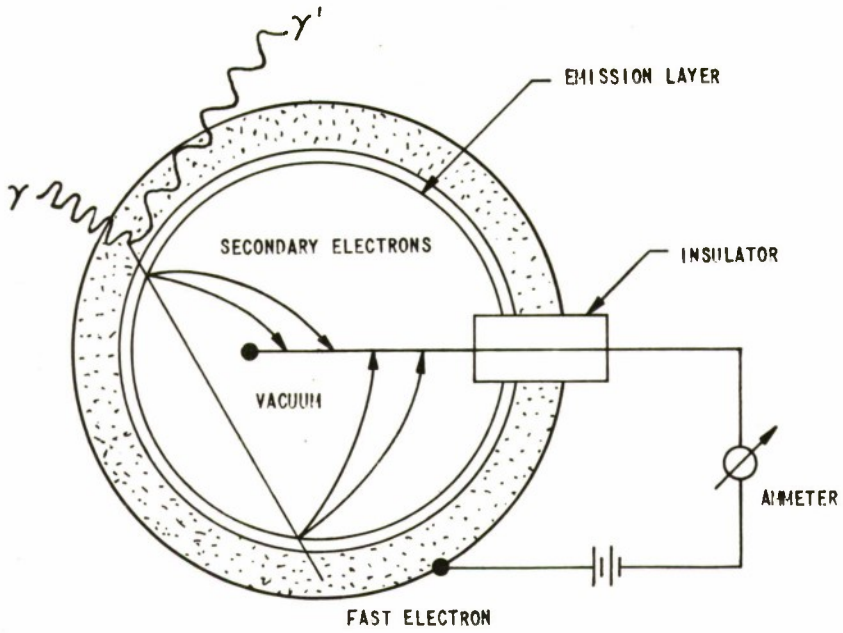


FIGURE 1.3A. *SEMIRAD detection mechanisms for gamma rays.*

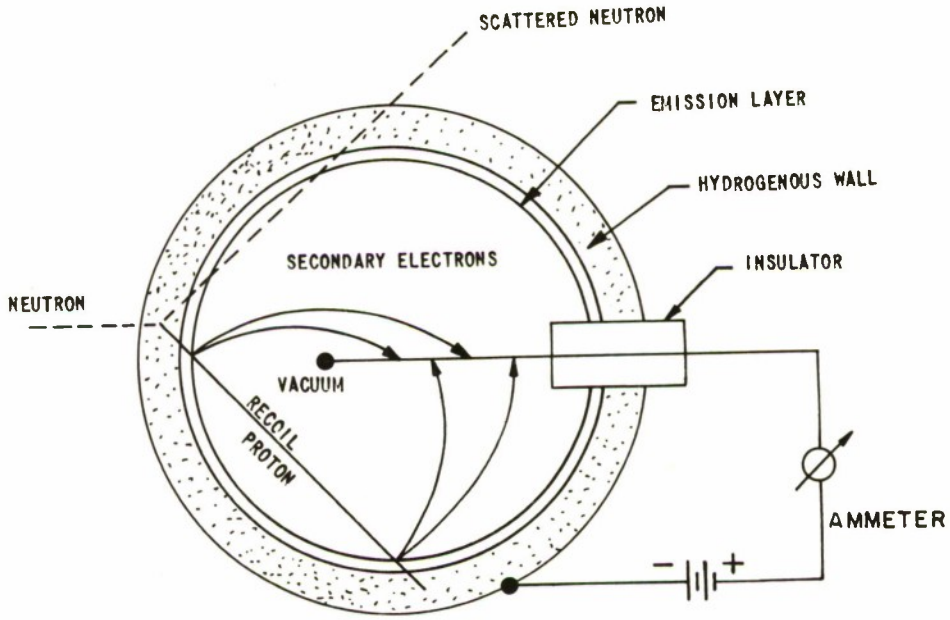


FIGURE 1.3B. *SEMIRAD detection mechanism for neutrons.*

which one desires to measure. If the measurement is to be performed in vacuum, as is the case in some outer space applications, one may replace the wall with a fine, positively charged wire mesh (collector). A hollow pipe centrally located in the mesh may serve as an emitter and the (negative) current flowing from the emitter indicates the electron dose rate.

CHAPTER 2

SEMIRAD VACUUM CONSIDERATIONS

Vacuum Requirements. The vacuum in SEMIRAD serves two main purposes: (1) it eliminates gas ionization, and (2) it makes possible the collection of low-energy secondary electrons. We can determine the vacuum requirements of SEMIRAD by considering these two purposes. A high vacuum also insures a constant and reproducible secondary-electron yield.

If we choose the arbitrary (but reasonable) limit for ion production in SEMIRAD as one ion pair for every 50 secondary electrons, then the contribution from the ionization will be two percent of the total. To achieve this goal, we must reduce the pressure of the gas within the detecting chamber until the sum of the production of ions by both primary radiation and ion multiplication is less than two percent of the number of secondary electrons produced.

The number of ions produced within an ion chamber by primary particles emerging from the wall of the chamber may be calculated from the following easily derived relation that assumes linear energy transfer of the primary particles.

$$N=\frac{E_pPd}{760\ wR} \tag{2.1}$$

where: N is the number of ion pairs formed per primary particle,
E_p is the energy of the primary particles (ev),
P is the gas pressure within the ion chamber (mm Hg),
d is the mean free path of the primary particle within the chamber (cm),
w is the energy expended in producing one ion pair in the gas (approximately 34 ev/ion pair for air),
and R is the range of the primary particle in the gas at normal pressure (cm).

If we use this relation and take into account the secondary-electron yield of the SEMIRAD surface, which is the number of secondary electrons emitted for each primary particle, the pressure required may be written as

$$P \leqq 760\ eRNy/E_pd \tag{2.2}$$

where: y is the yield of the SEMIRAD surface (secondary electrons/primary particle).

If we consider a 1-Mev electron whose range, R, is 400 cm in air, and use $w=34$, $N=2/100$, $y=2$, $E_p=10^6$ ev, and $d=2$ cm, the necessary air pressure is found to be 0.2 mm Hg. Similarly, for a 1-Mev proton whose range in air is 2.3 cm, we obtain a necessary pressure of 1.18×10^{-3} mm Hg, using the same constants as above.

In order to limit the production of gas ions by the passage of accelerated secondary electrons through the chamber to less than two percent of the total response of the SEMIRAD, we must limit the residual gas pressure so that the probability of formation of an ion pair by an individual secondary electron during its chamber transit is less than 2/100. We do this by adjusting the residual gas pressure within the SEMIRAD until the mean free path of the electrons becomes 50 times the collection distance (l).

Assuming linear energy loss, the mean free path of an electron in air can be expressed by:

$$L_e=4.1\times10^{-2}/P, \tag{2.3}$$

where L_e is the mean free path of the electron (cm), the pressure then becomes

$$P \leqq 4.1\times10^{-2}/50l. \tag{2.4}$$

For $l=2$ cm, the pressure required is 4.1×10^{-4} mm Hg. Since this pressure is less than either of the previously calculated pressures, it sets the vacuum requirements for SEMIRAD operation.

As a point of interest, note that the pressure requirements for ionization effects by secondary electrons may be entirely neglected if the collecting voltage of the SEMIRAD is not allowed to exceed the ionization potential of the gas (about 13 to 15 volts for air). In this case the only restriction for pressure is that specified in Equation 2.2. This fact may be of importance for SEMIRAD, which cannot be successfully operated at the vacuum indicated by Equation 2.4.

Vacuum-Suitable Materials. Although the pressure requirements that have been outlined are not

224-250 O-66—2

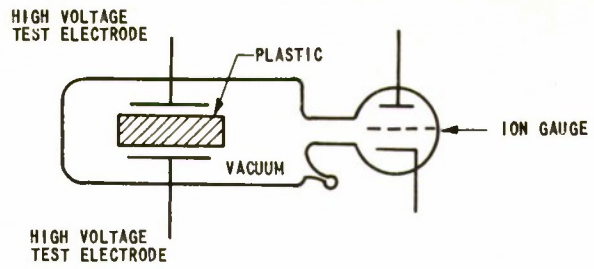


FIGURE 2.1. *Apparatus for testing the outgassing of plastics.*

difficult to obtain in conventional vacuum systems, the introduction of hydrogenous materials necessary to make SEMIRAD neutron-sensitive poses a serious problem. In general, organic materials introduced into a vacuum system to enhance fast-neutron sensitivity tend to outgas to the point of making them unsuitable for SEMIRAD construction.

A number of materials have been tested in the apparatus shown in Figure 2.1. The material under test was introduced into the apparatus, which was then thoroughly evacuated and hermetically sealed. Subsequent outgassing of the test material could then be observed by means of the attached ion gauge. The following materials have been tested and have been found to be unsatisfactory: paraffin (hard), apiezion hard vacuum wax, tissue-equivalent polyethylene, lucite, vacuum pitch, vacuum grease, and beeswax.

Most of these materials outgassed to the extent that the required vacuum could not be obtained prior to hermetical sealing of the sample. In the case of lucite and tissue-equivalent polyethylene, the samples outgassed indefinitely, and when the temperature was raised to 50° C, the vacuum was almost entirely lost.

The best hydrogenous materials for vacuum work have been found to be annealed polystyrene and mylar. Although these materials also tend to outgas, isolation of the instrument from the main vacuum system (so that oil and dirt from the vacuum system are not deposited on the samples) and pumping of the sample with a permanently attached ion pump or with a titanium getter pump for 15 minutes every 12 hours for about 10 days produce a vacuum that appears to be permanent at about 10^{-4} mm Hg.

The problems of maintaining a vacuum seem to be due not to high vapor pressures of the plastics but to outgassing of the occluded gases on the surface and absorbed water. To reduce the water content of plastic (e.g., mylar), we heat the latter in a vacuum to a temperature a few degrees below its melting point for approximately one hour. After this treatment, the sample can be exposed to air again for a short time, but should be handled carefully. The water must be removed before the surface of the material is coated with an evaporated layer of metal.

Research has been done on vapor pressure of plastic materials, and the results show that vapor pressures meet the SEMIRAD requirements for most suitable materials (Reference 1). The best way of introducing hydrogenous material into a permanently sealed vacuum system seems to be the use of hydrides. Some of these inorganic hydrogen compounds have a very low vapor pressure and can be baked at high temperatures in a vacuum furnace to drive the absorbed gas out of the material.

Titanium Pump. Use of the titanium pump has enabled the construction and operation of SEMIRAD with a hydrogenous wall in its initial development stage, without the necessity for permanent attachment to a bulky high-vacuum apparatus. This pump consists of a coil of titanium wire inserted into the vacuum with connections to the outside so that an electric current may be passed through the coil (see Figure 12.8). When the coil is heated, the titanium becomes an active getter, and most gases are absorbed or dissolved in the metal of the coil. In effect the getter becomes a vacuum pump and, in some cases, vacuum was improved by two or three orders of magnitude by the sole application of this getter.

Some of the experimental SEMIRAD described in Chapters 11 and 12 have had titanium pumps attached, thus making it possible for the instruments to be "pumped" again and again without disturbing the hermetic seal.

Ion Pump. An even more satisfactory way to keep a permanent vacuum in a closed SEMIRAD with a hydrogeneous wall is the application of a small ion pump that can be permanently connected to the instrument (see Figures 10.4 and 11.8). These ion pumps were recently developed and are obtainable in very convenient sizes for this application. They consist of the pumping chamber, which can be permanently sealed to the SEMIRAD body, and a permanent magnet that fits externally over the chamber. The pumps we used were Vac-Ion 0.2 liters/sec V–11651 models. Their pumping speed is .2 liters/sec at 10^{-2} mm Hg to 8 liters/sec at 10^{-6} mm Hg. An original vacuum of maximum 10^{-2} mm Hg, which is necessary for operation of the pump, can be raised to 10^{-7} mm Hg. This is far lower than the required pressure.

Another advantage of the built-in ion pump is that it serves simultaneously as a vacuum gauge. The pressure at any instant is related to the pumping current by a calibration curve and can thus be determined. The voltage applied on the pump depends on pressure and lies between 500 and 2800 V.

Use of Standard Getters in SEMIRAD. A good permanent vacuum can be obtained using a conventional getter that can be flashed before the "tipping off" operation. Certain precautions should be maintained, however, to avoid distribution of the gettering material over the secondary-electron emitter surface. Such contamination may affect the sensitivity by an uncontrollable change (mostly an increase) in the yield of secondary electrons, making the device irreproducible.

In the construction of gamma-sensitive instruments, we solved the above problem by subdividing the vacuum chamber into two compartments, one containing the collector electrode, and the other, with a much smaller volume, containing the getter. The two compartments are loosely separated, so that the remaining gas can travel between them. After it is flashed, the gettering material distributes itself exclusively throughout the getter compartment, which is a Faraday cage, and no contribution to the secondary-electron current can be obtained from this part of the SEMIRAD.

For neutron-sensitive instruments, where heat-sensitive hydrogenous materials are used, it is more difficult to use a conventional getter, because the hydrogenous material is destroyed during the flashing operation when heat is applied. Instruments with walls of outgassed titanium and no plastics inside (Figure 11.4) do not need any getters when carefully baked out in vacuum. The pressure in these instruments is in the order of 10^{-6} mm Hg.

The use of an all-titanium construction has still another advantage: when a large number of gammas or neutrons passes through an evacuated cavity, gas molecules are knocked out of the walls which may have considerable energy. Since the molecules stay in the vacuum, the pressure has the tendency to build up with increasing exposure to radiation. Not so in a chamber with titanium walls. Since the gas molecules are ejected from the walls with a considerable energy which is not altered during their travel through the vacuum, they impinge on the opposite wall and most of them are absorbed in the outgassed titanium.

The principle of this effect is the same as the principle of the operation of the titanium ion pump. This effect increases strongly when the exposure takes place while voltage is applied between the electrodes of the titanium SEMIRAD. The gas molecules leave the wall mostly in an ionized state and are then accelerated by the applied field to the opposite electrode, so their absorption probability increases.

CHAPTER 3

SEMIRAD DOSE-RATE LIMITATIONS

Since SEMIRAD are electronic diodes in which the electrons are generated by high-energy radiation rather than by thermionic emission, thus the limitations on current that apply to thermionic diodes may be directly applied to SEMIRAD. These limitations are the result of space-charge formation between the emitter and the collector, and were given by Langmuir and Compton (Reference 2). In this reference, limits are computed for several geometrical arrangements of the emitting and collecting electrodes. The results applicable to SEMIRAD are given below and are based on the assumption that the electrons are emitted with negligible initial velocities.

Parallel-Plate Geometry. The limiting current in a SEMIRAD whose electrodes are parallel plates may be expressed as:

$$i=\frac{\sqrt{2}}{9\pi}\left(\frac{e}{m}\right)^{1/2}\frac{V^{3/2}}{x^2}A, \text{ or } i=2.334\times10^{-6}AV^{3/2}x^{-2} \tag{3.1}$$

where

i is the maximum current through the SEMIRAD (amps),

e/m is the ratio of charge to mass of an electron (5.279×10^{17} esu),

V is the voltage applied to the SEMIRAD (volts),

x is the plate separation (cm),

A is the area of one plate (cm^2).

Coaxial Cylinder Geometry. The expression for the limiting current in a SEMIRAD with cylindrical geometry depends on which electrode is the emitter, and on the relative radii of the electrodes. The limiting current for both cases is given by the following parametric equation:

$$i=\frac{2}{9}\left(\frac{2e}{m}\right)^{1/2}\frac{LV^{3/2}}{r\beta^2}, \text{ or } i=14.66\times10^{-6}\frac{LV^{3/2}}{r\beta^2} \tag{3.2}$$

where r is the collector radius (cm)

L is the length of the cylinder (cm) ($L \gg r$ for negligible end-effect correction)

and β is a parameter depending on the geometry used. If r_e is the emitter radius, then for $r_e/r<1$ (external collector):

$$\beta=1+0.9769\left(\frac{r_e}{r}\right)^{2/3}\sin\left[1.0854\left\{\log\left(\frac{r}{r_e}\right)-1.0766\right\}\right] \tag{3.3}$$

If $r_e/r>1$, (internal collector), then

$$\beta^2=4.6712\left(\frac{r_e}{r}\right)\left[\log_{10}\frac{r_e}{r}-0.15045\right]^{3/2}. \tag{3.4}$$

Concentric Spherical Geometry. The limiting equation for current in a spherical SEMIRAD is also expressed parametrically and also depends on the relative radii of the electrodes. The limit is

$$i=29.34\times10^{-6}V^{3/2}\alpha^{-2} \tag{3.5}$$

where α is a parameter depending on the geometry used.

For $\frac{r_e}{r}<1$ (external collector)

$$\alpha^2=\frac{2}{3}ln\left(\frac{r}{r_e}\right)+0.5158\log\left[3.885\,ln\left(\frac{r}{r_e}\right)\right]. \tag{3.6}$$

For $r_e/r>1$ (internal collector)

$$\alpha^2=\left[1.11\left(\frac{r_e}{r}\right)-1.64\right]^{3/2}. \tag{3.7}$$

Table 3.1 lists both the maximum currents obtainable and the corresponding dose rates for typical SEMIRAD geometries using the Langmuir-Compton equations. An experimental value of 1.5×10^{-14} coulombs/rad/cm^2 of the emitter surface (titanium wall) has been used as the specific sensitivity for the construction of the table.

TABLE 3.1. *Maximum currents and corresponding dose rates obtainable from a typical SEMIRAD (for the specific sensitivity of 1.5 $\times 10^{-14}$ coulombs/rad/cm² emitter surface)*

Instrument type	Dimensions (cm)	(50 volts)		(3,000 volts)		Sensitivity (specific sen. × emitter area) (coulombs/rad)
		Maximum current (amp)	Maximum dose rate (rads/sec)	Maximum current (amp)	Maximum dose rate (rads/sec)	
Parallel plates	$A=3\times3$ $x=1/2$	2.97×10^{-2}	2.20×10^{11}	13.8	1.02×10^{14}	1.35×10^{-13}
Coax. cylinder internal collector	$r_e=3$ $r=0.1$ $L=10$	2.42×10^{-3}	8.58×10^{8}	1.13	4.01×10^{11}	2.82×10^{-12}
External collector	$r=3$ $r_e=0.1$ $L=10$	1.6×10^{-2}	1.70×10^{11}	7.44	7.89×10^{13}	9.43×10^{-14}
Coax. cylinder internal collector	$r_e=3$ $r=1$ $L=10$	1.99×10^{-2}	7.06×10^{9}	9.24	3.28×10^{12}	2.82×10^{-12}
External collector	$r=3$ $r_e=1$ $L=10$	3.37×10^{-2}	3.57×10^{10}	15.7	1.66×10^{13}	9.43×10^{-13}
Concentric spheres internal collector	$r_e=3$ $r=0.1$	5.8×10^{-5}	2.06×10^{7}	.027	9.57×10^{9}	2.82×10^{-12}
External collector	$r=3$ $r_e=0.1$	3.65×10^{-3}	3.87×10^{10}	1.69	1.79×10^{13}	9.43×10^{-14}

L length
r_e emitter radius
r collector radius
x distance
A area

CHAPTER 4

SEMIRAD SENSITIVITY

General. SEMIRAD are unique in that we can vary their sensitivity over wide ranges without changing the physical size of the devices (as is necessary in ion-chamber detectors). The SEMIRAD system is about 10,000 times less sensitive than an ion-chamber dosimeter with a similar geometry. To reduce the sensitivity in ion-chamber dosimeters (e.g. IM–93 fountain-pen dosimeters) and thus make them suitable for higher dose readings, one introduces condensers between the collecting electrodes. The dielectric material in these condensers must be of the highest quality; however, it is a source of many unwanted effects, partially explainable by persistent internal polarization, which may make the dose readings irreproducible. Considerable research has been done on these effects and is reported in References 3 and 4. In the case of SEMIRAD, the sensitivity can be increased by use of a large emitting surface coated with a high-yield secondary-electron emitter (for example, cesium-antimony coating such as used on photomultiplier dynodes). To lower the sensitivity of the instrument, we use a very small emitter area and a low-yield emitter coating (for example, carbon).

Although low-energy secondary electrons are emitted from both the positive and the negative electrodes in a SEMIRAD, the presence of the electric field causes the negatively charged electrons emitted from the positive electrode to return immediately to that electrode, and only the electrons emitted from the negative electrode traverse the detector. Therefore, only the negative electrode plays an important part in SEMIRAD secondary-electron generation. In some respects then, the negative electrode of a SEMIRAD is similar in action to that of the cathode of a thermionic diode and, as a consequence, the sensitivity of a SEMIRAD is proportional to the product of the yield and the area of the emitting (negative) surface.

If the subscripts 1 and 2 are used to denote the corresponding electrodes, we can write:

$$S_1 \propto A_1 Y_1 \text{ (for electrode 1 as the emitter)} \tag{4.1}$$

and

$$S_2 \propto A_2 Y_2 \propto \text{ (for electrode 2 as the emitter)} \tag{4.2}$$

where

S is the sensitivity of the SEMIRAD (coulomb/rad),
A is the area of the emitting electrode,
and
Y is the secondary-electron yield of the electrode (coulomb/rad/cm^2).

If both electrodes are made of material of identical composition and surface structure, then

$$Y_1 = Y_2$$

and

$$S_1/S_2 = A_1/A_2. \tag{4.3}$$

This relation, showing that the sensitivity ratio of a SEMIRAD operated with different electrode polarities is equal to the ratio of the emitter surface areas, has been tested experimentally several times and has been found to be true provided the vacuum is good enough (Figure 4.1). This polarity dependence is one identifying characteristic of SEMIRAD operation, and has been used to determine the degree of vacuum existing within SEMIRAD chambers. If for a cylindrical SEMIRAD S_1/S_2 is found to be closer to the value one than is its computed value, and if the absolute values of S_1 and S_2 begin to increase, the vacuum is probably poor, and ionization is taking place within the detector.

Two factors other than geometry influence the sensitivity of SEMIRAD devices: the emission of secondary electrons by high-energy primary electrons, recoil protons, or fission fragments; and the conversion of gamma rays into electrons or conversion of neutron energy into energy of recoil particles or neutron reaction products. The first factor will be discussed in Chapter 5 (Energy Dependence), and the second in Chapter 6 (Secondary Electron Emission). At this point it is important to emphasize that it is difficult to increase the sensitivity of SEMIRAD by coating the emitter surface with a high-yield secondary-electron-emission material that is an insulator (e.g. magnesium oxide).

If irradiated, the coating loses secondary electrons that cannot be replaced from the metal below be-

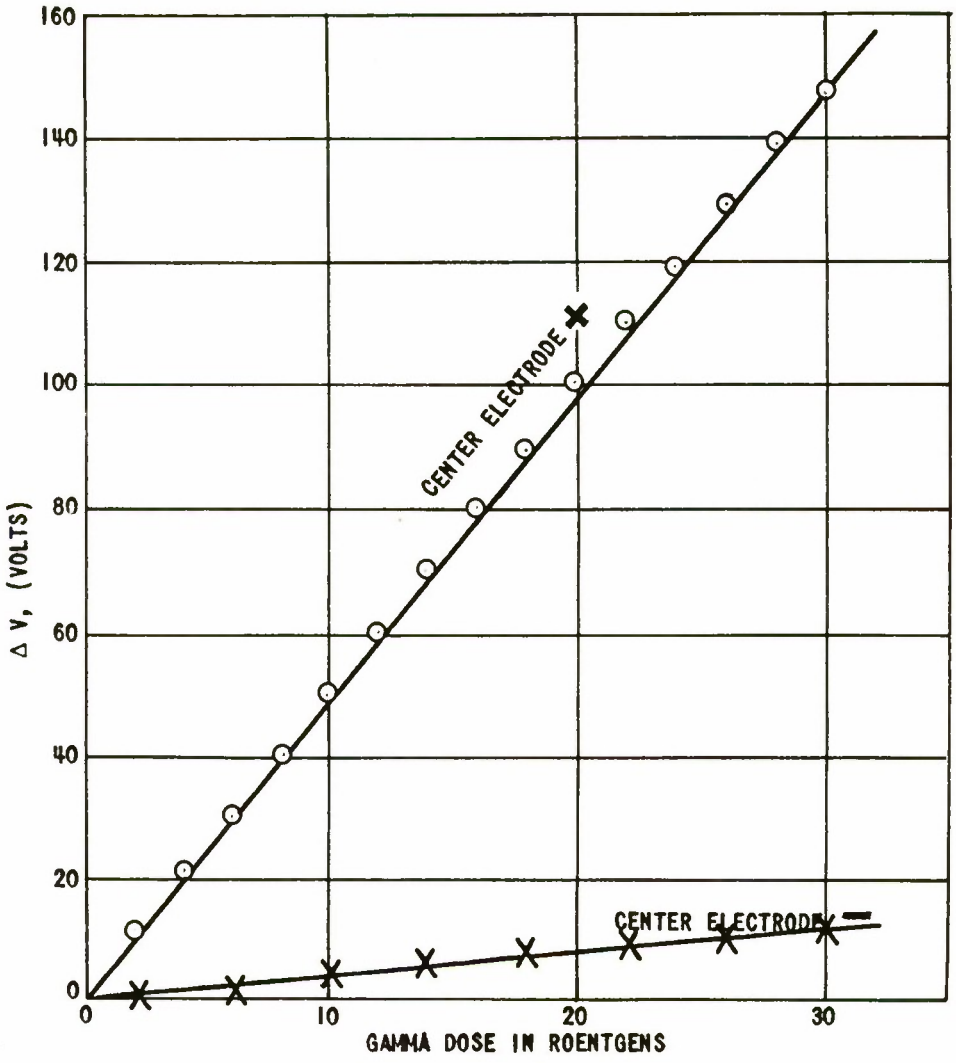


FIGURE 4.1. *Calibration of a SEMIRAD dosimeter with Co^{60} gammas, with normal and reversed polarity of the applied voltage. The ratio of the area of the center electrode to the area of the outside electrode was approximately 1:11.*

cause of its insulating properties. The coating surface becomes charged positively, and this charge may increase until it cancels the applied electric field or breaks down through the thin coating causing in the first case a steady variation of sensitivity and in the other a sudden strong variation. In some cases, the Malter effect (References 46 and 47) takes place, and an avalanche of electrons might be released.

We performed many unsuccessful experiments to avoid the above problems. For the same reason, the area of the insulator facing the vacuum that separates the collector from the emitter should be chosen as small as practicable to avoid distortion of the applied electric field due to charge buildup on the insulator surface.

High sensitivities may be obtained by coating the emitter surface with conductive high secondary electron yield materials. Such coatings are used in photomultiplier tubes and photocells and consist of mixtures of different materials, for example, Cesium Antimonide. The techniques of making such layers are very difficult, particularly if the coatings are deposited on metal in vacuum rather than on glass. We plan to work on this problem but presently no experimental data are available on this subject.

Sensitivity Dependence as a Function of the Applied Voltage. The sensitivity of the SEMIRAD devices as a function of the voltage applied between the collecting and the emitting electrodes depends on the ratio between the number of electrons

emitted into the vacuum and the number of electrons collected or repelled by the applied voltage. This ratio depends on the initial energy distribution and direction of emission of the primary particles and secondary electrons, on the geometry of the device, and on the electric field strength as a function of location. The initial energy distribution of the secondary electrons is considered in Chapter 6.

As far as secondary electrons are concerned, the current saturates at applied voltages equivalent to the energy of these electrons. Since the majority of secondary electrons lie within the order of several tens of electron volts, only a few more electrons can be collected (or repelled) by increasing the voltage beyond the corresponding value.

In practical cases, the saturation with voltage takes place at 30 volts collecting potential for the instruments illustrated in Figures 11.1, 11.3, and 11.4. One notices, however, that the output of a typical instrument is still changing slightly when we increase the voltage to several hundred or even several thousand volts. This happens because at high voltages we start collecting (or repelling) the low-energy component of the primary particles.

When the applied voltage approaches zero, the output current may vanish completely or partially, depending on the geometry used, whether the measured particles are neutrons or gammas, and on the wall material. In the case where one electrode completely surrounds the other, absorption for incident radiation in the central electrode is small, and where the surface structure and wall materials are the same for both electrodes, we obtain no response to radiation when the applied voltage is zero. In this case, all secondaries emitted from the central electrode arrive at the outer electrode. However, when we consider the secondaries emitted from the outer electrode, only that fraction determined by the ratio, S, of the area of the central electrode to the outer electrode arrives at the central electrode; therefore, the currents from the two electrodes nearly cancel one another.

Experimental Measurements of SEMIRAD Sensitivity for Fast Neutrons and Gamma Rays. These measurements were made using SEMIRAD dosimeters with a quartz-fiber electrometer built inside the vacuum chamber, the loss of charge on the electrometer being proportional to the total dose delivered. This loss of charge is read out as the voltage drop across the chamber, which is a capacitor. The instruments had a hydrogenous wall emitter coated with an aluminum layer, making them sensitive to both gammas and fast neutrons.

SEMIRAD were irradiated with fast neutrons and gamma rays generated by bombardment of a beryllium target with 2-Mev deuterons on the USASRDL Van de Graaff accelerator. Since the gamma contamination of the neutron beam was about 25 percent of the neutron dose, the delivered dose for gammas and for fast neutrons was measured separately. This was accomplished by exposing a series of calibrated ion-chamber quartz-fiber dosimeters capable of measuring neutron and gamma doses in a mixed neutron-gamma field.

In order to separate the sensitivities of the SEMIRAD for gamma and neutron doses, we irradiated the SEMIRAD under two neutron-to-gamma ratios: first, directly with neutrons and gammas from the beryllium target; and second, behind a moderator of 9 cm of paraffin which increased the gamma-to-neutron ratio. Under these conditions, the following analysis was made:

If S_n = SEMIRAD sensitivity to neutrons (volts/rad),
S_γ = SEMIRAD sensitivity to gamma radiation (volts/rad),
n_1, n_2 = Neutron dose (rads),
γ_1, γ_2 = Gamma dose (rads),

and

ΔV_1, ΔV_2 = Voltage drop indicated on the SEMIRAD,

and if the subscripts 1 and 2 indicate first (unmoderated) and second (moderated) irradiations respectively, one obtains:

$$S_n n_1 + S_\gamma \gamma_1 = \Delta V_1 \tag{4.4}$$

and

$$S_n n_2 + S_\gamma \gamma_2 = \Delta V_2. \tag{4.5}$$

By use of these expressions, we obtained the following sensitivities by substituting experimental values for ΔV_1, ΔV_2, n_1, n_2, γ_1, and γ_2:

$S_\gamma = .10$ volts/rad;
$S_n = .067$ volts/rad.

Although these values are not precise, they are at least accurate enough to indicate that the sensitivities of this particular SEMIRAD for gammas and fast neutrons were of the same order of magnitude.

Since the capacitance of the SEMIRAD was measured at about 10 $\mu\mu$f, and since the emitter area of this SEMIRAD was 6.5 cm^2, we can compute

the absolute neutron sensitivity by using the following formula:

$$Y_n = C\Delta V/A\phi e \text{ secondary electrons/incident neutron} \quad (4.6)$$

where

Y_n is the secondary-electron yield in secondary electrons per incident neutron,
C is the capacitance of the system,
ΔV is the voltage drop corresponding to the given neutron dose (volts),
A is the area of the emitting surface (cm^2),
ϕ is the neutron flux density (n/cm^2) and,
e is the charge on an electron (1.6×10^{-19} coulombs).

For the sensitivity of .067 volts/rad (2.5×10^8 n/cm^2), this formula results in a value of 2.6×10^{-4} secondary electrons per incident fast neutron. To check this sensitivity, we computed the number of secondary electrons produced per incident neutron and used the following formula computed by Moyer (Reference 5) which gives the number of recoil protons emerging from the surface of a hydrogenous material under fast neutron irradiation

$$N_p = O_i N_H A\phi(E_n)\sigma_{n,p}(E_n)R(E_n). \quad (4.7)$$

Here N_H is the number of hydrogen atoms per cm^3 of the irradiated material or

$$N_H = n_H \frac{\rho A_n}{W_m} \quad (4.8)$$

where

$\phi(E_n)$ is the neutron flux density per unit range of energy,
$\sigma_{n,p}(E_n)$ is the n, p scattering cross section,
A is the area of the hydrogenous material,
$R(E_n)$ is the range-energy function (cm) for protons, (Figure 4.2A, 4.2B),
n_H is the number of hydrogen atoms per molecule of the material,
ρ is its mass density,
A_n is the Avogadro number (6.02×10^{23} atoms per gram-mole), and
W_m is the molecular weight of the material.

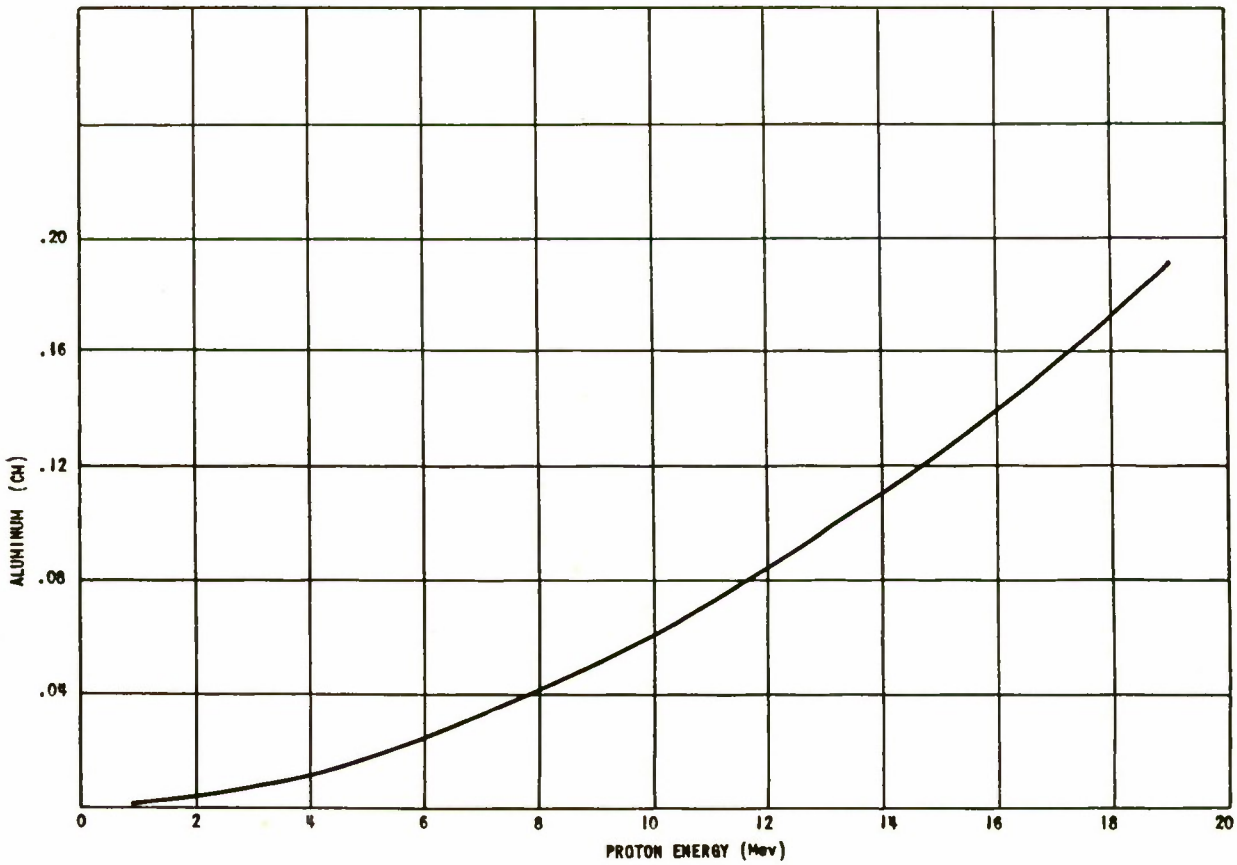


FIGURE 4.2A. *Range of protons as a function of energy in aluminum.*

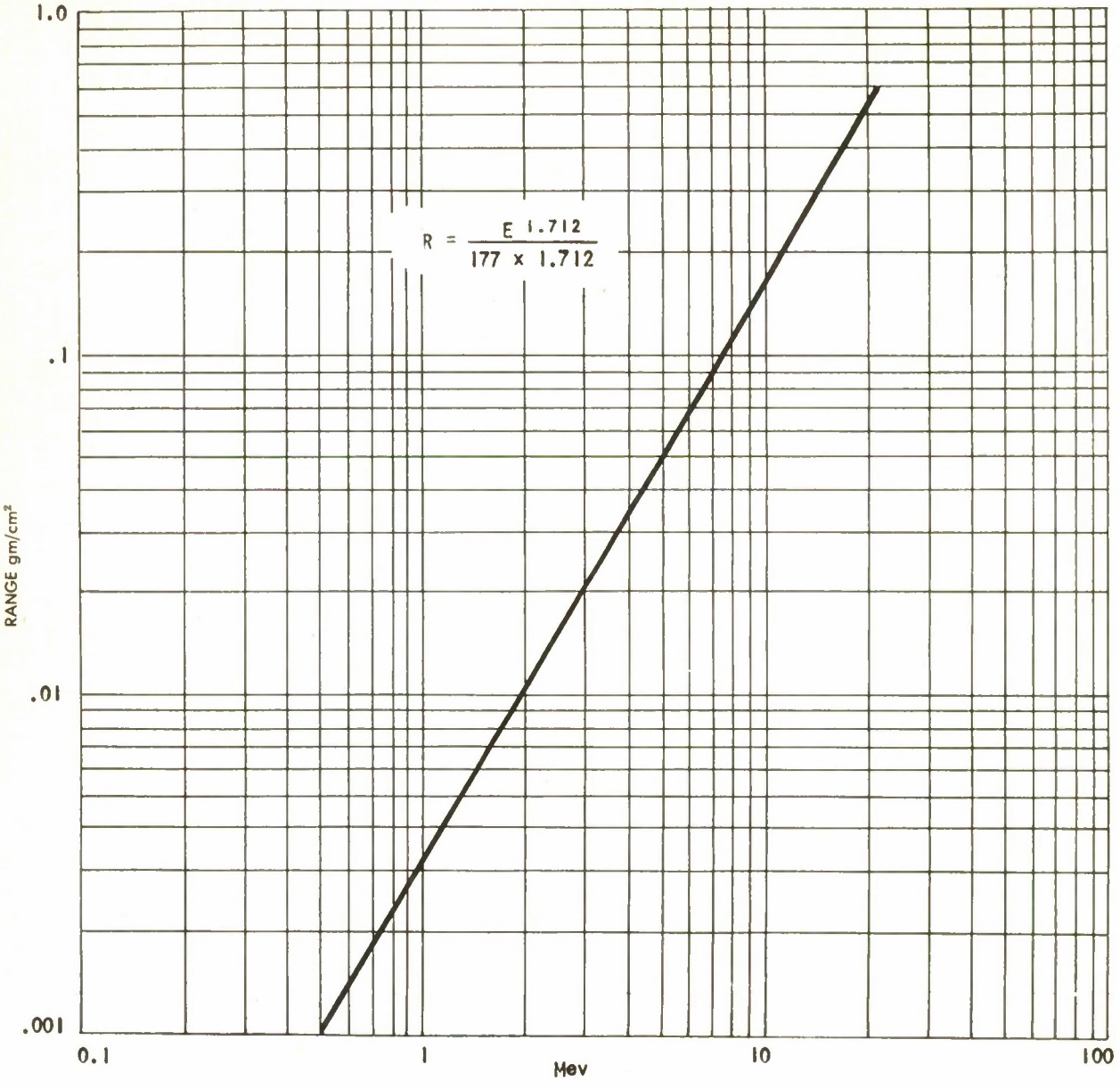


FIGURE 4.2B. *Range of protons as a function of energy in plexiglas.*

For 2-Mev neutrons incident on polyethylene, we find that approximately one proton emerges from the polyethylene for every 10,000 incident fast neutrons. Since each proton that emerges from the wall of a cylindrical geometry SEMIRAD also reenters the wall and therefore has two chances to produce electrons, result these considerations in an average proton-produced secondary-electron yield of about one, which agree roughly with the measured yield values in the case of isotropically incident protons at these specific energies.

Theoretical Computation of SEMIRAD Neutron Sensitivity. To compute more accurately the sensitivity of a given hydrogenous-wall SEMIRAD for fast neutrons, we must know the energy distribution of protons escaping from a hydrogenous wall produced by neutron irradiation and the yield for proton-produced secondary electrons as a function of the proton energy. The energy distribution of protons emerging from a fast-neutron-irradiated slab of hydrogenous material was computed by Kronenberg and Murphy (Reference 6).

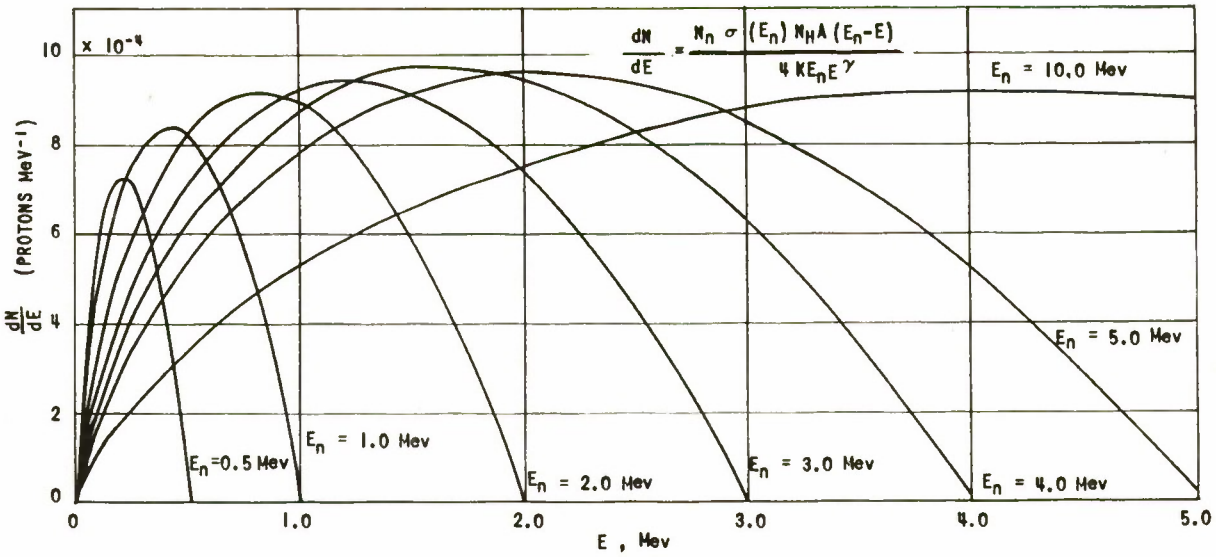


FIGURE 4.3. *Energy distribution of recoil protons leaving the surface of a plexiglas slab when irradiated isotropically with mono-energetic neutrons. Neutron flux—1 neutron/cm².*

This computation was made under the assumptions that the thickness of the hydrogenous slab is chosen so that it is smaller than the mean free path of the lowest-energy fast neutron under consideration and thicker than the range of the highest-energy recoil proton. Furthermore, the neutrons impinge upon the material isotropically. This last requirement is always closely realized when the inside of a closed cavity is under consideration. The general result for the proton spectrum is

$$\frac{dN_p}{dE}=\frac{N_H A E^{-\gamma}}{4K}\int_E^{\infty}\left[\int_{E_0}^{\infty}E_n^{-1}\sigma_{n,p}(E_n)h(E_n)dE_n\right]dE. \tag{4.9}$$

where the symbols have the same meaning as in Equation 4.7, and in addition γ and K are material constants defined by the rate of energy loss of a proton traversing a material,

$$-dE/dD=KE^{\gamma} \tag{4.10}$$

and $h(E_n)=\dfrac{dN_n}{dE_n}$ is the fast-neutron spectrum. Some typical values for K and γ are given in Table 4.1.

For mono-energetic neutrons Equation 4.9 becomes

$$\frac{dN_p}{dE}=N_H N_n A E^{-\gamma}E_n^{-1}\sigma(E_n)(E_n-E)\frac{1}{4K} \tag{4.11}$$

This energy distribution is illustrated in Figure 4.3 for some typical neutron energies. The yields for secondary-electron emission as a function of incident proton energy are discussed in Chapter 6. From this data we theoretically obtain the hydrogenous SEMIRAD fast-neutron sensitivity, S, as:

$$S=\int_0^{\infty}\frac{dN_p}{dE}(E)Y_i(E)edE \tag{4.12}$$

where e is the electron charge, and $Y_i(E)$ is the average number of secondary electrons per incident proton for isotropic irradiation of a target. As outlined in Chapter 6, $Y_i=2Y$, where Y is the yield for perpendicular incidence. The sensitivity S may be expressed in coulombs of collected charge per incident neutron or in coulombs per rad of incident neutrons.

TABLE 4.1. *Material constants γ, K, N_H for some materials which may be used to generate recoil protons. The dimension of K is $Mev^{1-\gamma}\ cm^2g^{-1}$; γ is dimensionless.*

Material	γ	K	N_H
Plexiglas ($C_5H_8O_2$) ($\rho=1.185$)	−.719	273.2	5.71×10^{22}
Tissue ($C_5H_{40}O_{18}N$) ($\rho=1.0$)	−0.70	280	6.03×10^{22}
Water ($\rho=1.0$)	−.737	279.4	6.69×10^{22}
Polyethylene ($\rho=0.912-0.965$)	−0.727	305.9	8.06×10^{22}

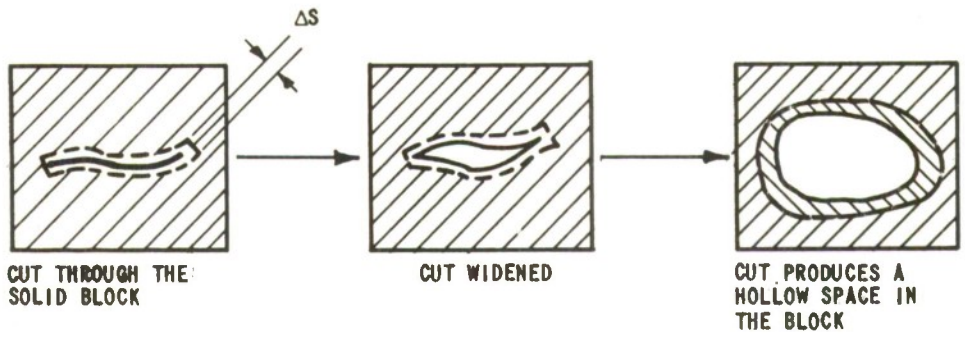


FIGURE 4.4. *A cut inside of a block of material is spread out to generate an evacuated cavity (1/2ΔS indicates the thickness of the escape layer).*

Theoretical Computation of SEMIRAD Gamma Sensitivity. An expression similar to Equation (4.12) can be written for the SEMIRAD sensitivity to gamma radiation, in which the sensitivity can be expressed in coulombs per rad or coulombs per incident gamma ray, as follows:

$$S=\int_0^{\infty}\frac{dNe}{dE}(E)Y_i(E)edE \tag{4.13}$$

where $\frac{dNe}{dE}$ is the energy distribution of fast electrons emerging into the vacuum from the gamma-irradiated wall, and the yield, $Y_i(E)$, is the average number of secondary electrons per fast electron analogous to its use in Equation (4.12). The yield, in this case, is dependent on the energy of the incident particle just as it is in Equation (4.12). The function $\frac{dNe}{dE}$ was computed by Fetkovich (Reference 7), in which he calculated the energy distribution $F(E)$ of electrons traversing an imaginary plane inside a block of matter irradiated by gamma rays with energy W. The result (Equation 4.14), includes all electrons from Compton scattering, photo effect, pair production, and also from back scattering.

$$\frac{dNe}{dE}(E,\theta)=N\frac{I}{A\Delta\Omega}\frac{\cos\theta}{\frac{dE}{dX}}=I \tag{4.14}$$

$$I=\int_{E_i=\infty}^{E_i=E}[\sigma_w^{ph}(E_i)+\sigma_w^{\text{compt.}}(E_i)+\sigma_w^{pr}(E_i)]dE_i$$

In the above equation θ is the angle between the perpendicular line to the imaginary surface in the block of material and the direction of the electron,

I is the gamma intensity,

A is the area of the imaginary surface,

$\sigma_w^{ph,\,\text{compt.},\,pr}$ are the cross sections for the incident gammas of energy W for photoelectric effect, Compton scattering and pair production, respectively, and $\Delta\Omega$ is the solid angle where $\Delta\Omega=2\pi\sin\theta d\theta$. This expression is valid if the following conditions are satisfied: The distance between any point of the imaginary surface and the exterior of the block is larger than the range of the fastest electron available (corresponding to the energy of the gamma rays), and smaller than the mean free path of the gammas. If a cut is made along the previously mentioned imaginary plane and the opening thus produced is spread out, one obtains an evacuated cavity surrounded by walls similar to a SEMIRAD chamber (Figure 4.4). This operation does not affect Equation 4.14. Setting $\theta=0$ and $\Delta\Omega=1$, we obtain the following expression for the energy spectrum of electrons in the evacuated SEMIRAD with the wall of the cavity serving as the emitter electrode:

$$\frac{dNe}{dE}(E)=\frac{NI}{A}\frac{1}{\frac{dE}{dx}}\int_{E_i=\infty}^{E_i=E}$$

$$[\sigma_w^{ph}(E_i)+\sigma_w^{\text{compt.}}(E_i)+\sigma_w^{pr}(E_i)]dE_i \tag{4.15}$$

By substituting this expression for $\frac{dNe}{dE}(E)$ in Equation 4.13, we find the sensitivity of a SEMIRAD to gamma radiation.

CHAPTER 5

SEMIRAD ENERGY DEPENDENCE

A dosimetry system's energy dependence is its sensitivity as a function of the quantum energy of the incident radiation. Any statement on energy dependence of an instrument will thus depend on the units in which we measure the quantity of the incident radiation. The quantity of radiation can be expressed in (a) the number of particles incident on a unit area at the point of the measurement, (b) the total energy (in ergs) that passes through a unit area at the point of measurement, (c) the energy delivered by the incident radiation to a sample of a certain material with a given volume or mass, or (d) the number of ion pairs that radiation can produce in a given volume of gas.

In the study of radiation effects, the dose absorbed in the irradiated sample is in most cases the important factor, and so many investigators prefer to measure it in rads. A dose of one rad is delivered when a sample of a given material with a mass of one gram receives 100 ergs of energy. The dose is dependent on the irradiated material and therefore we speak of aluminum rads, tissue rads, etc., for both gammas and neutrons. In the case of neutrons, the number of neutrons per cm^2 is a unit that is also used. The corresponding dose rate or intensity is defined as the number of neutrons incident per second on a unit area. Table 5.1 shows the conversion factors between neutrons per square centimeter and rads. In an analogous way, gamma intensity can be expressed by Mev gamma per cm^2 per sec.

SEMIRAD Energy Dependence for Gamma Radiation. Suppose a gamma-sensitive SEMIRAD is irradiated with gamma rays that have the spectral distribution $\frac{dI}{dE}(E)$ where I is the spectral intensity measured in rads. These gamma rays cannot transmit their energy to the wall of the instrument directly, but they form high-energy electrons by means of the photoelectric effect, Compton effect, and pair production. We consider the case where the emitter wall thickness is much smaller than the mean free path of the lowest energy gamma rays in the enviroment and larger than the range of any electron that the gamma spectrum can produce (Figure 5.1). According to the first collision theory, the electrons in the cavity will then be in an energy equilibrium (as outlined in Chapter 4). An electron spectrum that can be experimentally measured inside the SEMIRAD cavity may be defined as

$$\frac{dI_e}{dE}(E) = F\left[\frac{dI_\gamma}{dE}(E)\right], \tag{5.1}$$

where F contains the wall material as parameter. If we choose a very thin layer of material at the surface of the cavity wall, with thickness ΔX, where ΔX is very small compared to the effective electron range, then the energy deposited in the layer by the electrons or indirectly by the gamma rays (which is the energy delivered to the volume $A\Delta X$, A being the cavity area) will be

TABLE 5.1. *Conversion factors between neutrons per cm^2, r, and rads as function of energy (First collision dose)*

Energy (Mev)	Dose (n/cm^2 rad)	Dose (r/rad)
Thermal	15. 10^8	.....
0.01	96. 10^8	1.15
0.015	69. 10^8	1.17
0.03	39. 10^8	1.19
0.04	31. 10^8	1.18
0.05	26. 10^8	1.17
0.06	22. 10^8	1.14
0.08	18. 10^8	1.11
0.10	15. 10^8	1.10
0.15	11. 10^8	1.08
0.2	9. 10^8	1.07
0.3	6.8 10^8	1.07
0.4	5.7 10^8	1.07
0.5	5.0 10^8	1.07
0.6	4.5 10^8	1.07
0.8	3.9 10^8	1.07
1.0	3.4 10^8	1.07
1.5	2.8 10^8	1.07
2.0	2.5 10^8	1.07
3	2.1 10^8	1.07
4	1.9 10^8	1.08
5	1.8 10^8	1.09
6	1.7 10^8	1.09
8	1.6 10^8	1.10
10	1.6 10^8	1.11

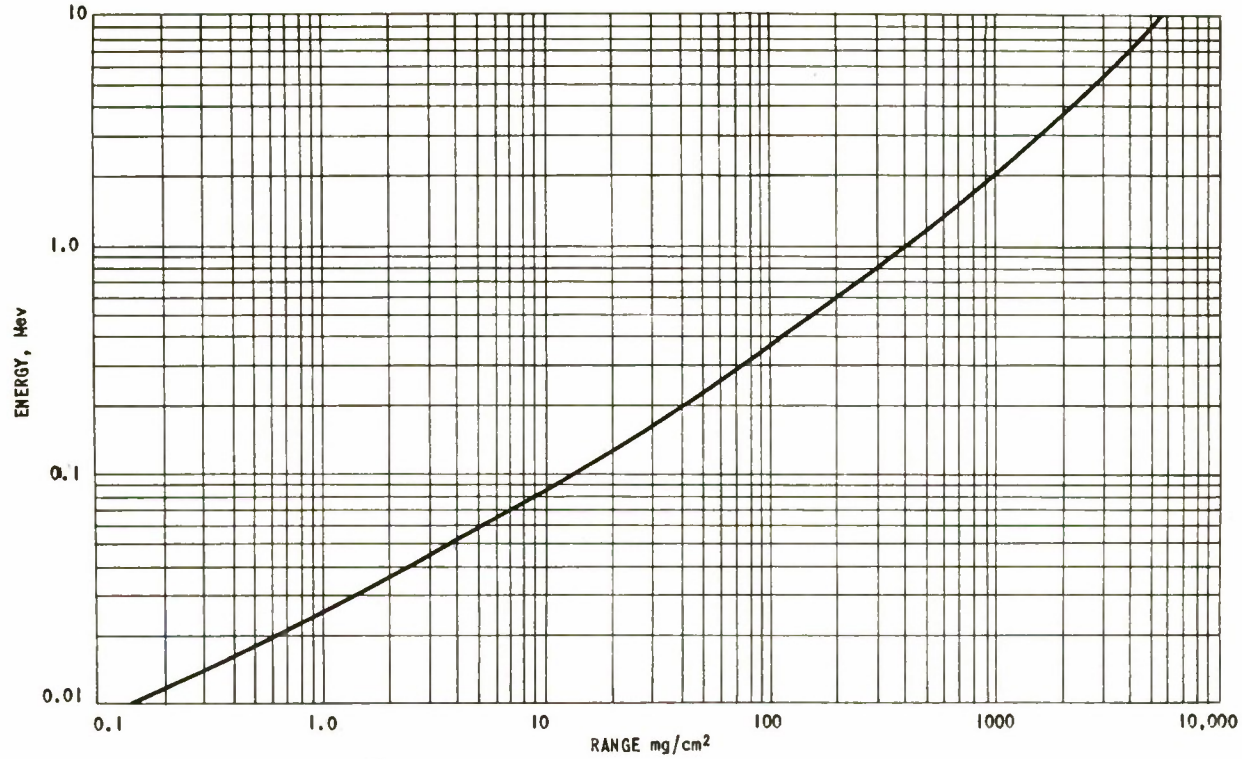


FIGURE 5.1. *Beta particle range-energy curve.*

$$D=\int_{E=0}^{\infty}\frac{dI_e}{dE}(E)\frac{dE}{dx}(E)\Delta X2A\,dE\ (\text{rads}) \qquad (5.2)$$

where $\frac{dE}{dx}(E)$ is the energy loss of the fast electron per unit distance traveled in the wall material, which is a function of the electron energy but can be assumed constant in the thin layer ΔX because the change of the electron energy caused by this layer is small. The energy dependence for $\frac{dE}{dx}$ for electrons is shown in Figure 5.2, plotted according to Reference 36. The factor 2 in the expression 5.2 indicates that every electron traversing the vacuum crosses ΔX twice.

If $Y_i(E)$ is the isotropic yield for production of low-energy secondary electrons by fast primary electrons with energy E, then the total charge released from the wall in the form of secondaries by primary electrons with spectral distribution $\frac{dI_e}{dE}(E)$ will be

$$Q=\int_{E=0}^{\infty}\frac{dI_e}{dE}(E)Y_i(E)2eA\,dE \qquad (5.3)$$

According to statements in Chapter 6, the yield $Y_i(E)=2Y(E)$ is, according to calculations and measurements, proportional to the energy delivered by the primaries to a thin surface layer of the target from which the secondary electrons can escape, or

$$Y_i(E)=K\frac{dE}{dx}(E)\Delta S \qquad (5.4)$$

where K is a proportionality factor and S is the thickness of the escape layer. This expression should apply only to primaries with a range greater than the thickness of the escape layer. Substituting the last expression in the previous one, we obtain

$$Q=\int_{E=0}^{\infty}\frac{dIe}{dE}(E)K\frac{dE}{dx}(E)\Delta S2eA\,dE. \qquad (5.5)$$

Setting $\Delta S=\Delta X$, and considering Equation 5.2 we obtain

$$Q=eKD$$

where K is a proportionality factor which does not depend on gamma energy. The charge collected

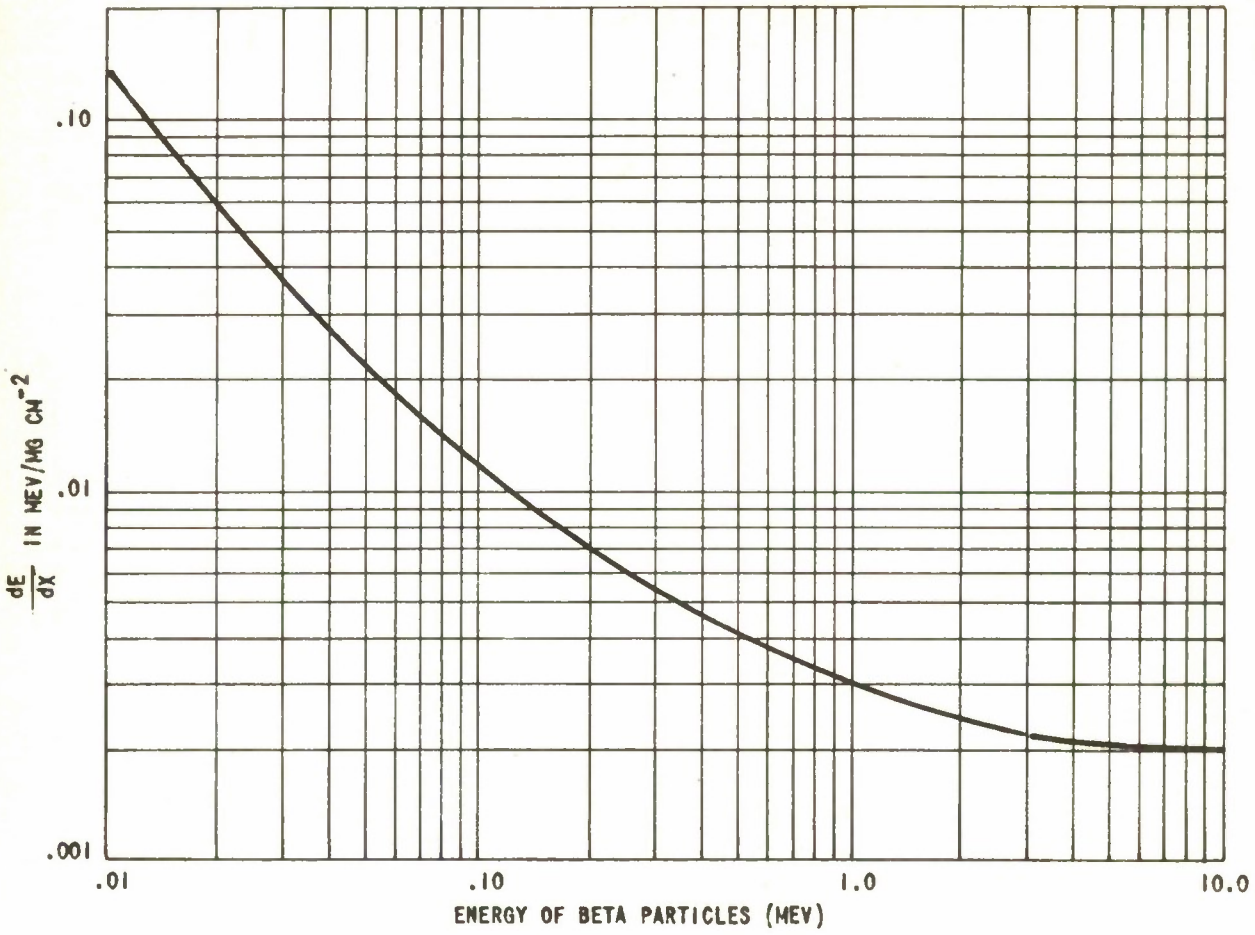


FIGURE 5.2. *Energy loss per unit distance traveled as a function of energy for electrons.*

in a SEMIRAD exposed to a certain gamma-ray dose measured in rads is thus proportional to this dose regardless of the energy of the incident gamma rays, provided that we observe the restrictions under which this expression was derived. In addition to these restrictions, this statement applies only to a closed-cavity geometry.

SEMIRAD Energy Dependence for Fast Neutrons. Analogous considerations apply in the case of a hydrogenous wall neutron SEMIRAD. If $\frac{dI_n}{dE}(E)$ is the incident neutron spectrum, and

$$\frac{dI_p}{dE} = F\left[\frac{dI_n}{dE}(E)\right]. \tag{5.6}$$

is the resulting spectrum of recoil protons in the evacuated cavity (see Equation 4.9) then the dose delivered to the escape layer is

$$D = \int_{E=0}^{\infty} \frac{dI_p}{dE}(E)\,\frac{dE}{dx}(E)\Delta S 2\,dE \tag{5.7}$$

For the electric charge collected due to this dose, we obtain

$$Q = \int_{E=0}^{\infty} \frac{dI_p}{dE}(E) Y_i^{\text{prot.}}(E) 2e\,dE. \tag{5.8}$$

In this case, the following also applies:

$$Y_i^{\text{prot.}}(E) = L\,\frac{dE}{dx}(E)\Delta S \tag{5.9}$$

where $\frac{dE}{dx} = -KE^{\gamma}$ (see Equation 4.10); (5.10)

therefore $Q = eLD$

where the constant L does not depend on neutron energy. Here, as in the case of gamma radia-

tion, similar restrictions apply. The thickness of the hydrogenous wall must be smaller than the mean-free path of the lowest energy neutron in the spectrum and larger than the range of the highest energy proton that the neutron spectrum can produce. The instrument should have a cavity-type geometry and the metallic emission layer on the surface of the cavity should be very thin. The energy dependence of $\frac{de}{dx}(E)$ for protons is shown in Figures 5.3 through 5.6 for some typical materials. Figure 4.2b shows the proton range as a function of proton energy in plastic. For neutron SEMIRAD with no hydrogenous wall, but where a wall coating of boron or fissionable material is responsible for the neutron sensitivity, different considerations apply. The total charge of the secondary electrons emitted by fission fragments will be

$$Q \propto \int_{E=0}^{\infty} \frac{dI_n}{dE}(E)\sigma_{\text{fiss}}(E)H(E)dE \tag{5.11}$$

where σ_{fiss} is the fission cross section, and $H(E)$ is the average number of secondary electrons emitted when one fission event takes place in the SEMIRAD wall coating. $H(E)$ depends on the kind and energy distribution of the fission fragments and will vary slowly with the energy of the incident neutrons (up to several Mev, one can assume $H(E)$ to be a constant).

One may define the absorbed dose as loss of the primary neutrons (in terms of energy) in the fissionable material without involving the interaction energy. This way of defining the absorbed neutron dose is very unusual, however, and we find difficulty in obtaining a correlation between a uranium rad and, for example, a tissue rad. The fast neutrons produced in the fission process can be completely neglected because their number is small compared to the number of the incident neutrons. With this definition, we can obtain the dose delivered by the incident neutrons as

$$D \propto \int_{E=0}^{\infty} \frac{dI_n}{dE}(E)\sigma_{\text{fiss}}(E)dE, \tag{5.12}$$

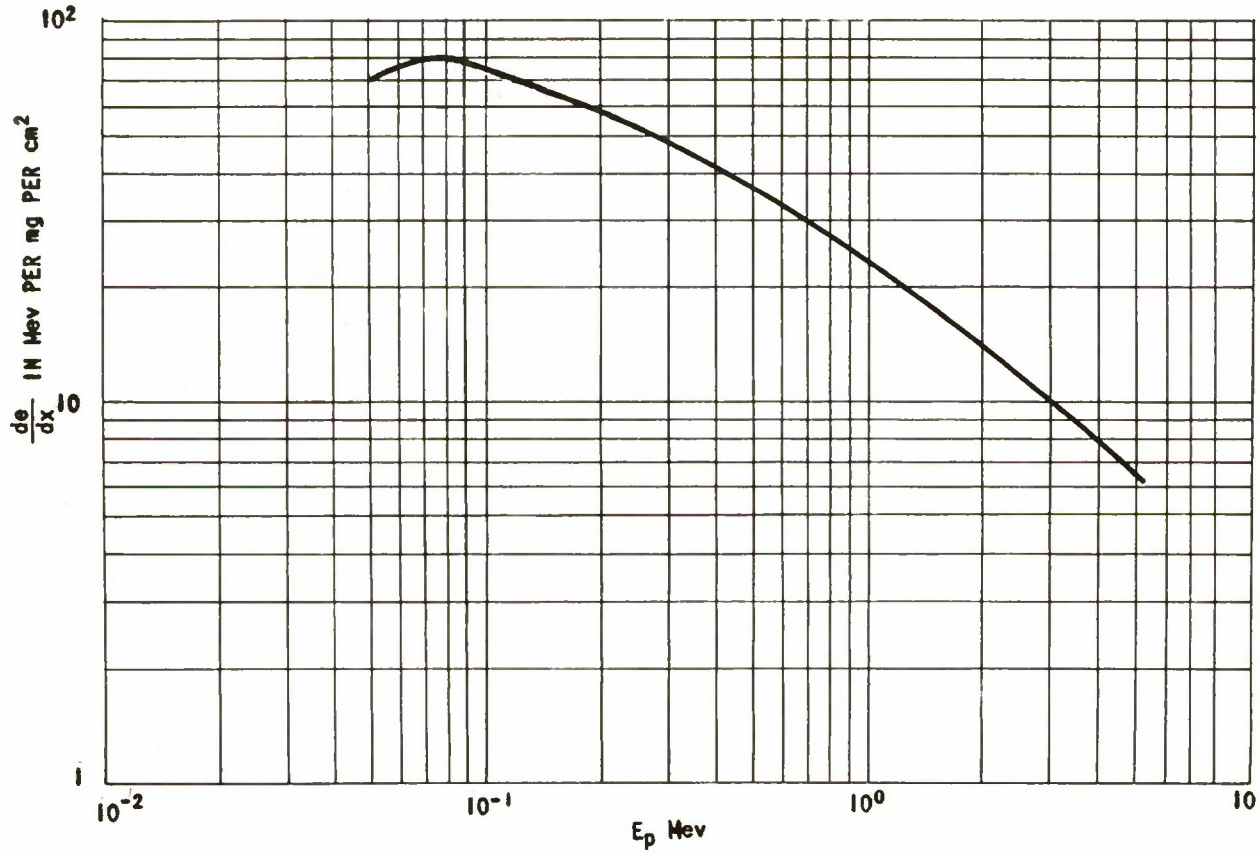


FIGURE 5.3. *Energy dependence of* dE/dx *for protons incident on beryllium.*

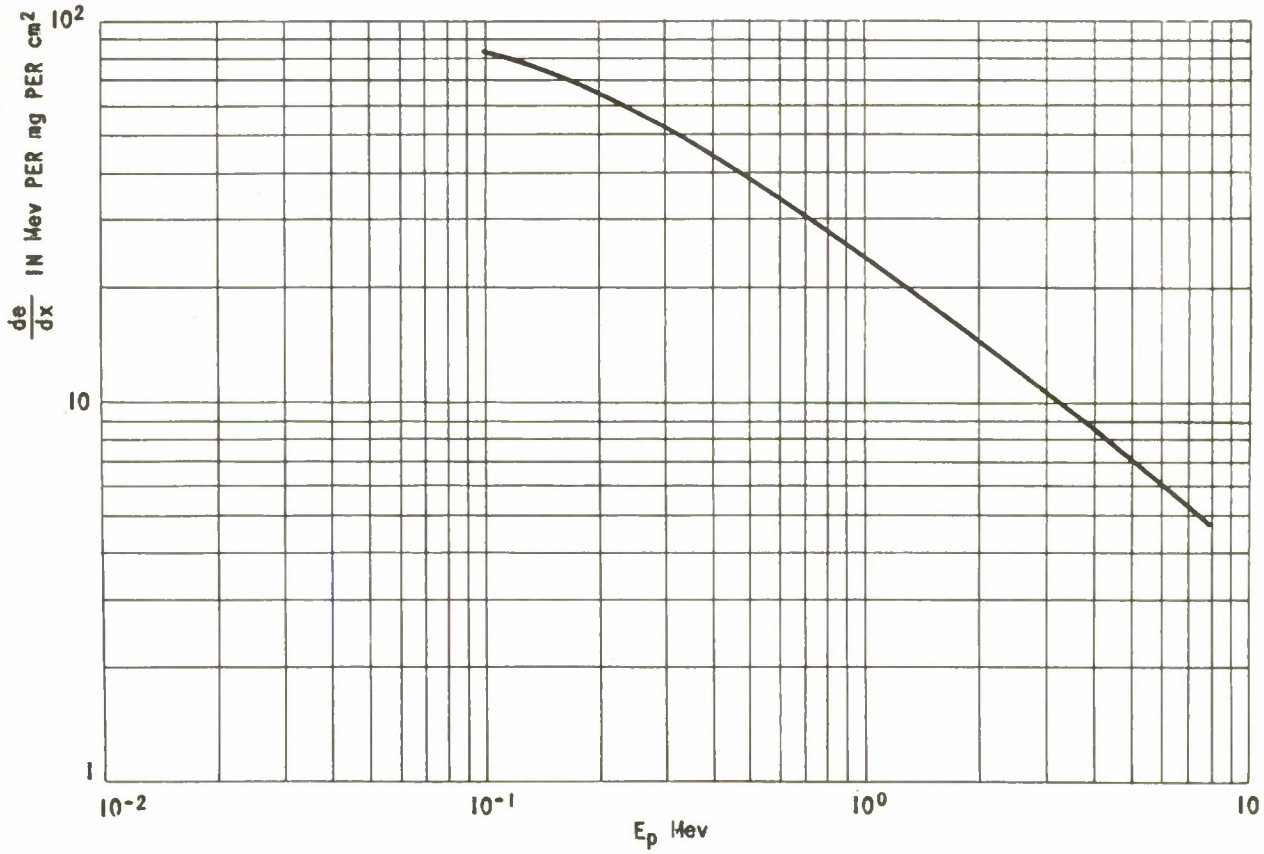


FIGURE 5.4. *Energy dependence of* dE/dx *for protons incident on carbon.*

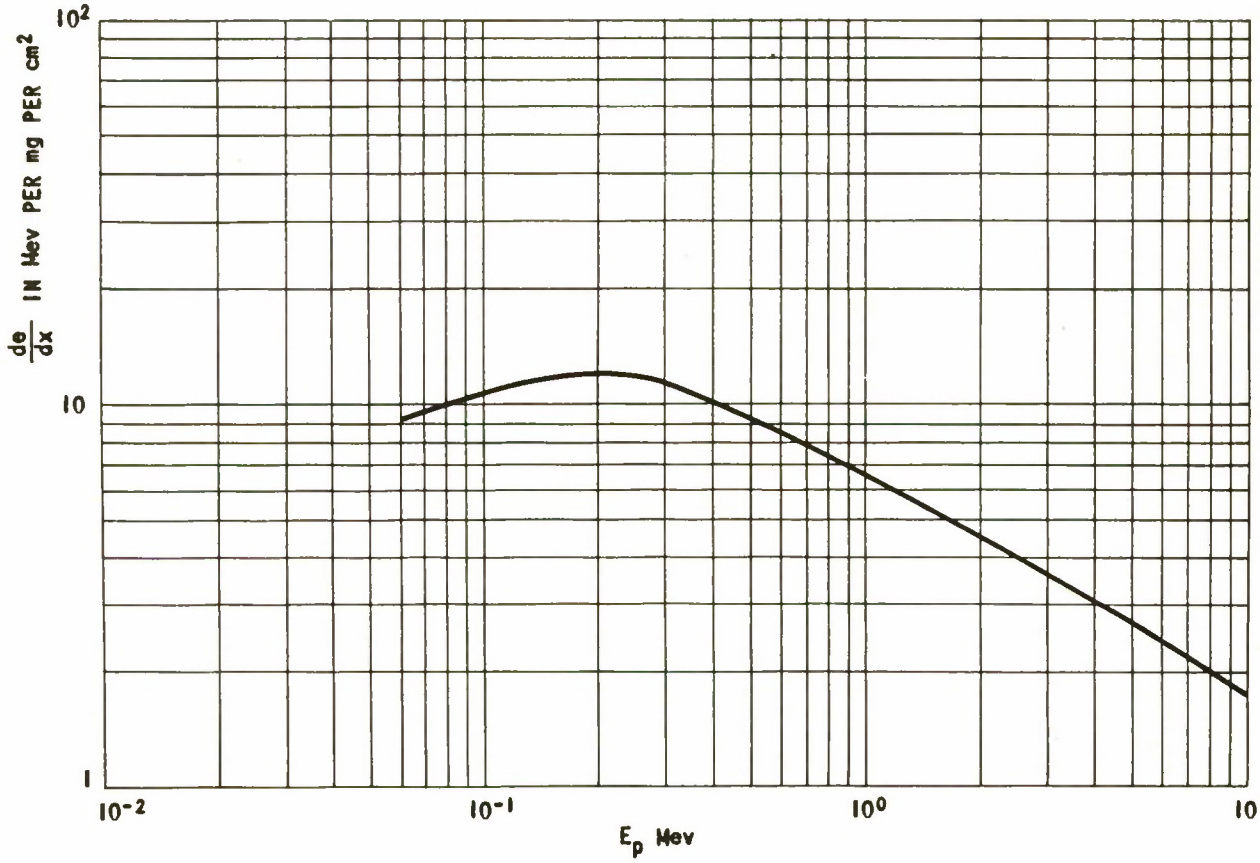


FIGURE 5.5. *Energy dependence of* dE/dx *for protons incident on gold.*

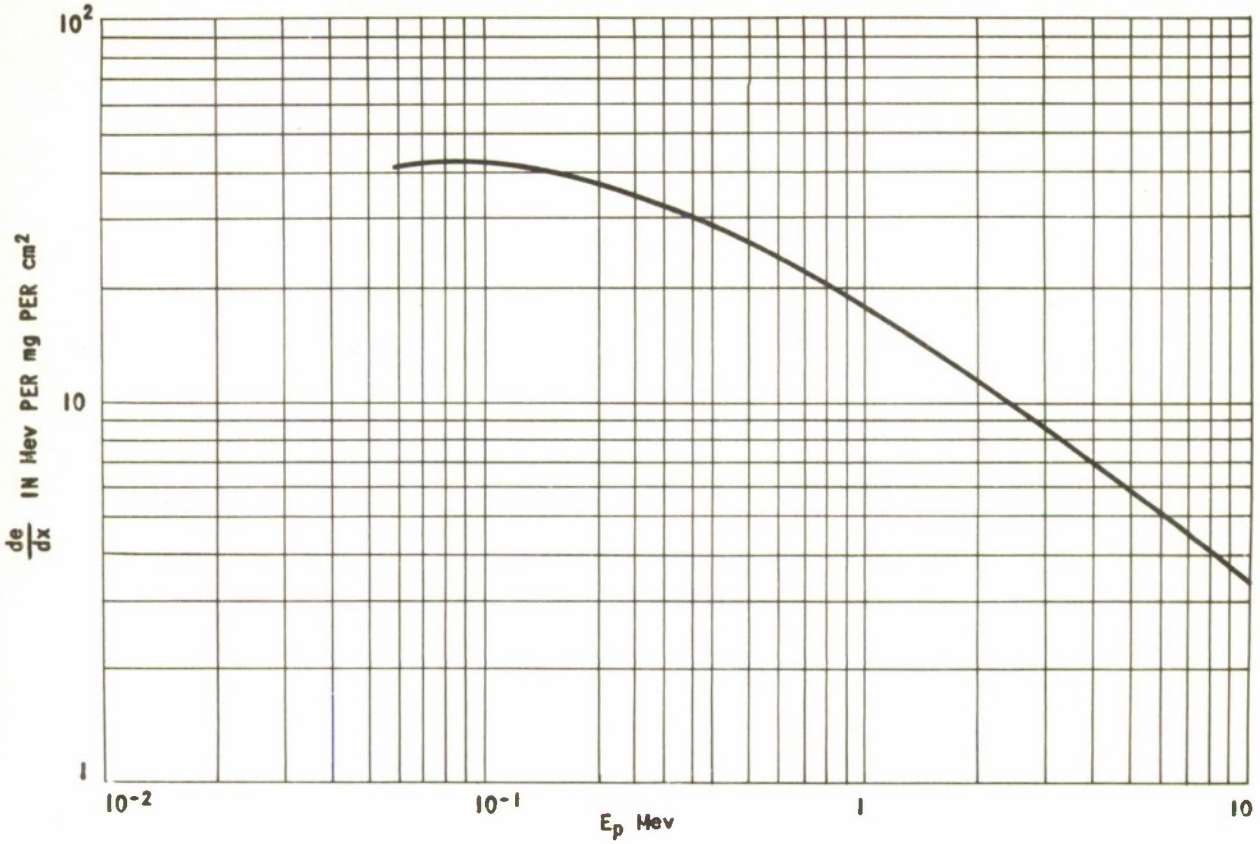


FIGURE 5.6. *Energy dependence of* dE/dx *for protons incident on aluminum.*

and see again that the absorbed dose is proportional to the collected charge

$$D \propto Q \tag{5.13}$$

This last result, however, must be considered useless for practical application, and only an experimental comparison with a tissue-equivalent dosimeter can provide real data on the energy dependence of the fission SEMIRAD. We see from the above that the fission or boron SEMIRAD cannot be applied to the measurement of radiation in units of delivered dose, but it is a very useful instrument for the measurement of neutron fluxes. If the cross section in Equation 5.11 does not vary too strongly with energy, or if an average value can be assumed, then for neutron energies such that $E_n \ll$ Energy released in the reaction, we find that

$$Q \propto \int_{E=0}^{\infty} \frac{dN_n}{dE_n}\, dE_n = N_n \tag{5.14}$$

where N_n is the total number of neutrons (slow or fast depending on the wall coating) that passed through the SEMIRAD area.

CHAPTER 6

EMISSION OF SECONDARY ELECTRONS BY HIGH-ENERGY PARTICLES

General. When electrons, protons, or heavy particles collide with a solid surface in a vacuum, secondary electrons are produced from this surface. In this chapter, we outline the physics of this effect on which the operation of SEMIRAD is based. Secondary-electron emission can be expressed in terms of the yield function which is defined as the number of secondaries emitted per incident particle. In the case of emission of electrons by electrons or electrons by protons, all particles involved carry a single electron charge, and therefore

$$Y=\frac{|I_s|}{|I_p|} \tag{6.1}$$

where I_s is the secondary-electron current, and I_p is the primary-particle current. The yield depends on many parameters which are discussed below.

Dependence of the Yield on the Angle of Incidence. The incoming particle excites the target electrons; those that acquire sufficient energy and are produced close enough to the surface can diffuse to the outside and become free. We may define the depth underneath the surface from which the emission can take place as the escape layer ΔS (Figure 6.1). According to these considerations, the yield is proportional to the distance traveled by the incident particle in ΔS, or

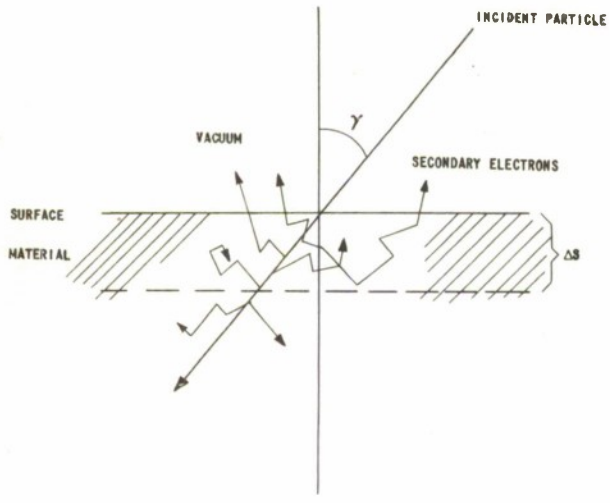


FIGURE 6.1. *The emission layer for secondary electrons.*

$$Y(\varphi)=K\frac{1}{\cos\varphi} \tag{6.2}$$

This behavior can be verified experimentally; a typical measurement is shown in Figure 6.2 for deuteron incident on aluminium, and in Figure 6.3 for fast electrons (Reference 8). Electrons travel in absorbers along a zig-zag path, but in practice ΔS is always small compared to the mean free path of the high-energy electrons and Equation 6.2 applies in this case also. From Equation 6.2, we can derive the yield for particles that strike the surface from random directions. Such a yield applies to SEMIRAD in most cases and we call it the isotropic yield Y_i.

When a plane surface with area A is bombarded isotropically on one side by incident particles, the number of particles impinging on A is

$$I_p=\int_0^{\frac{\Pi}{2}} AN2\Pi\sin\varphi\cos\varphi d\varphi=\frac{1}{2}AN2\Pi \tag{6.5}$$

where N is the particle flux, and φ is the angle between the normal to A and the direction of the particle. The number of secondaries emitted by these particles, considering Equation 6.2, is

$$I_s=\int_0^{\frac{\Pi}{2}} AN2\Pi\sin\varphi\cos\varphi\frac{Y}{\cos\varphi}d\varphi=YAN2\Pi \tag{6.4}$$

For the isotropic yield Y_i defined as I_s/I_p, one obtains

$$Y_i=2Y \tag{6.5}$$

where Y is the yield for perpendicular incidence.

We measured this relation experimentally by inserting a small, polished spherical target in a parallel beam of 2- and 1-Mev protons and the results agreed with the calculation within experimental errors. For rough surfaces, Y is always higher than for polished surfaces. A rough surface results in the impingement of incident particles at random angles even when these particles are directed perpendicular to the surface. The actual surface area can be increased by roughing, and we can use this effect to increase the SEMIRAD sensitivity.

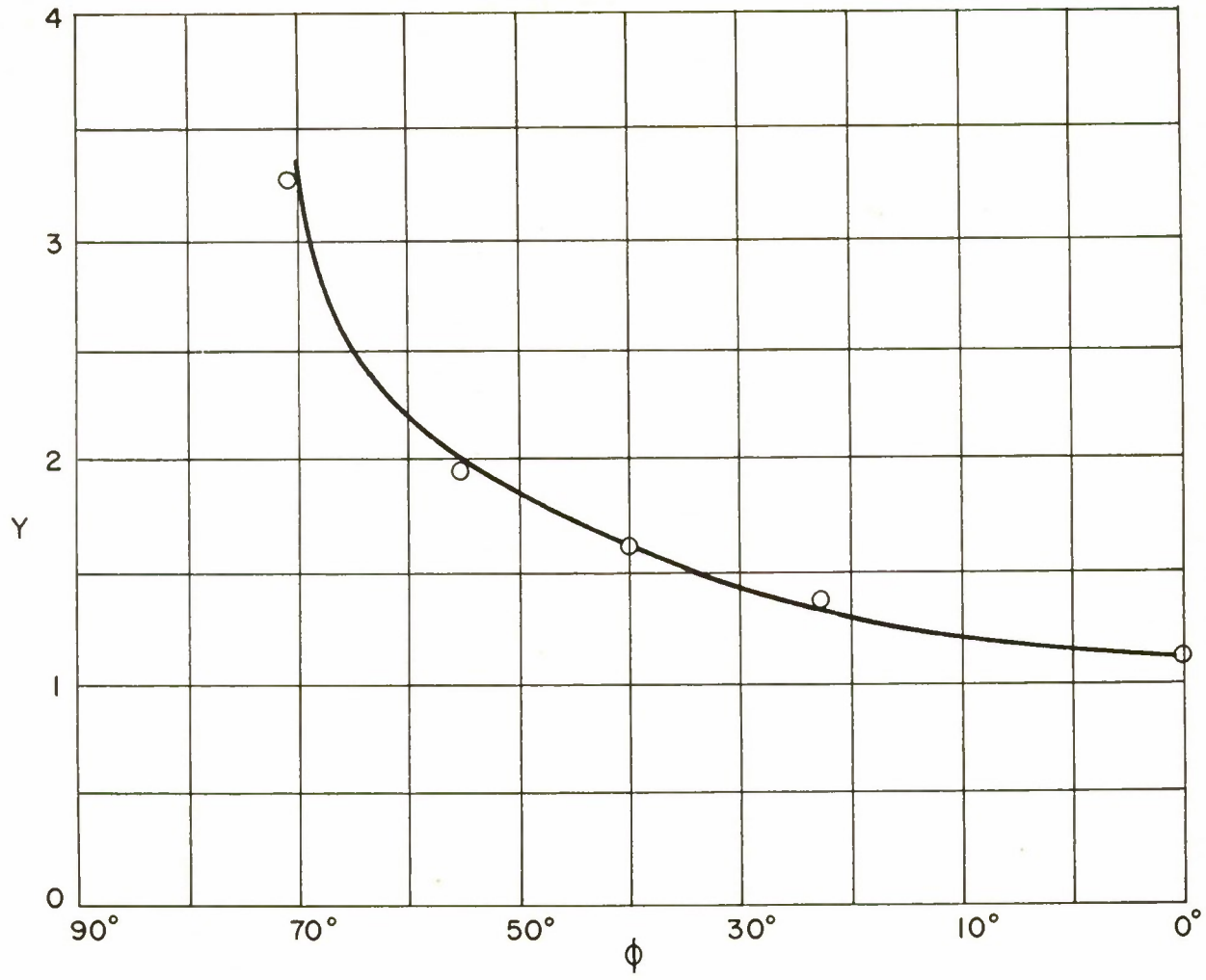


FIGURE 6.2. *Angular dependence of the secondary electron yield produced by 2 Mev deuterons on aluminum. Solid curve:* $\frac{Y(\varphi=0)}{\cos\varphi}$

Experiments were performed with thin foils to determine the yield difference for forward and backward incident particles. Protons with 1- to 2-Mev energies were directed through a thin foil against a block of metal. The collecting electrode was in the vacuum between the foil and the target (Figure 6.4). The secondary-electron current in the forward direction from the foil and the current in the backward direction from the block were compared. The difference between these two currents was found to be negligible (Reference 9). Mironov and Nemenov (Reference 10), however, noticed a difference between the forward and the backward yield for protons. For aluminum they obtained about 1.2 as the ratio between the forward and backward yield. This ratio does not seem to vary with the energy of the incoming particles (Figures 6.5 and 6–6).

Yield versus Surface Conditions. Clean surfaces generally have a lower yield than unoutgassed or contaminated surfaces. Unclean surfaces provide a yield that is not reproducible and changes with time and handling of the target. This fact applies especially when the incident particles are electrons or protons below 100 kev. To make the surface of a target clean, we found that it should be heated to 400° C for 15 minutes. In the literature on this subject, some authors mention that they have obtained clean surfaces by bombarding targets for extended periods of time with a high-energy particle beam. Our experiments did not substantiate this thesis. We found that targets cleaned by heating gave a constant and reproducible yield, whereas after prolonged bombardment the yield became unsteady.

Secondary Electron Yield as Function of Inci-

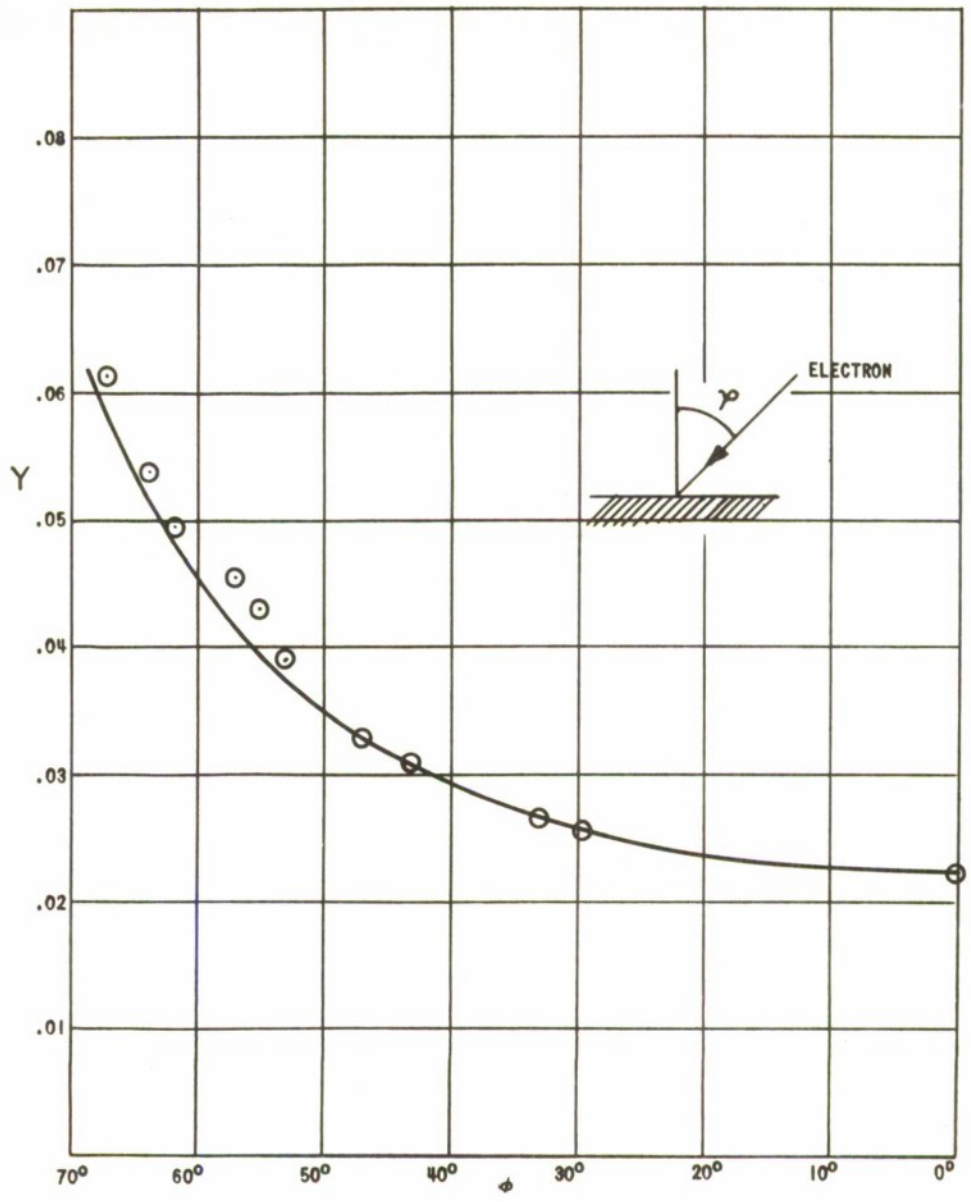


FIGURE 6.3. *Dependence of the secondary-electron yield on the angle of incidence (energy of primary electrons: 1.3 Mev). Solid curve:* $\frac{Y(\varphi=0)}{\cos\varphi}$.

dent Particle Energy. Many authors report the yield measurements as a function of energy of the incident particle for electrons, protons, and heavy ions. Most of the work was done in the low-energy range (up to 10 kev), and only few data are available for the energy range of interest for radiation dosimetry with SEMIRAD (between several kev and several Mev). The measurements show that, for most materials, there is a sharp, almost linear increase of the yield with energy (starting with zero energy). At energies ranging between several hundred ev and several kev for electrons, and several tens of kev for protons, a plot of the yield versus energy reaches a flat maximum then decreases rapidly at first, and more slowly toward the high-energy end.

We offer the following qualitative explanation of such behavior. We define a layer beneath the target surface from which some of the electrons excited by the incoming particle can escape, and below which none can escape. The number of electrons emitted per incident particle, i.e., (the

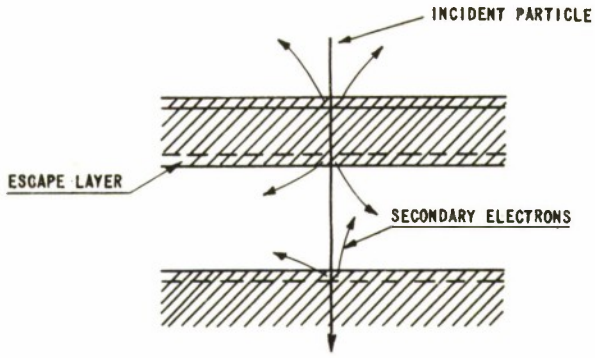


FIGURE 6.4. *Measurement of the ratio between the forward and backward yield for the emission of secondary electrons.*

yield) is dependent on the amount of energy deposited by the incident particles in ΔS. For particles with an energy such that their range R in the target material is shorter than ΔS, the yield should increase with energy. For $R \sim \Delta S$ a flat maximum should be reached, and for $R \gg \Delta S$ the yield should depend on energy in the same way as the energy dissipated by the particle per distance traveled. This corresponds qualitatively with the observed data for incident heavy ions and electrons.

Experimental measurements of $Y(E)$ taken from the literature are illustrated in Figures 6.5 to 6.7 and Table 6.1 for different materials irradiated with electrons, protons, and heavy ions. The curves in Figures 5.2 through 5.6 show the energy loss per unit distance traveled for the incident particles. Normalizing the $dE/dx(E)$ curve to any point of the corresponding secondary-electron yield curve, we find that from the purely experimental point of view the relationship

$$\frac{dE}{dx}(E) \propto Y(E) \tag{6.6}$$

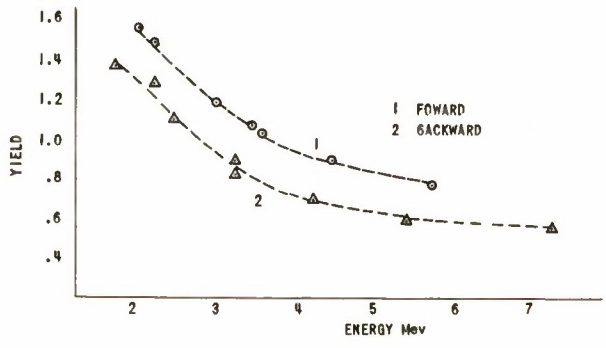


FIGURE 6.5. *Energy dependence of the secondary-electron yield for protons incident on nickel.*

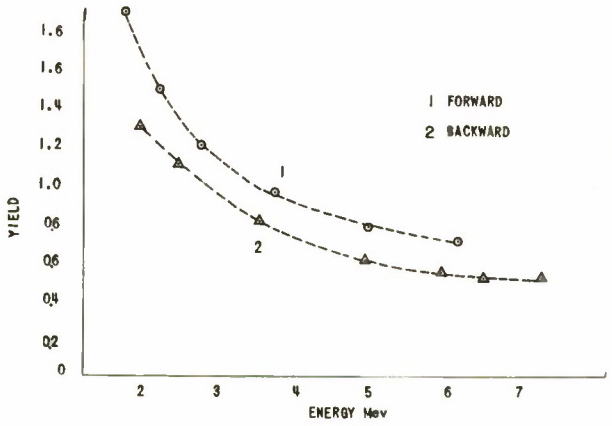


FIGURE 6.6. *Energy dependence of the secondary electron yield for protons incident on aluminum.*

applies very closely in most cases above a certain low value of E (Figures 6.8A and 6.8B).

For experimental work with SEMIRAD, the discrepancy at low energies is of little consequence because in the case of gammas or neutrons in the Mev range there are only a few recoil protons or electrons below the energies where Equation 6.6 starts to apply (see Figure 4.3). The theoretical explanation for Equation 6.6 was given by Sternglass (Reference 11), who analyzes the secondary-electron emission by high-energy ions from the point of view of the Bohr-Bethe theory of ionization. The secondary electrons and delta rays formed in the bulk of the target lose their energy through different collision processes, and a small part of the inter-

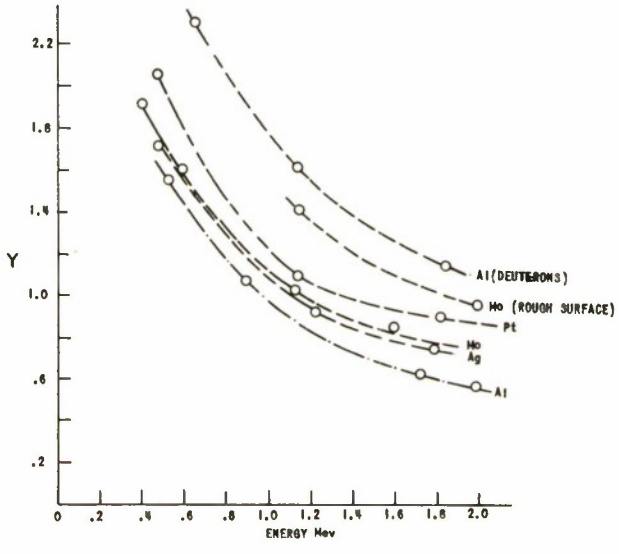


FIGURE 6.7. *Energy dependence of the secondary yield for different materials.*

TABLE 6.1. *Emission of secondary electrons under positive ion bombardment (reference 17).*

Bombarding energy (kev)	Yield for the emission of secondary electrons								
	Molybdenum target		Copper target		Aluminum target		Lead target		
	H_2+	$H+$	H_2+	$H+$	H_2+	$H+$	H_2+	H_c+	$H+$
78	6.31	4.10	6.68	3.88	6.08	4.19	8.29	12.8	4.23
107	6.59	3.77	6.64	3.61	6.30	3.82	7.74	13.3	3.87
142	6.40	3.27	6.45	3.41	6.23	3.51	7.58	13.9	3.56
213	6.19	2.76	6.26	2.90	6.43	3.01	7.46	14.1	3.12
284	5.56	2.35	6.30	2.52	6.29	2.68	7.34	14.3	2.89
355	5.45	2.18	5.71	2.44	5.98	2.19	6.99	14.3	.....
456	.....	2.01	5.60	2.21	5.46	2.17	6.61	14.1	2.50

A Van de Graaff generator was used in this experiment. Most secondaries had energies less than 30 ev.

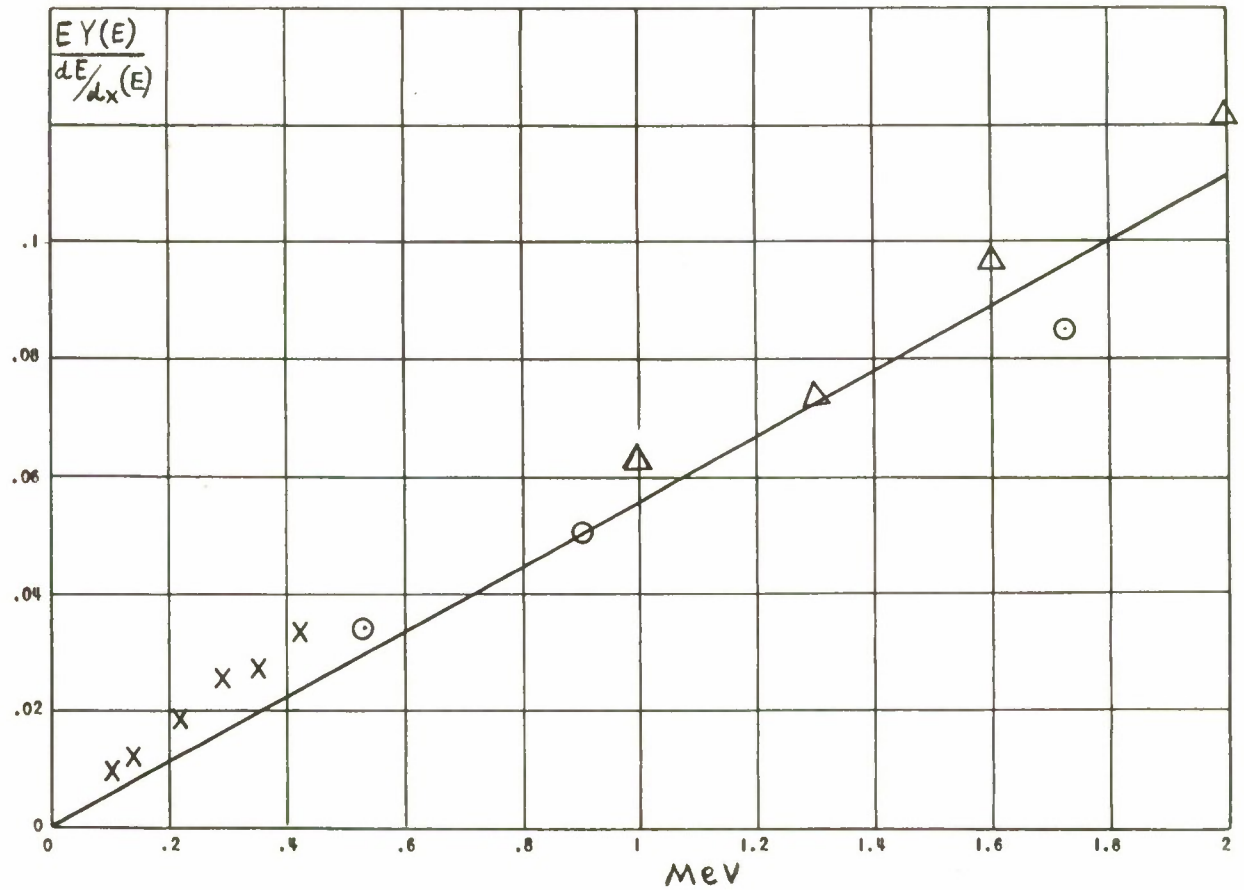


FIGURE 6.8A. *Secondary-electron emission by protons from aluminum. Proton energy times secondary-electron yield divided by the energy loss of the proton per unit distance traveled, versus proton energy. Yield is expressed in number of secondary electrons per incident proton; energy in Mev; and distance in mg/cm² of aluminum. Yield data are: X from Reference 17; Δ from Reference 18; and ⊙ from Reference 19.*

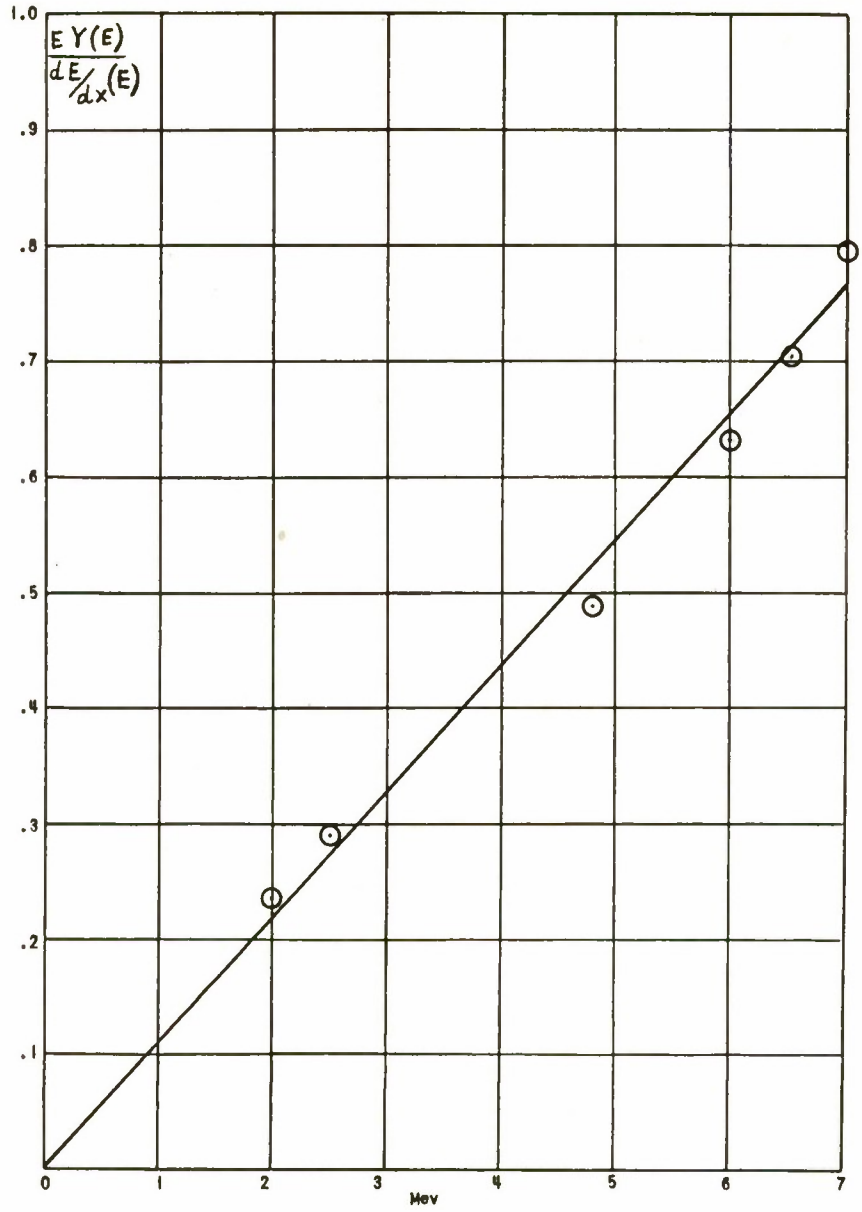


FIGURE 6.8B. *Same as for 6.8A, but for higher incident proton energies computed from the yield data from Reference 10.*

nally formed exeited eleetrons escape through the surface and become free. Sternglass obtains the following expression for the secondary-electron yield:

$$Y(E)=\frac{1}{2}\frac{1}{E_0}\frac{dE}{dx}(E)TAL_s[1+F(V)] \qquad (6.7)$$

where E_0 is the mean energy lost per secondary formed in the interior of the target.

T is the probability that an electron arriving at the surface from the interior will be able to escape.

A is a constant (about 0.6), and

L_s is a distance whose order of magnitude is equal to the mean free path of the internally formed secondary electrons.

The function $F(V)$ is given by $F(V)=\left(1+\frac{L\delta}{L_s}\right)^{-1}$ where $L\delta$ is the effeetive penetration distance of the delta rays formed in the target. The comparison of this expression with experimental data is shown in Figure 6.9. From the derivation of the yield formulas, Sternglass concludes that the yield function is not dependent on the work function of the

target and does not vary strongly for different target materials which agree very well with experimental results.

For secondary-electron emission by high-energy incident electrons, considerations apply similar to those in the case of protons if the mean free path of the incident electrons is much greater than the escape layer. The unexcited electrons in the escape layer cannot distinguish the mass of the incoming particle; all that matters is the velocity and charge of the incident particle as long as it travels on a straight line through the escape layer and does not reenter the escape layer later by scattering. The fact that the electrons carry a negative charge while the protons are positive has no bearing on the secondary emission. In a practical case, however, the incident electrons do backscatter in the target and while entering or leaving the target, they produce low-energy secondary electrons within a wide energy range.

In addition to this effect, the probability that the primary electrons lose a large amount of their energy in a single collision with a target electron within the escape layer is not negligible. Miller and Porter (Reference 12) measured the total yield and the contribution to the yield from high-energy secondaries. Some of the data given by these authors is shown in figure 6.10. Figures 6.11 and 6.12 give curves from Reference 13. Miller and Porter found that for the low-energy component of the secondaries,

$$Y_{\text{slow}} \propto \frac{dE}{dx}(E) \tag{6.8}$$

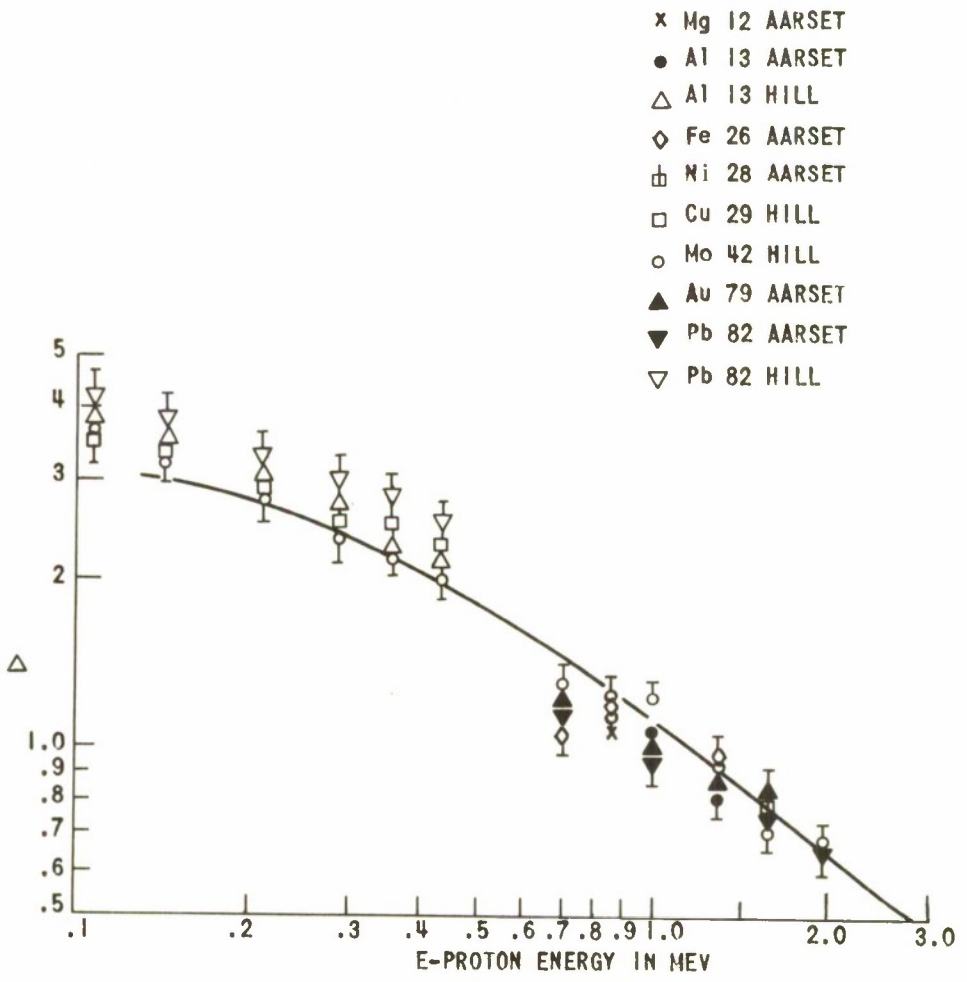


FIGURE 6.9. *Theoretical curve from Reference 11 according to the Expression 6.7 compared with experimental data.*

over a wide energy range while the contribution of the high energy component increases with the increasing energy of the primaries so that there is a considerable deviation from Equation 6.8 for the total yield. The above difficulty may seriously affect the energy dependence of the SEMIRAD for gamma radiation as discussed in Chapter 5, but we avoid this by setting the SEMIRAD collecting potential so that only the low-energy secondaries contribute to the current, and thus Equation 6.6 is closely fulfilled.

Energy Distribution of Secondary Electrons Emitted by Electrons. As mentioned in the previous paragraph, the energy spectrum of secondary electrons produced by electrons can be subdivided into two groups: low-energy (0 to about 50 ev), and the high-energy components (from 50 ev up to the energy of the incident electrons). The spectrum for the low-energy component was measured by Miller and Porter (Reference 12), and is shown in Figure 6.13 for gold with primary energies between 22 kev and 1.06 Mev. Trump and Van de Graaff (Ref-

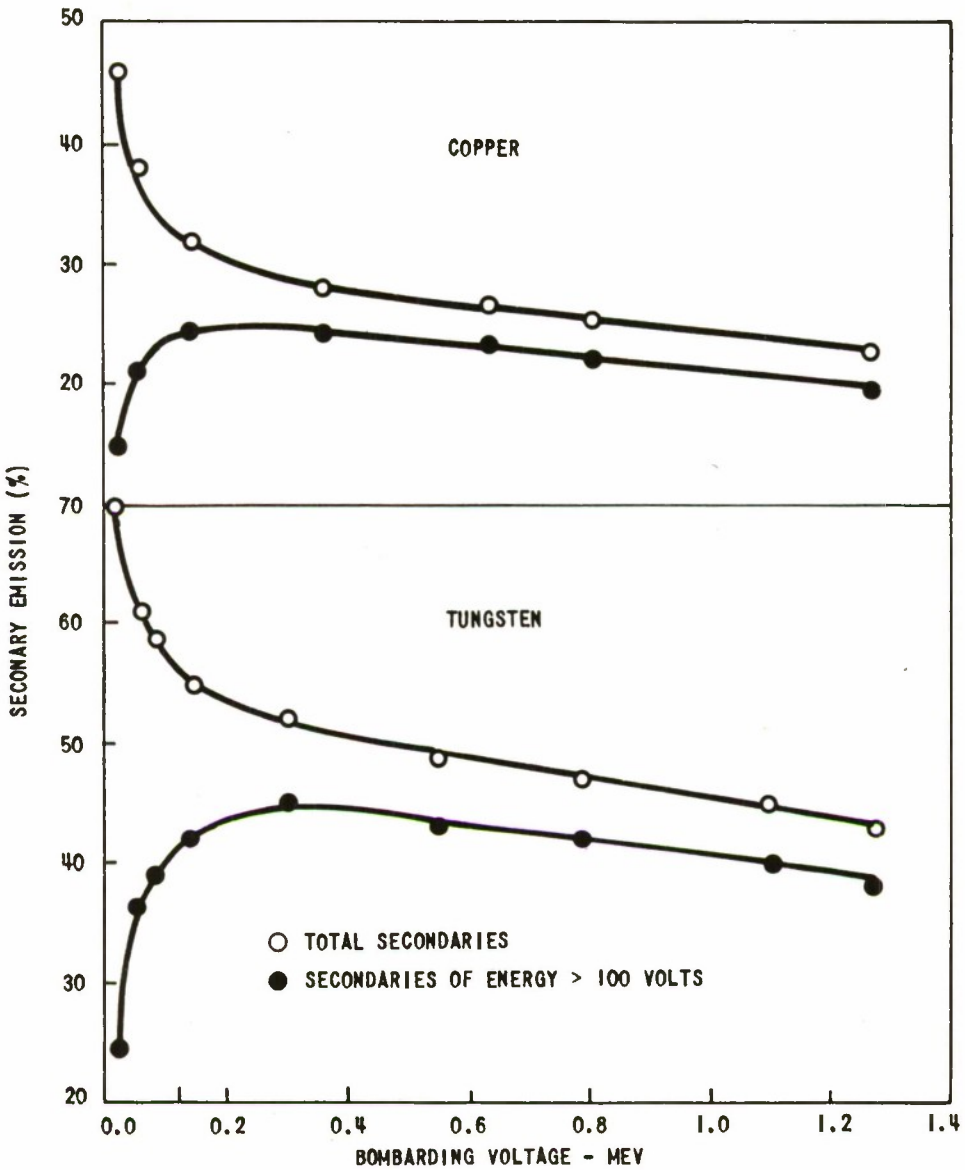


FIGURE 6.10. *Secondary electron emission yield in percent as a function of the energy of primary electrons incident on copper and tungsten.*

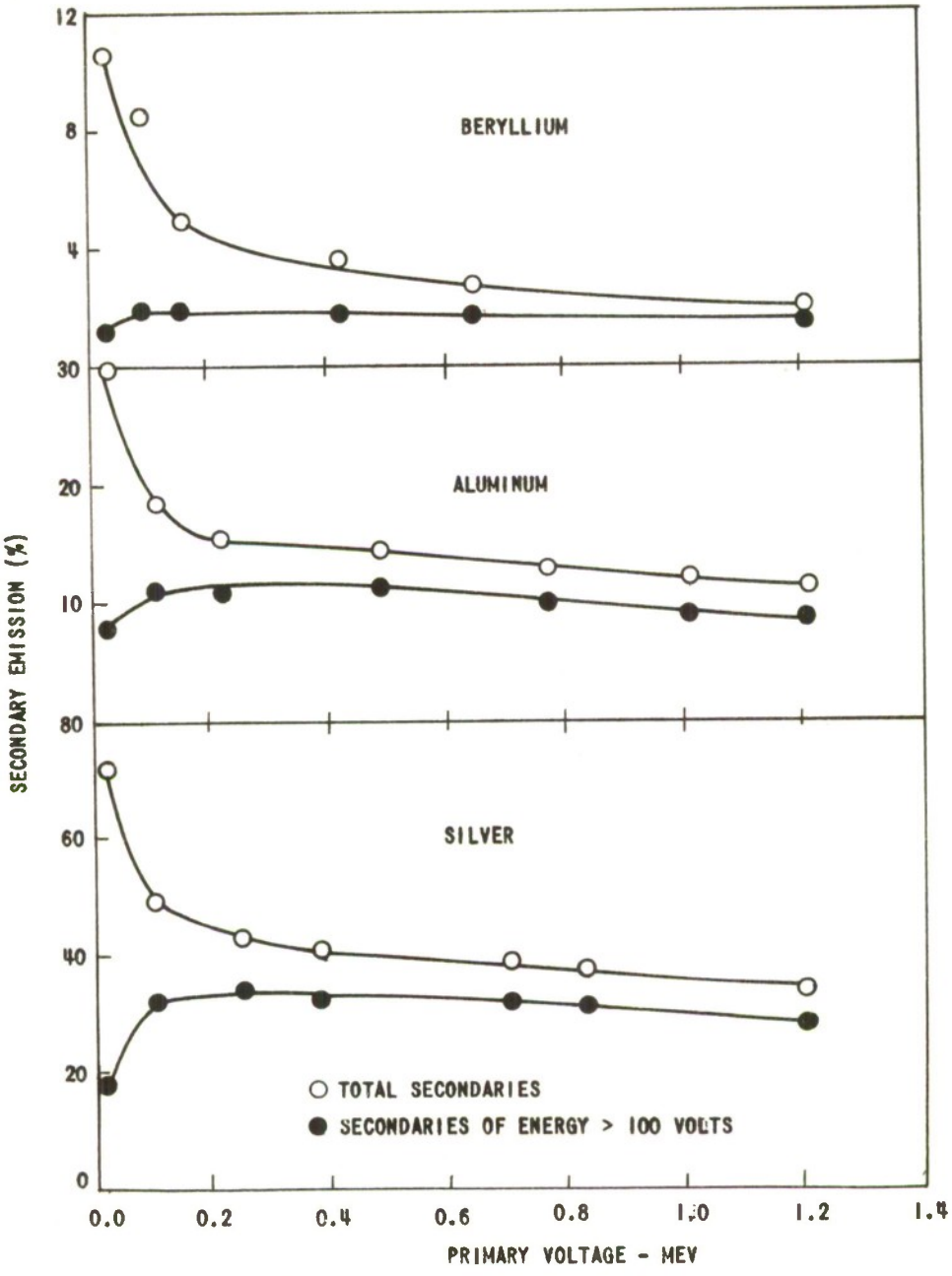


FIGURE 6.11. *Same as Figure 6.10 for beryllium, aluminum, and silver.*

erence 13) reported similar measurements for tungsten and steel (Figure 6.14) with primary energies between 36 and 256 kev.

These data indicate that the energy spectrum of the low-energy component does not depend on the energy of the primary particles. The average energy of the high-energy secondaries increases with the primary energy. Contrary to the low-energy secondaries, the yield of the high-energy secondaries increases strongly with the Z of the bombarded material, as shown in Figure 6.15 (see also Reference 12). The origin of the high-energy component seems to be, as the high-energy yield dependence on Z of the target indicates, elastic nuclear scattering rather than inelastic nuclear or electron-scattering (Reference 14).

Energy Distribution of Secondary Electrons Produced by Heavy Ions. One of the first theoretical

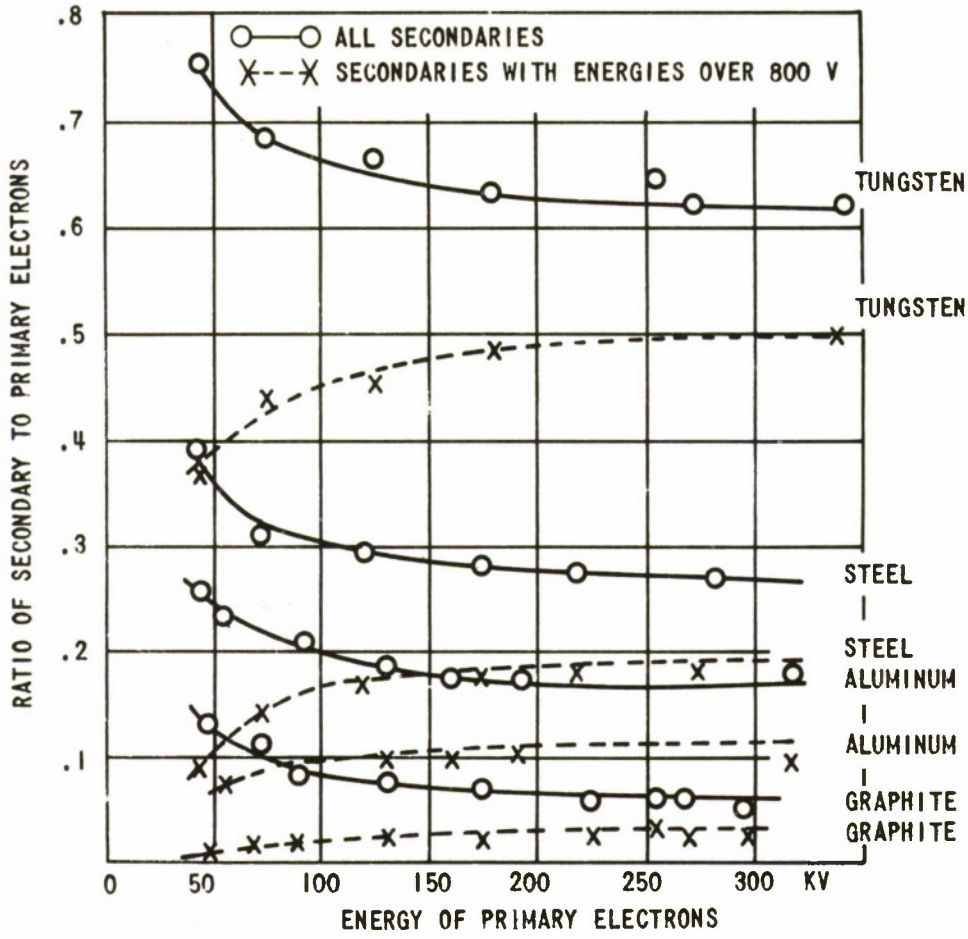


FIGURE 6.12. *Secondary emission of electrons by electrons with energies up to 340 kev.*

papers on secondary-electron emission by heavy ions was published by Kapitza (Reference 15), who developed a theory according to which the incoming particle excites a column of matter in the target along its path. The amount of excitation, which is proportional to the energy deposited by the ion per unit distance traveled, raises the temperature in this column and thus produces thermoionic emission from the target surface. The quantitative results of such a theory are difficult to justify, because a well-defined temperature and therefore thermal equilibrium are necessary to provide values for yields and energy distributions (which is not the case for a heavy-particle track in a solid).

Kapitza computed for the secondary-electron spectrum a Maxwellian distribution in energy extending from 0 to about 6 ev. Earlier experimental data agree with this estimate (References 16, 17, and 18) and, recently, new experiments were performed on this subject (Reference 19). Targets of Be, Al, Cu, and Au were bombarded with protons. The resulting secondary electrons were investigated with respect to their intensity, energy distribution, and energy distribution as a function of the angle of emission. The findings show that, contrary to previous investigations, electrons with energies higher than those corresponding to the local-heating effect contribute considerably to the total yield. About 75% of the secondaries are emitted at low energies, and the remaining part is emitted with high energies (up to 2000 ev for 1-Mev protons). The electron spectrum decreases rapidly toward the high-energy end. The high-energy component is not emitted isotropically, but preferentially backwards in the direction from which the protons arrive.

Figure 6.16 gives an example of a secondary-electron spectrum (integrated) produced by 1-Mev

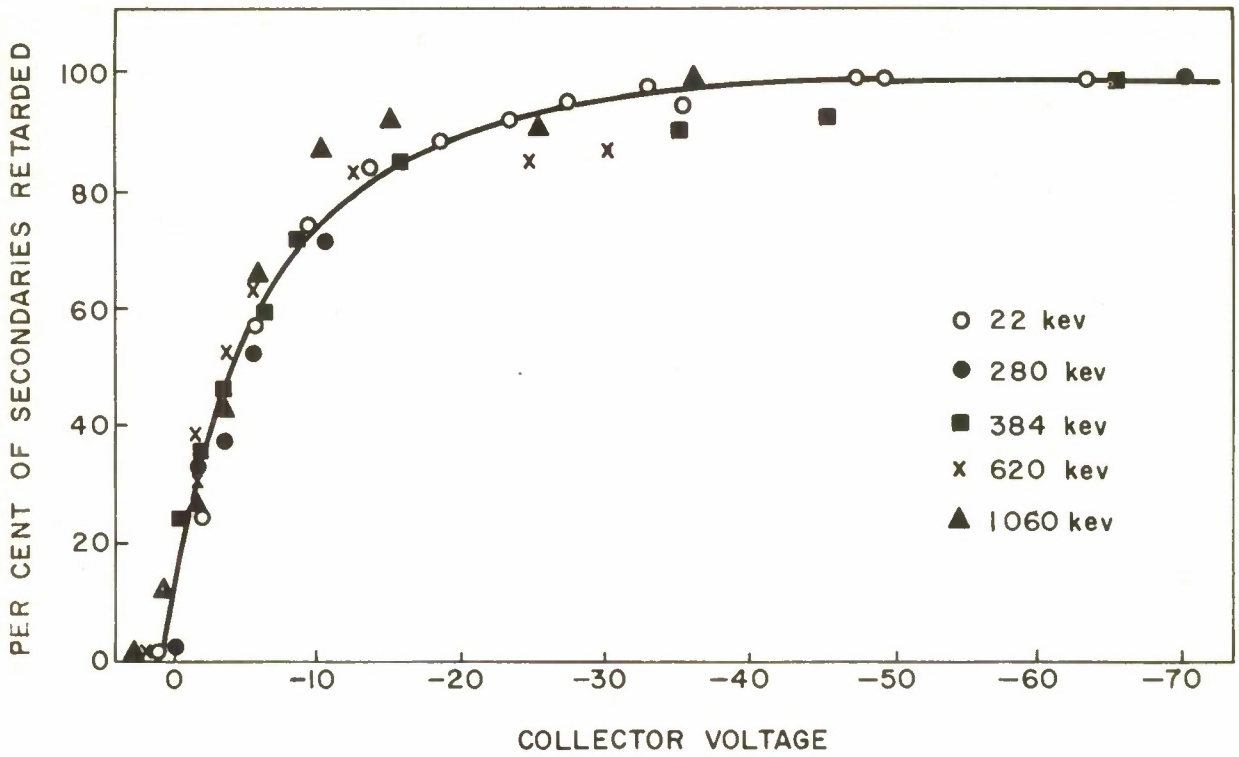


FIGURE 6.13. *Energy spectrum of slow secondaries emitted by electrons for gold.*

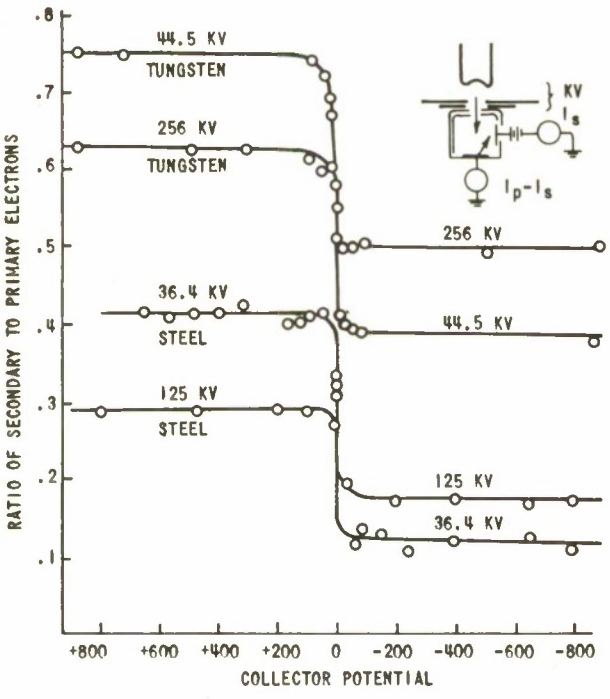


FIGURE 6.14. *Variation of secondary emission with collector potential (primary particles: electrons).*

224-250 O-66—4

protons. Figure 6.17 shows the differential yield spectrum of the high-energy component from 100 ev up for different angles of emission. The differential yield is defined as the number of secondary electrons per incident proton with energies higher than E emitted under an angle φ with respect to the incident protons, for the solid angle $4\pi/2$. The relation between the differential yield and total yield is

$$Y(E)=\int_0^{\frac{\pi}{2}} Y(E,\varphi)\sin\varphi d\varphi \tag{6.9}$$

In Figure 6.17 one can see that the maximum energy of the secondary electrons is about 2000 ev for 0.96 Mev incident protons. This corresponds closely with the maximum energy a proton can deliver to an electron through coulomb scattering. In the laboratory coordinate system this energy is given by

$$E_{\max}=4\frac{m_e}{m_p}E_p, \tag{6.10}$$

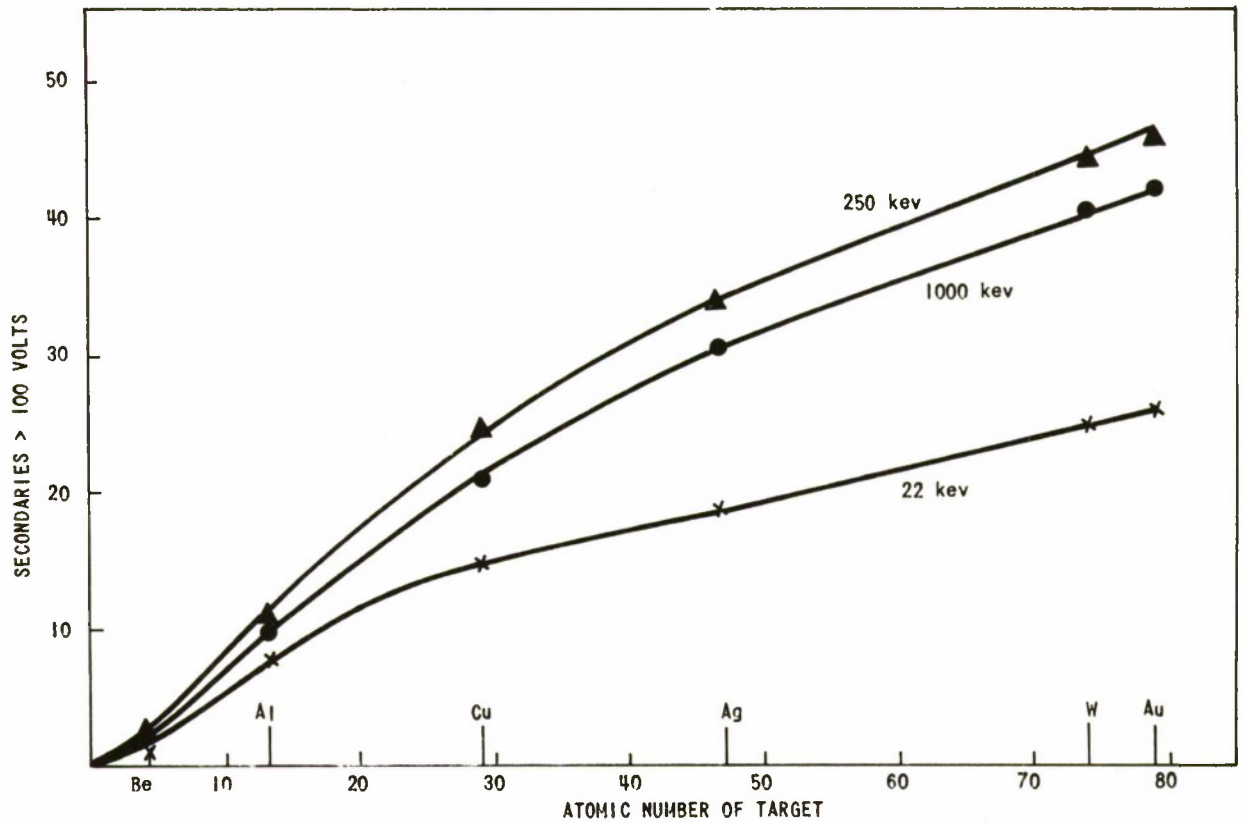


FIGURE 6.15. *Emission of fast secondary electrons versus the atomic number of the target material.*

where m_e and m_p are the masses of electron and proton respectively. For 0.96-Mev protons, $E_{max} = 2092$ ev.

The data for dependencc of energy on emission angle also seem to confirm the explanation of the high-energy component by coulomb scattering. In the case of secondary-electron emission by high-energy protons and deuterons, we observed that the energy distribution of the secondaries is not dependent on the target material for both the low- and high-energy component if the energy of the primaries is constant, which is very different from the case of electron emission by electrons. The energy distribution of the low-energy component in the former case does not depend on the energy of the primary particles, and the high-energy component shifts toward higher energies with increasing primary energy (as explained in the previous example, Equation 6.10). The probability is rather low that the expression $Y(E) \propto \frac{dE}{dx}(E)$ applies to the high-energy component as it does to secondary electrons below about 50 ev. Therefore, if SEMIRAD readings for fast neutrons are to be in rads, one should avoid the collection of the high-energy component hy setting the collector potential at about 50 volts for a typical cylindrical diode with an internal collector (see Chapter 5). A choice of low voltage will, however, influence the collection time of the secondaries, and will lowcr the dose rate at which the instrument saturates.

Secondary Electron Yield as a Function of Vacuum Level. In recent experiments, we observed that in most cases the sensitivity of the instruments depends to some degree upon the level of the vacuum in the chamber. This is the case even when the vacuum is sufficiently low to exclude any possibility of a contribution by the ionization current to the output. The typical value for this sensitivity change is about 15 percent increase in sensitivity for each decade of increase in pressure. The measurements were taken using gamma rays (primary particles are electrons) at the vacuum levels between 10^{-7} to 10^{-3} mm mercury. We did not yet make measurements using fast neutrons (primary particles) to study this puzzling effect. Its explanation is not available at this time, but one may guess that the change in the work function of

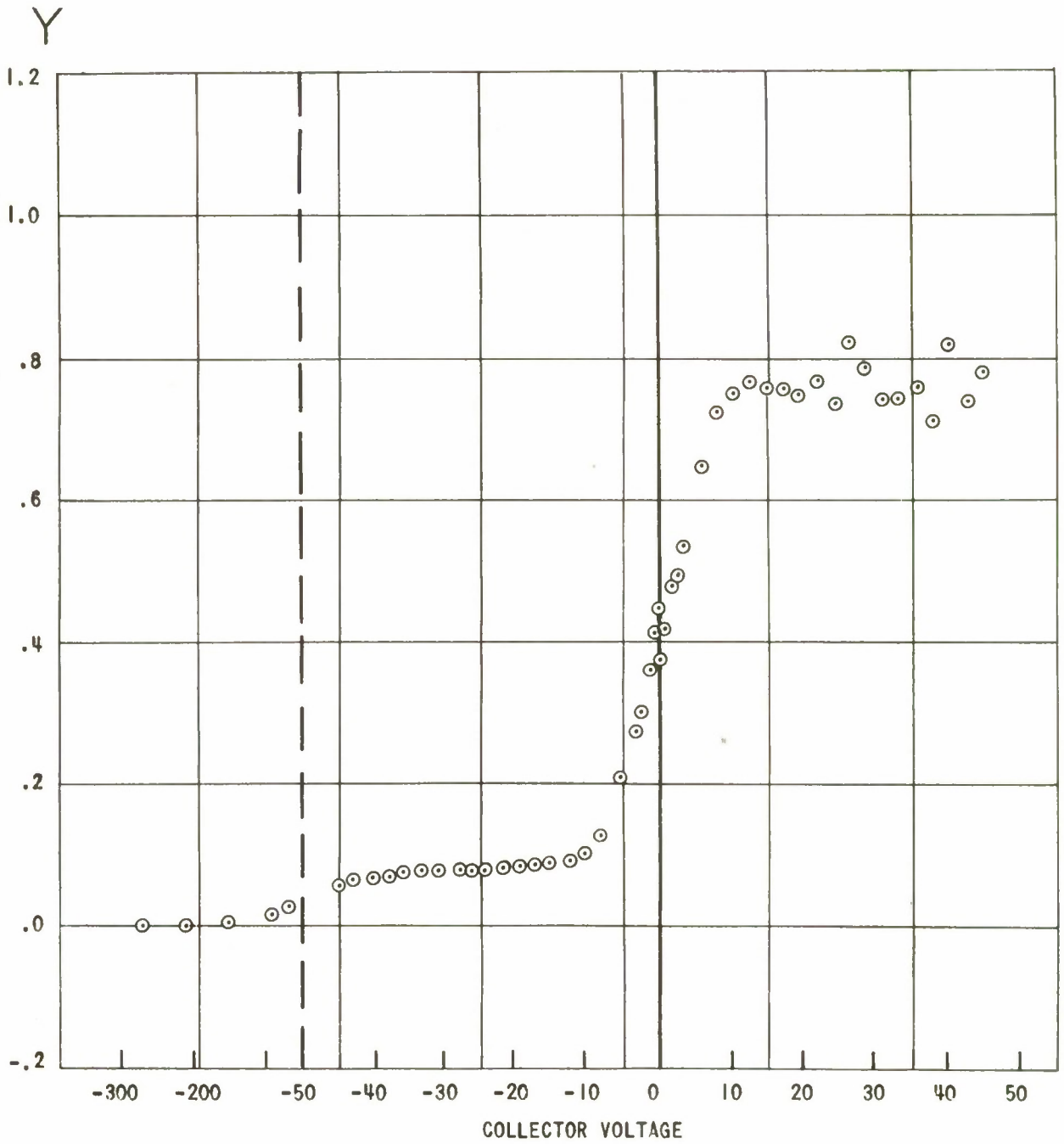


FIGURE 6.16. *Integral energy distribution of secondary electrons emitted by 1.034 Mev protons from aluminum.*

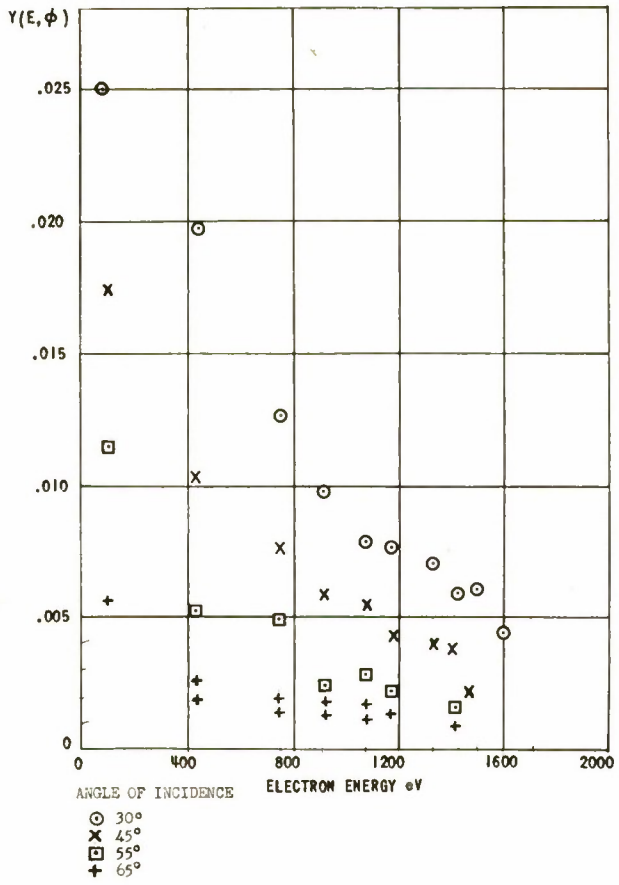


FIGURE 6.17. *High-energy component of secondary electrons emitted by 0.96 Mev protons from aluminum.*

the wall material as a function of pressure may be responsible for it.

This effect presents a serious problem in keeping the calibration of the permanently evacuated instrument constant over an extended period of time, because the vacuum level in the chamber drifts slowly. The problem of avoiding recalibration of instruments can be solved easily for units which have a permanently attached ion pump. One must simply note the pumping current (which is proportional to the air pressure) during the calibration and restore it to this rate by pumping before the instrument is used.

CHAPTER 7

SEMIRAD PULSE AMPLIFICATION AND CABLE CONNECTION

General. As its usage requires, the SEMIRAD is a very insensitive device; accordingly, only in the case of a high-radiation intensity is it possible to connect the SEMIRAD output directly to the oscilloscope, or, better still, directly to the deflection plates. The advantages of a direct connection are minimum distortion of the pulse, and fastest possible time resolution. If the coaxial cable is longer than about five feet, it must be terminated with an impedance-matching resistor in order to avoid signal ringing. A typical value of a terminating resistor is 75 ohms for the coaxial line RG59, and is given in general by the expression $Z_0=\frac{138}{\sqrt{\epsilon}}\log_{10}\frac{D}{d}$, where D is the inside diameter of the outside conductor, d is the diameter of the inside conductor, and ϵ is the dielectric constant of the insulator.

Once the cable is properly terminated, the shape of the signal is little affected by the length of the cable. For the best time resolution, the impedance of the SEMIRAD must be matched to the transmission line by using applicable geometry in designing the detector itself. The time resolution then is two times the length of the SEMIRAD divided by the velocity of light C. If S is the sensitivity of the SEMIRAD in coulomb/rad, and R is the terminating resistor (or any input resistor), then

$$SAR=\frac{\Delta V}{\Delta D_r}K \qquad (7.1)$$

Where $\frac{V}{D_r}$ is the voltage rise with dose rate at the input of the readout scope in volts/rad/sec of incident radiation, and A is the attenuation factor of the cable. This attenuation factor is proportional to the length of the coaxial line and depends on the frequency of the signal.

In operating with pulsed radiation, one mostly encounters single rather than periodic pulses; therefore, in some cases where the attenuation is high or strongly frequency-dependent (mostly for pulses of very short duration or in the case of long transmission lines), one must go through the following procedure: split the obtained pulse recording into its frequency components by means of Fourier analysis, multiply the amplitude of each component by the attenuation factor which is a function of frequency, and add the corrected components again. We thereby obtained a recording that possessed the true shape of the radiation pulse. One may also invert the integral

$$F(t)=\int_0^\infty f(\lambda)g(t-\lambda)d\lambda$$

where $g(t)$ is the function of the resolution of the system, $f(t)$ is the input function (signal), and $F(t)$ is the output function.

The dependence of the attenuation factor on frequency can be obtained in some cases from the catalogues of the cable manufacturers. Since the value of the terminating resistors is very low (about 100 ohms), the voltage drop may be too small at low-radiation dose rates. In this case a high-impedance input is necessary and is obtained by means of a preamplifier with a high-impedance input and low-impedance output. The preamplifier should be located as close as possible to the detector to reduce the capacitance of the lead between the components. This capacitance adds to the capacitance of the collector, and thus, according to Equation 4.6, reduces the sensitivity. An unterminated line between sensor and preamplifier that is too long may induce unwanted ringing of the signal; but, on the other hand, the preamplifier should be sufficiently removed from the radiation field to avoid internal ionization and other transient or permanent radiation effects on its components. In view of this, the preamplifier should be shielded as well as practicable against gamma rays and neutrons. An example for a typical connection between preamplifier and detector is in one of our measurements on Godiva II where 2-meter-long cables were used with total collector circuit capacitance equal to 150 $\mu\mu f$.

Protection Against External Ionization. The sensitivity of a typical SEMIRAD is approximately 1/10,000 of the sensitivity of a corresponding ion chamber; therefore, we must be very careful to eliminate any possibility of external ionization currents that could overshadow the relatively faint SEMIRAD effect. The signal lead must be hermetically surrounded by an insulating material

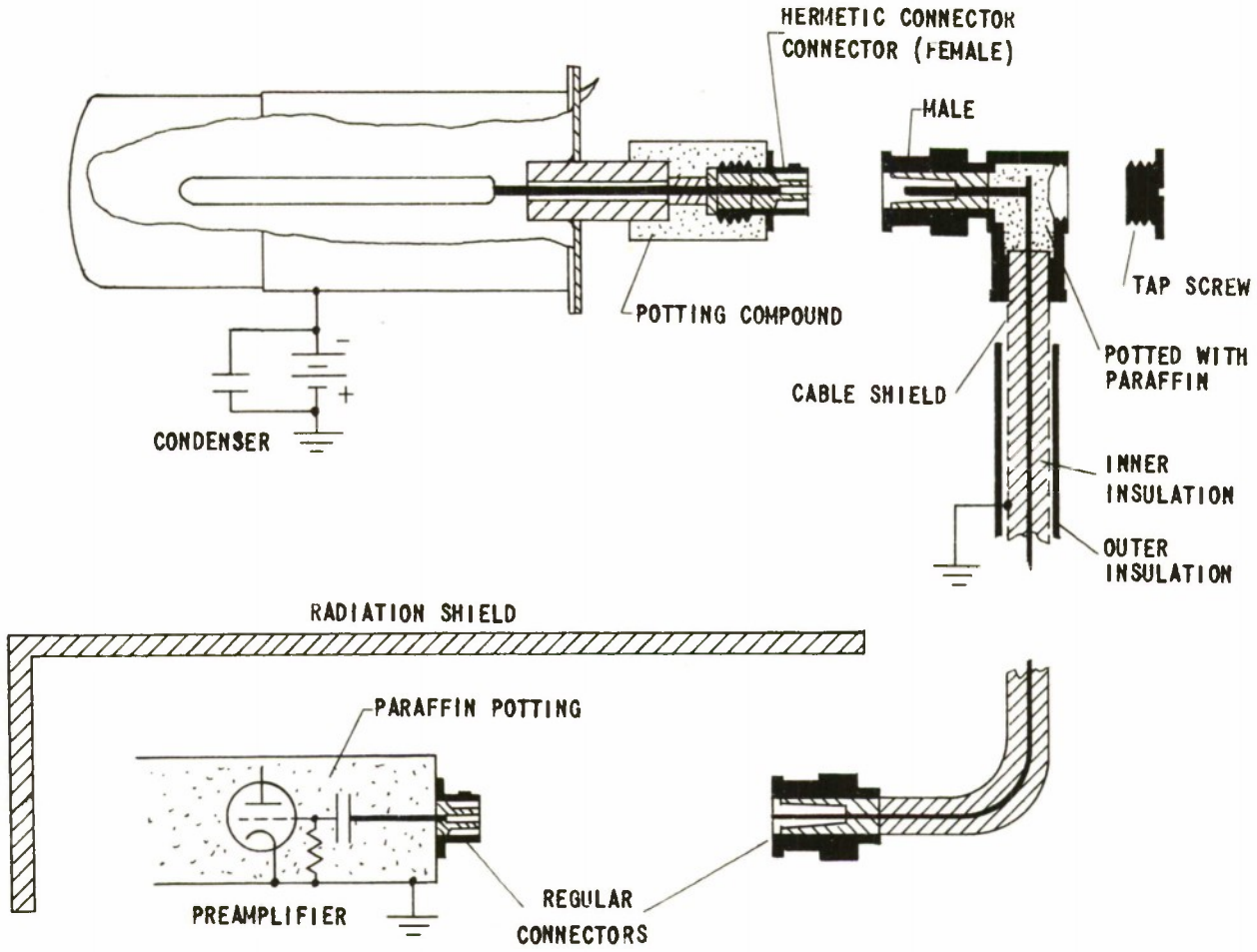


FIGURE 7.1. *Protection against external ionization of a SEMIRAD diode.*

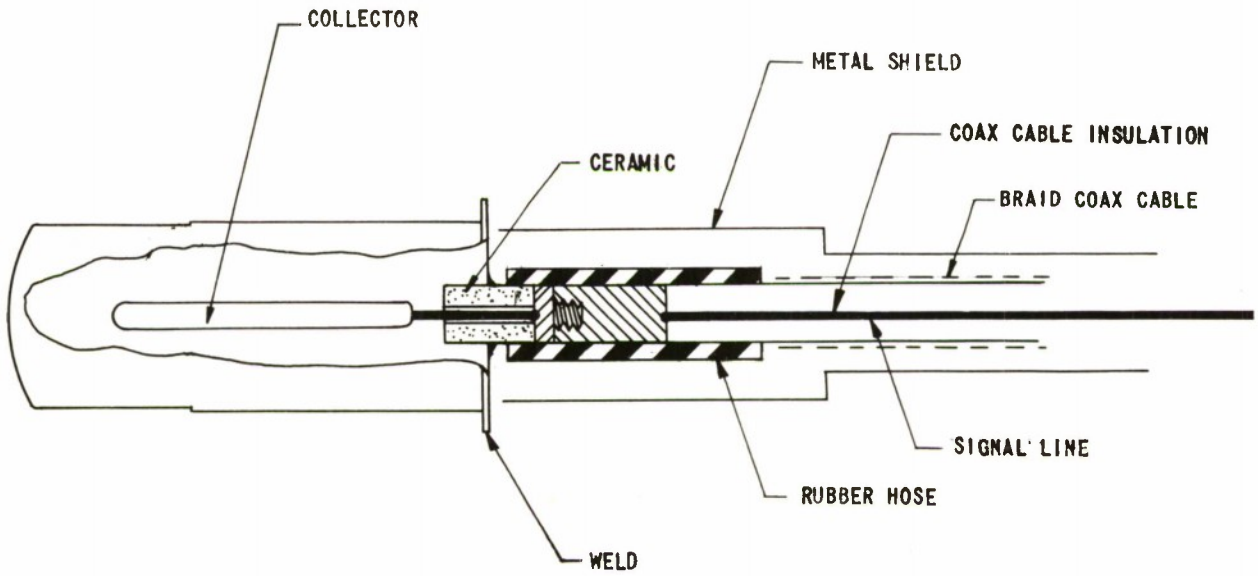


FIGURE 7.2. *A simple method to protect an exposed SEMIRAD diode against external ionization.*

through which the ions cannot travel, and this insulator must be externally shielded with a metallic braid. Any kind of a hermetically sealed connector can be used.

A simple solution of the connector problem is shown in Figure 7.1, where BNC connector AMPHENOL 31-850 and UG 1034/U91145 was used. The male part of this connector combination is designed so that the center lead can be soldered to the center pin and then the surrounding area filled out with paraffin or epoxy resin. The opening through which the paraffin is poured can then be closed with a screw supplied with the connector. Formerly, ceramic insulators were used with the coaxial cable soldered to them and the joint was protected against ionization with a piece of latex rubber hose (Figure 7.2).

The protection of the SEMIRAD system against external ionization becomes less important, or even unnecessary, if one works at radiation intensities higher than 3×10^7 rads per second. In a system consisting of an ion chamber and a SEMIRAD in parallel, the following considerations apply for its performance: The ion chamber efficiency as a function of the radiation dose rate is given (References 55, 56, and 58) for a parallel plate and a cylindrical geometry by the following expressions:

$$f_{\mathrm{Pl}} = \frac{2}{1+\sqrt{1+\xi_{\mathrm{Pl}}^2}} \qquad f_{\mathrm{cyl}} = \frac{2}{1+\sqrt{1+\xi_{\mathrm{cyl}}^2}}$$

$$\xi_{\mathrm{Pl}} = md^2 \frac{\sqrt{g}}{Vi} \qquad \xi_{\mathrm{cyl}} = m(a-b)\kappa_{\mathrm{cyl}}^2 \frac{\sqrt{g}}{Vi} \tag{7.2}$$

where d and $(a-b)$ are the distances between the electrodes (in cm), m is a characteristic gas constant (15.9 for air at 760 mm Hg 20° C), Vi is the applied voltage in volts, g is the ionization intensity in esu cm^{-3} sec^{-1} and

$$\kappa_{\mathrm{cyl}} = \sqrt{\frac{\frac{a}{b}+1}{\frac{a}{b}-1}} \frac{lm\frac{a}{b}}{2}. \tag{7.3}$$

From the above expressions one can see that the dose rate limitations for a chamber of a few centimeters diameter starts becoming important at the dose rates of 3×10^3 rads per second and at 3×10^5 rads per second almost complete limitation is obtained. Up to this level the SEMIRAD sensitivity is approximately 10^{-4} times the ion chamber sensitivity but past the saturation level of the ion chamber the SEMIRAD output still increases linearly with the dose rate while the ion chamber output remains constant. Hence at approximately 3×10^7 rads per second the two outputs become comparable, and at 3×10^9 rads per second or higher the ion chamber output becomes negligible compared to the SEMIRAD output.

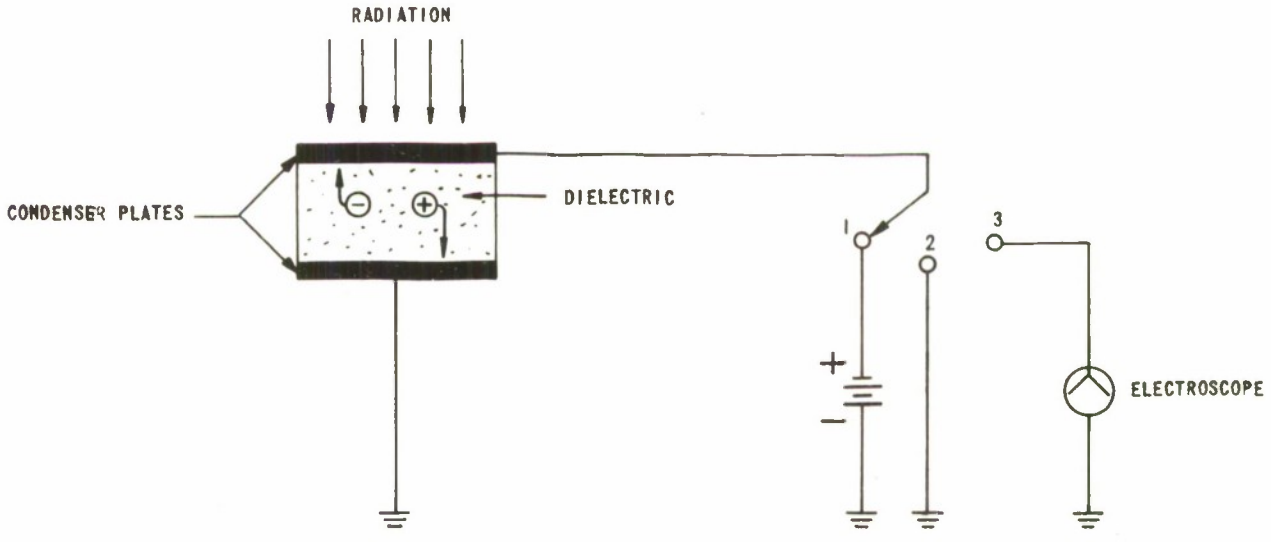


FIGURE 7.3. *Principle of the persistent internal polarization caused by radiation.*

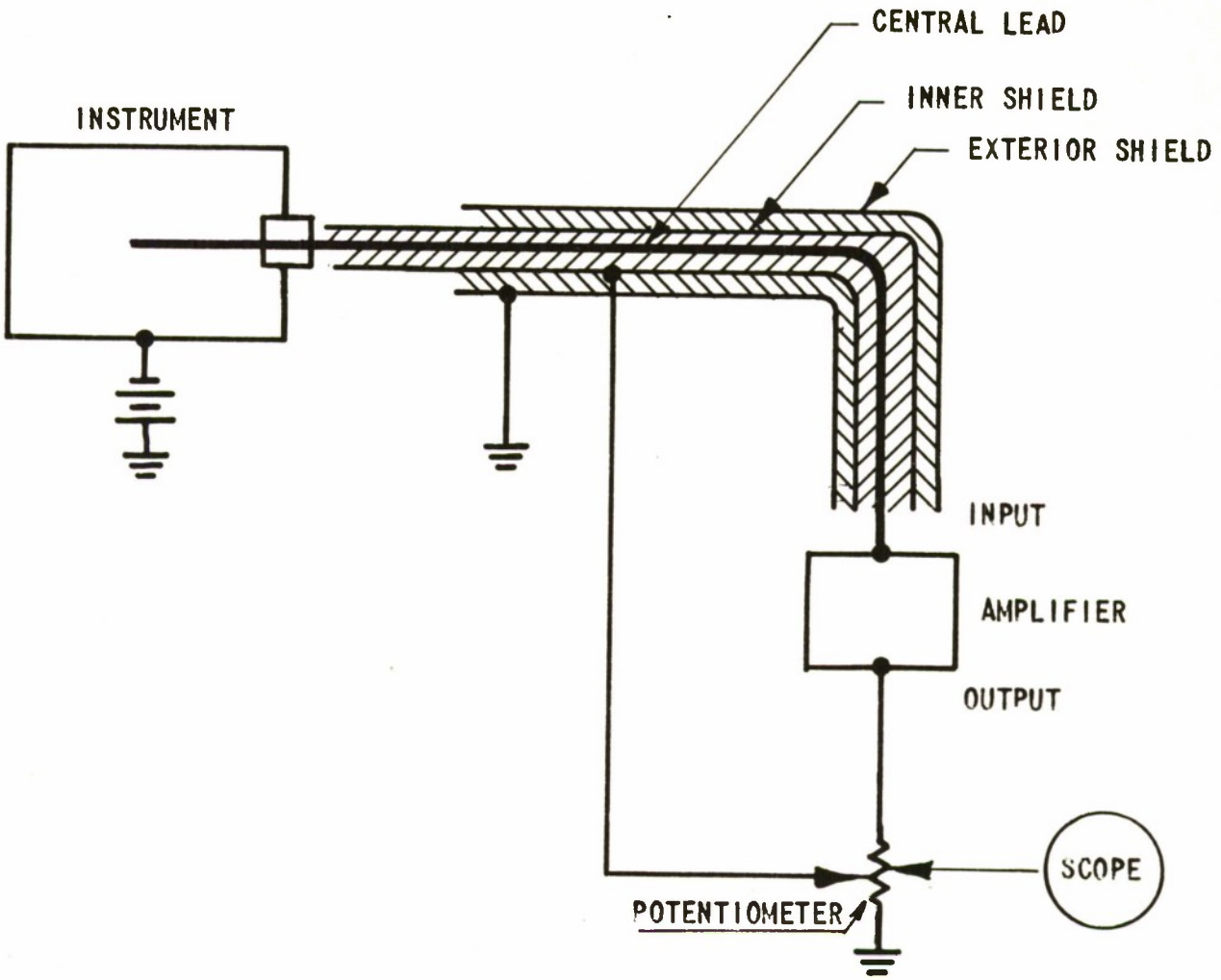


FIGURE 7.4. *Circuit designed to prevent persistent internal polarization by maintaining the voltage between the center and the outside of the connecting cable.*

Persistent Internal Polarization and Its Effect on the Transmission of the Pulse. When some insulators are irradiated with penetrating ionizing radiation in the presence of an electric field, the electric charges that are freed by the incident radiation can shift in the electric field during their lifetime. This shift results in a permanent polarization of the material, or, in other words, the material becomes an electret. This effect was discovered by Kallmann and his associates (Reference 3) during work on radiation-induced photoconductivity in insulating materials. The importance of this effect in working on radiation dosimetry (including SEMIRAD) is illustrated by the following experiment. In Figure 7.3, a suitable insulator is exposed between two condenser plates to gamma rays, which produce free charges throughout it. One plate is grounded, and the other can be connected to a battery (Position 1), to ground (Position 2), or to an electrometer (Position 3).

When the radiation is on and voltage is applied (Position 1), the internal polarization builds up. With the radiation off and the condenser grounded (Position 2), the polarization is compensated by the induced charge on the plates. If the plate is then connected to the electrometer (Position 3), no charge is apparent without radiation; but when radiation is applied, the internal charge recombines and the charge previously bound to the plates is visible on the electrometer. If the condenser was previously irradiated with both plates grounded, no such charge could be released when irradiated again in Position 3.

From the experiment described above we see that, depending on the kind of insulators used and the voltages applied across them, the signal output of the SEMIRAD may depend not only on the instan-

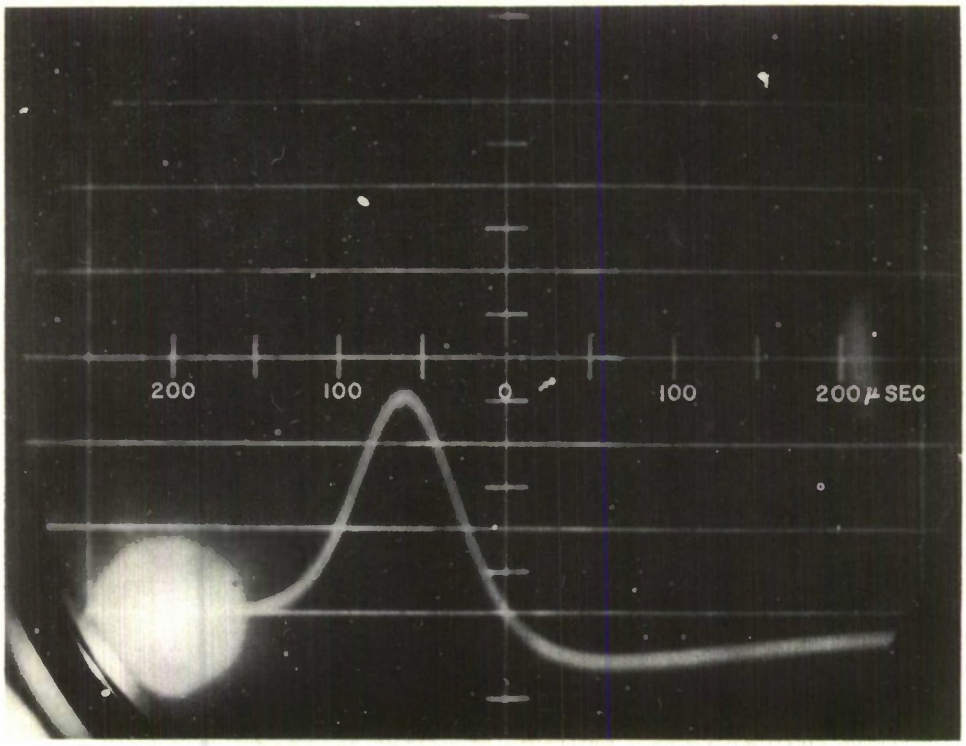
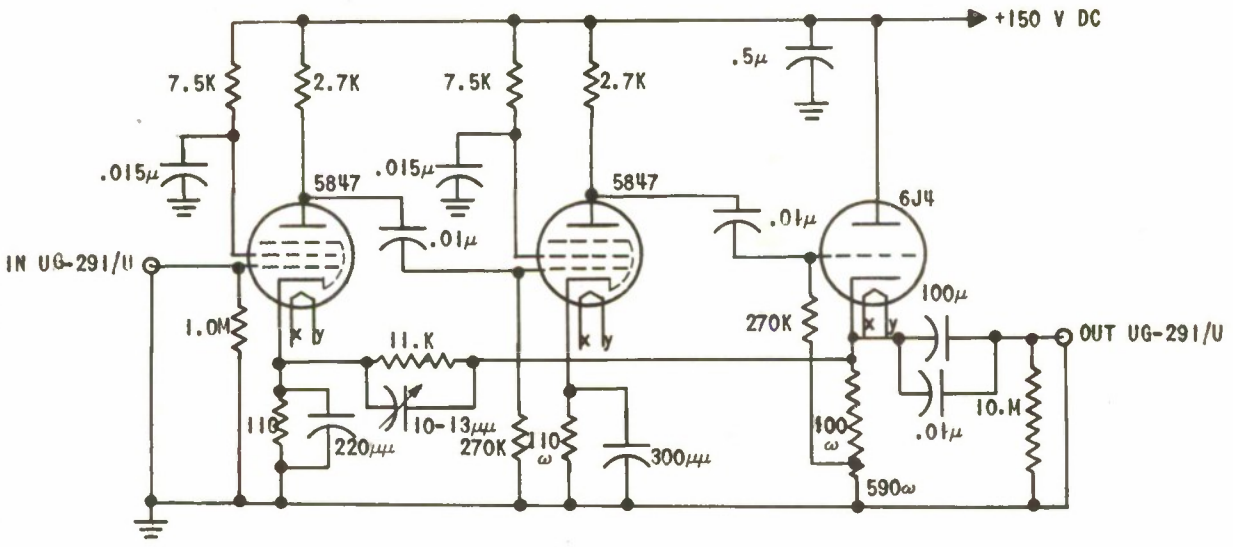


FIGURE 7.5. *Example of an "undershoot."*



FAST SEMIRAD PREAMPLIFIER. GAIN: 100 (20 db). RISE TIME: .06 μSEC. CLIPPING TIME: 2500 μSEC. OUTPUT IMPEDANCE: APPROX. 75 OHMS. VOLTAGE REQUIREMENTS: 150 V D.C. AT 50 ma; 6. V D.C., AT 1.0A.
NOTE THAT SIGNAL IS NOT INVERTED.

FIGURE 7.6. *Fast preamplifier circuit.*

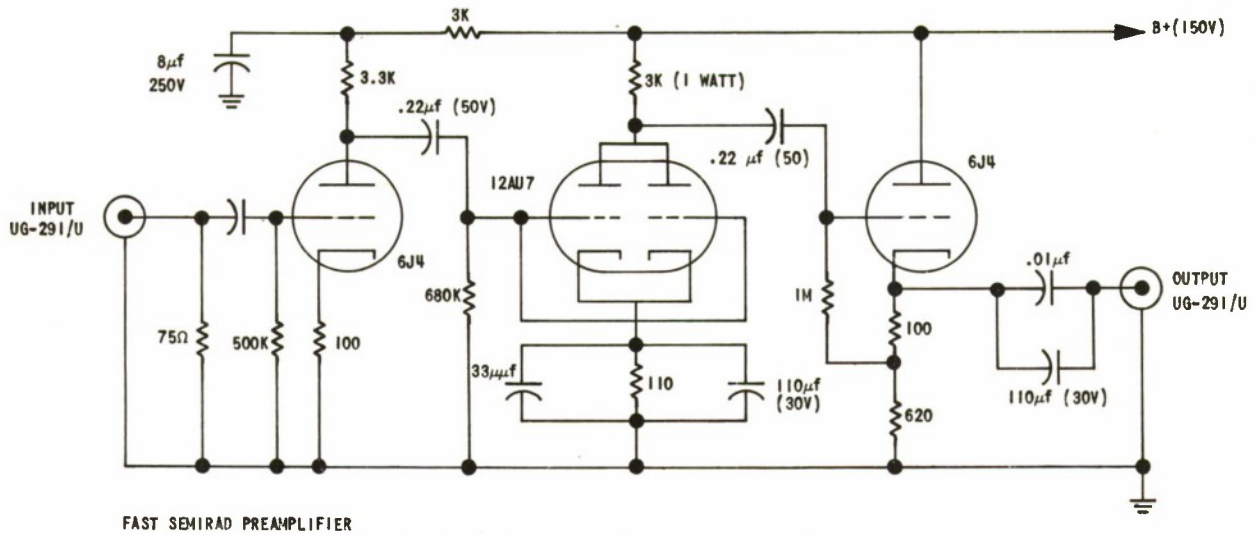


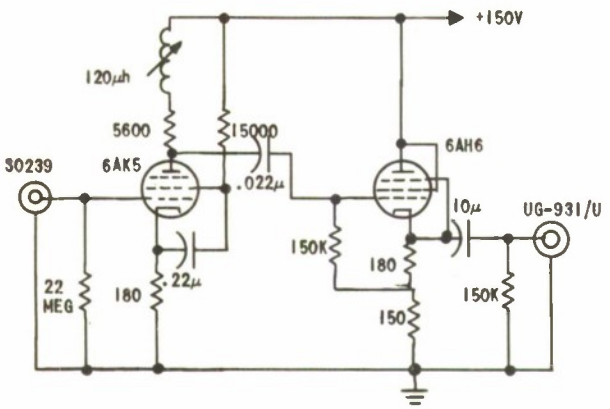
FIGURE 7.7. *Fast preamplifier circuit.*

taneous intensity of the radiation, but on the previous history of the whole arrangement. To avoid this dependence, the voltage between the central conductor of the coaxial cable, which is attached to the SEMIRAD, and its braid should always be kept to a minimum. This precaution becomes more important as the total dose to the cable increases. We can obtain this minimum voltage by connecting the battery to the instrument so that a net voltage appears across the insulator of the coaxial cable only during the time the pulse is transmitted. Such a circuit is shown in Figure 7.1.

In the case of a strong voltage signal and a high total dose delivered to the cable, we may even have to operate without any voltage across the insulator of the coaxial cable. In Figure 7.4, the cable has two concentric shields, wherein part of the amplified pulse at the input (the scope amplifier may be used) is applied to the inner braid of the cable, and is so adjusted in strength that at any given time the voltage between this braid and the center wire vanishes. The outermost braid is grounded and any voltage between the two braids is of no consequence for the transmission of the pulse. The choice of insulating materials is also very important. From experience we know that paraffin, polyethylene, polystyrene, and alumina ceramics do not exhibit persistent internal-polarization effects strong enough to disturb the measurement of a Godiva pulse. Teflon insulation, on the other hand, shows a very strong persistent internal polarization from radiation and should be avoided.

In some cases the influence of the cable effects and other side effects on the measurement of radiation intensity can be obtained during this calibration of the instruments and during a high-intensity pulse recording. An example of such an estimate is given at the end of Chapter 10.

Guard Ring Design. An excellent way to avoid leakage and photoconductivity caused by radiation in the insulator located between the wall of the instrument and the collecting electrode is by means of a guard ring. In such a device the insulator consists of two parts, one attached to the wall of the instrument (where the collecting voltage is applied) and the other to the collecting electrode which is grounded through the input resistor at the oscilloscope; between these two insulators is inserted a piece of metal which is at the ground potential. It must be constructed in such a way that it separates completely the dielectric which touches the collector from the dielectric connected to the charged wall. In this construction there is no voltage observable across the insulator which touches the output, and the collecting voltage is applied only between the guard ring and the wall of the instrument. Obviously, a current caused in the insulator by radiation may flow between the wall and the



PREAMPLIFIER CIRCUIT, SERIES "C"
GAIN: 10, OUTPUT Z: 70 OHMS
RISE TIME: 0.1 μS
CLIPPING TIME: 1600 μS
POWER REQ.: 6V @ 0.63A
150V @ 22.5μA

FIGURE 7.8. *Fast preamplifier circuit.*

guard ring but this does not influence the output current of the instrument. A system of this kind has been constructed and it is recommended that all future designs use this design. The instruments with the guard ring show a very constant time independent calibration regardless if they were calibrated at low intensity, DC radiation or at high-intensity pulsed radiation.

Construction of Amplifiers and Preamplifiers For Use With SEMIRAD Dose Rate Meters. The amplifiers used to measure radiation pulses with SEMIRAD should satisfy the following requirements: (a) the output should be proportional to the input over a wide signal range, or follow closely a given function, e.g., the case of the logarithmic amplifier; (b) the time resolution should be much faster than the fine structure of the radiation pulse one intends to measure, and (c) the clipping time of the preamplifier defined as the time for the output signal of an amplifier to fall from peak value required to 1/e of that value following the application of a step-function voltage input to the amplifier, should be much longer than the duration of the expected pulse (about a factor of 100) to avoid "undershoots." Such an undershoot is shown in Figure 7.5. Figures 7.6, 7.7, and 7.8 show the circuit diagrams of three very reliable preamplifiers suitable for SEMIRAD work. Tubes have been chosen rather than transistors, because the latter suffer radiation damage

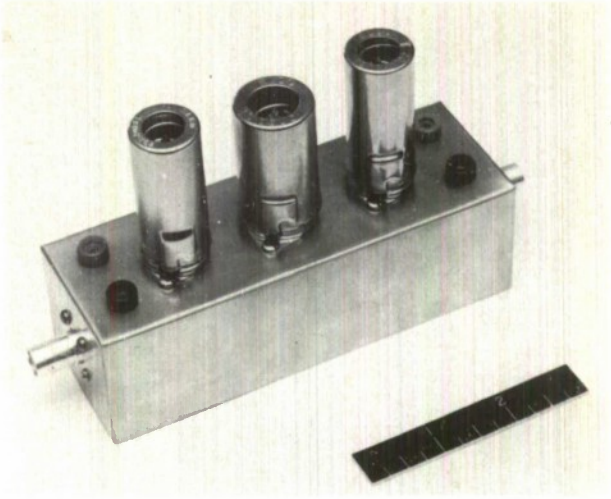


FIGURE 7.9. *Typical assembled preamplifier. The chassis is filled with potting compound.*

more easily and are in general less reliable in radiation environments. The inside of the chassis containing the components of the preamplifier was solidly filled with paraffin. Figure 7.9 shows the external construction of such a preamplifier.

Amplifiers with time constant much longer than the duration of the pulse show as their output the total accumulated dose as a function of time. Figures 12.18 and 12.19 show the pulse of the General Atomic LINAC in both the rate-versus-time and accumulated dose-versus-time form. All amplifiers described here resemble Hi-Fi amplifiers. Their response is constant within five percent (about 0.02 db) over a wide frequency range.

Recording of Pulses. Pulses of less than several milliseconds duration must be recorded by means of oscilloscopes. The choice of a suitable oseilloscope is determined by its rise time, sensitivity, input resistance, and range of time settings. To record single pulses, the scope must be equipped with a "single sweep" arrangement.

The triggering can be accomplished in two different ways: (a) by an external trigger signal that is supplied by some independent apparatus just before the radiation pulse starts, and (b) by a part of the pulse from the radiation sensor self-triggering the scope while the main part of the pulse is sent to the input through a delay line.

For all recordings of pulses longer than a few mieroseconds, the input of the readout oscilloscope should be set to DC. For shorter pulses both DC and AC input settings can be used.

CHAPTER 8

CALIBRATION OF SEMIRAD

SEMIRAD dosimeters or dose rate meters supply the readout in electric charge or in electric current as a function of time. To obtain readings in rads or in rads per second at any instant of time, we must convert the electric charge or current at that time into these units. There are two ways to accomplish this: (1) calibrate the sensitivity at constant low-radiation rates and thereby obtain the absolute sensitivity of the instrument in a/rad/sec, or (2) calibrate the sensitivity during the measurement of a high-intensity pulse.

Calibration at Low Intensities. SEMIRAD diodes are very insensitive devices. The signal output at several hundred rads/sec, as delivered from a typical laboratory X-ray machine, is very small. Thus we must use sensitive current-detection methods.

Figure 8.1 shows the experimental setup for calibration. The collector electrode is connected by means of a shielded cable to the input of a standard high-voltage electrostatic voltmeter outside of the radiation area. The shielding of the coaxial cable is kept at the same potential as its center to avoid persistent internal polarization of the dielectric, and to prevent leakage currents across the dielectric and other cable effects. The center of the cable can be connected by means of a high-resistance switch to a 300-volt battery or grounded through a high resistor (about 10^{12} ohms).

Using a stopwatch, one measures the discharge times of the voltmeter through the resistor with the radiation on and then with the radiation off. The voltage interval over which the discharge takes place should be small and selected so that the discharge can be assumed to be linear with time. Here one has to consider that the loss of charge of a condensor from leakage through a resistor is an exponential function of time, while the discharge from secondary-electron production by the SEMIRAD is linear with time.

The sensitivity of a SEMIRAD in a/rad/sec is given by the expression

$$S=\frac{V_0+V_1}{2}\frac{1}{RD_r}\left[\frac{t_0}{t}-1\right] \tag{8.1}$$

where V_0 = initial positive voltage on the collector assembly

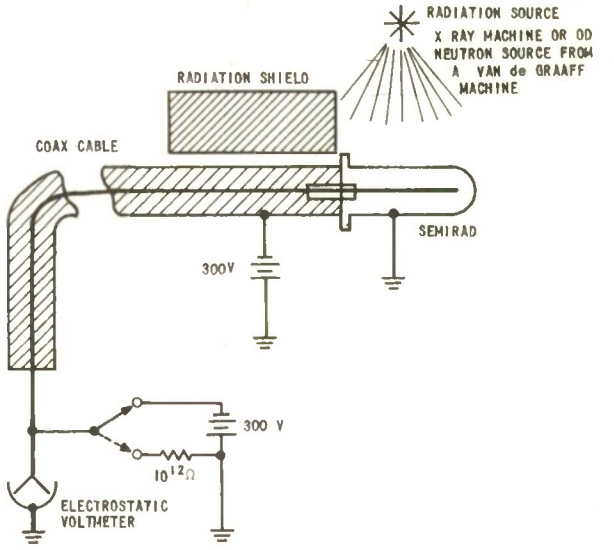


FIGURE 8.1. *Calibration of a SEMIRAD diode at constant, low radiation rates.*

V_1 = voltage after partial discharge of the system

t_0 = time necessary to discharge the system from V_0 to V_1 through the resistor without radiation

t = same as t_0 but with radiation applied ($t_0 > t$)

R = value of the resistor to ground

D_r = constant dose rate of the radiation delivered to the instrument in rads/sec

and $\frac{V_0+V_1}{2}$ is the average voltage during the discharge.

The process should be repeated several times to check whether the results are reproducible. A similar process can be applied to calibrate SEMIRAD using a sensitive electron-tube electrometer. Here one measures directly the current through the instrument produced by a constant radiation dose rate from the radiation source. Division of the current by the dose rate gives the sensitivity.

Calibration During Exposure to a High-Intensity Pulse. Assume $I=I(t)$ is the measured current from the SEMIRAD as a function of time for a given radiation pulse measured with the SEMIRAD.

Then $$\int_0^\infty I(t)dt = Q \tag{8.2}$$

where Q is the total eharge of seeondary eleetrons delivered from the instrument during the pulse. Aeeording to the prineiple of operation of the SEMIRAD

$$Q = KD \tag{8.3}$$

where D is the total dose of radiation delivered during the pulse. D ean be measured by use of an independent method for measuring total radiation doses delivered at high rates.

Threshold dosimeters, for example, ean be used for neutrons and film dosimeters for gamma rays. The total eharge Q is obtained from the graphical or numerical integration of the eurve $I(t)$, and so the proportionality faetor K ean be determined. Differentiation of Equation 8.2 gives the eurrent during the duration of the pulse as a funetion of dose rate (whieh is a function of time).

$$I(t) = \frac{dQ}{dt} = K\frac{dD}{dt} = KD_r(t)$$

$$\text{or } I(t) = \frac{Q}{D}D_r(t) = \frac{1}{D}\left[\int_0^\infty I(t)dt\right]D_r(t) \tag{8.4}$$

This is the conversion from eurrent reading to dose rate in rad/see. Equation 8.4 ean therefore be used to calibrate the SEMIRAD during the pulse reading.

Both methods described in this ehapter should be used with every instrument. The low-intensity calibration ean be used to determine the sensitivity, and one ean use these data to estimate the neeessary input resistor, sensitivity setting on the readout seope, and other data vital for the successful recording of the high-intensity radiation pulse. Calibration during the pulse is neeessary to express the results in radiation dose-rate units.

CHAPTER 9
Instruments With Wide Sensitivity Range (Electron-Multiplier SEMIRAD)

Some advantages of dosimeters and dose-rate meters based on the SEMIRAD principle over ion-chamber detectors are superior energy-dependence characteristics and superior time resolution. We find it useful to have instruments that cover not only the high-intensity radiation but also the low radiation rates. One method of achieving a wide sensitivity range is the use of a sensitive instrument with a high-gain amplifier. Another system, which we find to be more desirable, uses a modified photomultiplier tube as a detector, where the multiplier dynodes represent a built-in amplifier in which the gain is a function of the applied dynode voltages

In the latter system, the tube has a modified cathode, where the photosensitive coating is replaced with a thick layer of a metallic conduetor. Instead of the regular photomultiplier operation where, by means of a scintillator, radiation is eonverted to light that produces photoelectrons from the photoeathode, the radiation in this case releases Compton electrons in the cathode that produce secondaries from the surface of the cathode and are then multiplied by the dynodes.

In most conventional applications of the photomultiplier, the pulses produced by single particles are measured. Here we measure the dose rate as a function of time by recording the output current of the device as a function of time without resolving the pulses from the single particles. A speeial multiplier circuit for this purpose is described below.

Construction of the Electron-Multiplier SEMIRAD. A tube similar to any conventional photomultiplier tube can be used; however, the transparent photomultiplier cathode should be replaced by a layer of metal. The change should be made by the tube manufaeturer during the assembly of the tube before the pumping, baking, gettering, and activation procedure of the device. The finished tube should have no bakelite base eonnected to the bottom. Two typical wiring diagrams are shown in Figures 9.1 and 9.2. The bleeder resistors supply the correct voltages to the dynodes, and the later stages have condensers connected in parallel to maintain the dynode voltages in case of a heavy currcnt surge of short duration. The resistors and eondcnsers should be loeated in a suitable container next to the tube. To prevent ionization of gas between the leads, we must fill the container with a suitable potting compound as outlined in Chapter 7. For practical applications it is not necessary to shield the dynode

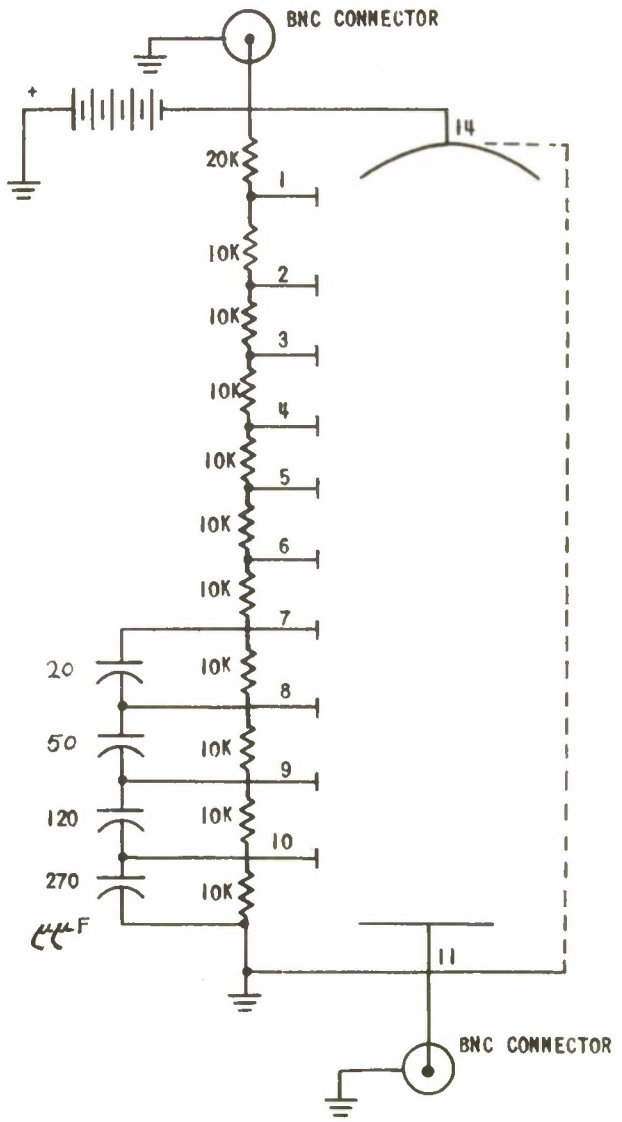


FIGURE 9.1. *Electron-multiplier SEMIRAD circuit (modified RCA 5819).*

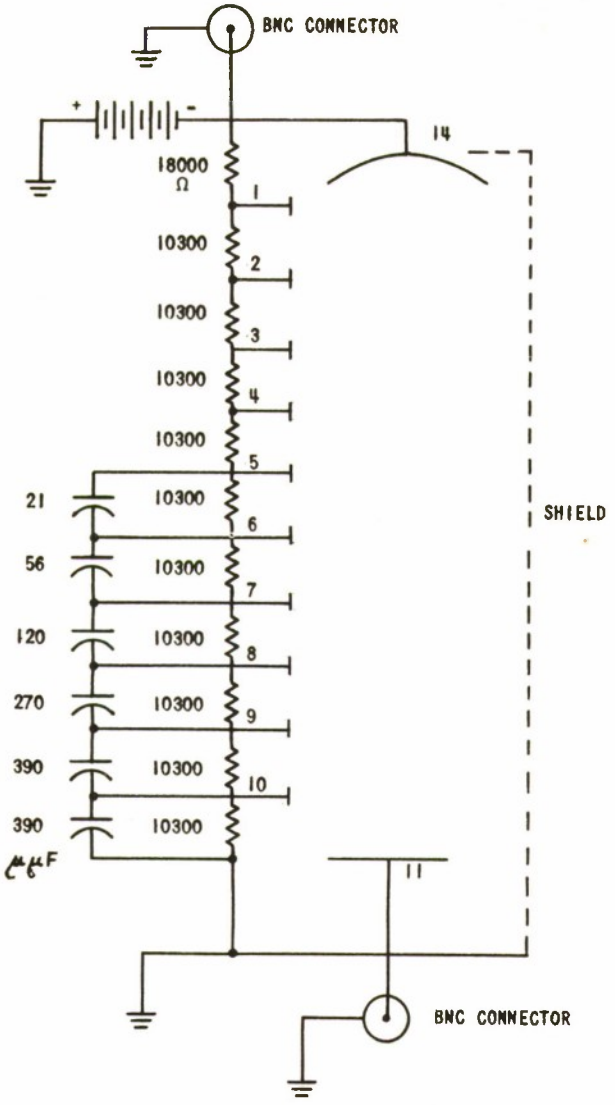


FIGURE 9.2. *Electron-multiplier SEMIRAD (modified Dumont 6292 tube).*

stack from incident radiation. The buildup of dynode current is given by

$$I_n = I_0 Y^n \tag{9.1}$$

where I_n = current through the nth dynode
I_0 = initial current
and Y = gain per dynode

I_n increases very rapidly with n, and an additional response due to emission of secondaries by Compton electrons from the dynodes is negligible. Even in the case of such a contribution of the dynode effect to the sensitivity, this additional current simply adds to the total current and is included in the sensitivity during the calibration of the instrument.

Use of Conventional Photomultiplier as Electron Multiplier SEMIRAD. It is possible to use any conventional photomultiplier tube as an electron-multiplier SEMIRAD without any interior changes. The only disadvantages of such a system as compared with the modified tube are sensitivity to light and a rather high cathode resistance. After removal of the bakelite base, the glass on the base of the tube should be painted black (e.g., with glyptal) to prevent light caused by possible fluorescence in the potting compound under irradiation from entering the tube. After the device is assembled as outlined in the previous section, one obtains a very useful inexpensive and simple instrument. Its sensitivity to radiation is higher than in the case of a solid metallic cathode because the secondary-electron yield from the photosensitive coating is higher than from an ordinary metal coating. Some tubes do have metallic photocathodes already and therefore do not require a modification. Typical tubes of this kind are the PM 931A and its successors.

Characteristics of Electron-Mulitplier SEMIRAD. One can obtain a very wide sensitivity range in such a device by variation of the dynode voltages. If V is the applied voltage on the resistor stack, D_r the radiation dose rate, and I the output current, then

$$I = D_r e^{BV+K} \tag{9.2}$$

The empirical constants B and K depend on the type of multiplier used. Figure 9.3 shows typical experimental data on the sensitivity dependence with voltage. The tube shown is an RCA 5819 photomultiplier with a conventional cathode. Other photomultiplier tubes yield similar results. The applied voltage may be raised to the maximum allowable voltage specified by the tube manufacturer, or even slightly higher for maximum sensitivity. The amplification factor then becomes very large and for an equivalent tube, the RCA 6810, it is 6.6×10^7 (Reference 20).

In the high-gain application, one has to be careful not to exceed the maximum allowable current; otherwise deviation from linearity of input to output will result. For the RCA 6810, the maximum allowable current is 0.7 amp. Experimental data yield a sensitivity of 0.58 a/rad/sec at the maximum applied voltage for this tube.

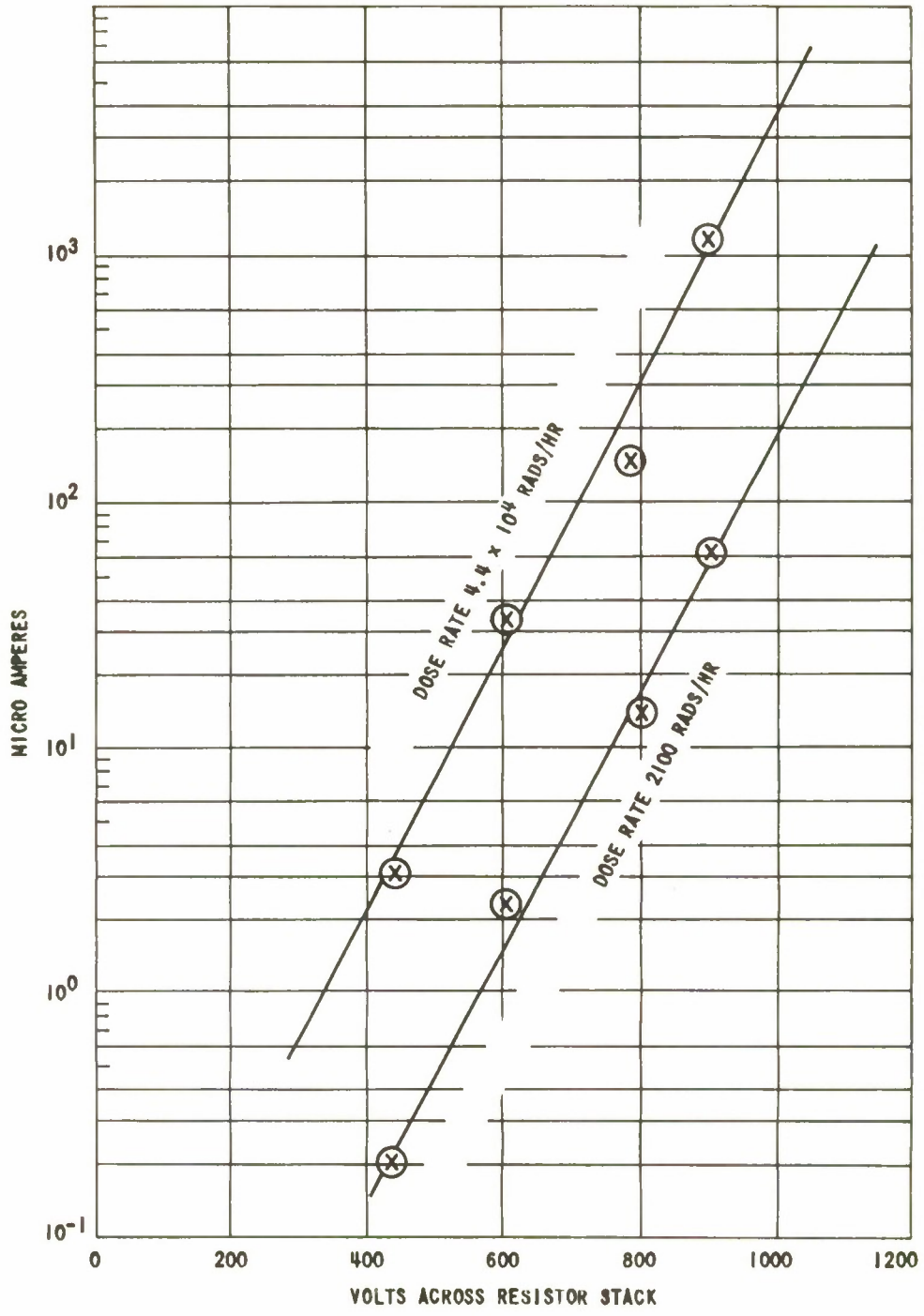


FIGURE 9.3 *Sensitivity of a typical electron-multiplier as a function of dynode voltage.*

Constant Current Methods. In the wide sensitivity range detector system, it is advisable to use a readout arrangement where the anode current of the multiplier is kept constant by means of a feedback circuit that raises or lowers the voltage across the dynode stack when the current shows a tendency to drop or to increase. Here one records the applied voltage as a function of time across the dynodes, which is necessary to maintain a constant current rather than the multiplier current. The result is a linear relationship between the logarithm of the radiation

224-250 O-66—5

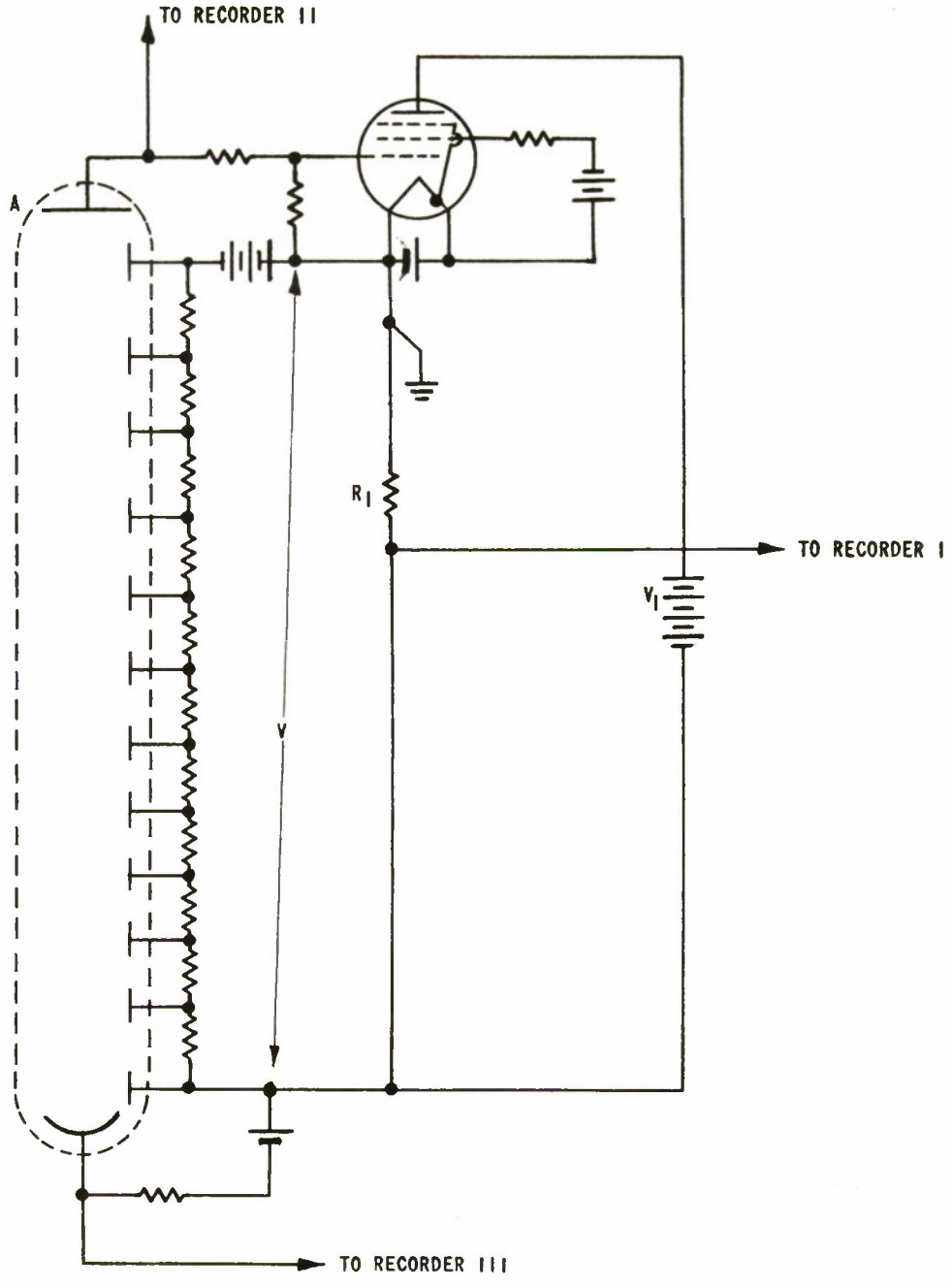


FIGURE 9.4. *Constant-current electron-multiplier circuit.*

dose rate and the applied voltage, both as a function of time.

$$V(t) = C - K \ln D(t) \tag{9.3}$$

The constant C and K can be determined in each case experimentally. Figure 9.4 shows a typical circuit diagram that can be used for this purpose. The pentode in series with resistor R acts as a potentiometer. For high currents through the multiplier anode A, the resistance of the pentode decreases and this causes the voltage V across the dynode stack to drop. This voltage is then recorded (Recorder I) and is proportional to the logarithm of dose rate as a function of time. The electron-multiplier current may also be displayed to provide a cross check on the dose-rate recording in case the current should vary with time (Recorder II).

The circuit shown here does not affect the voltage between the last dynode and the multiplier anode.

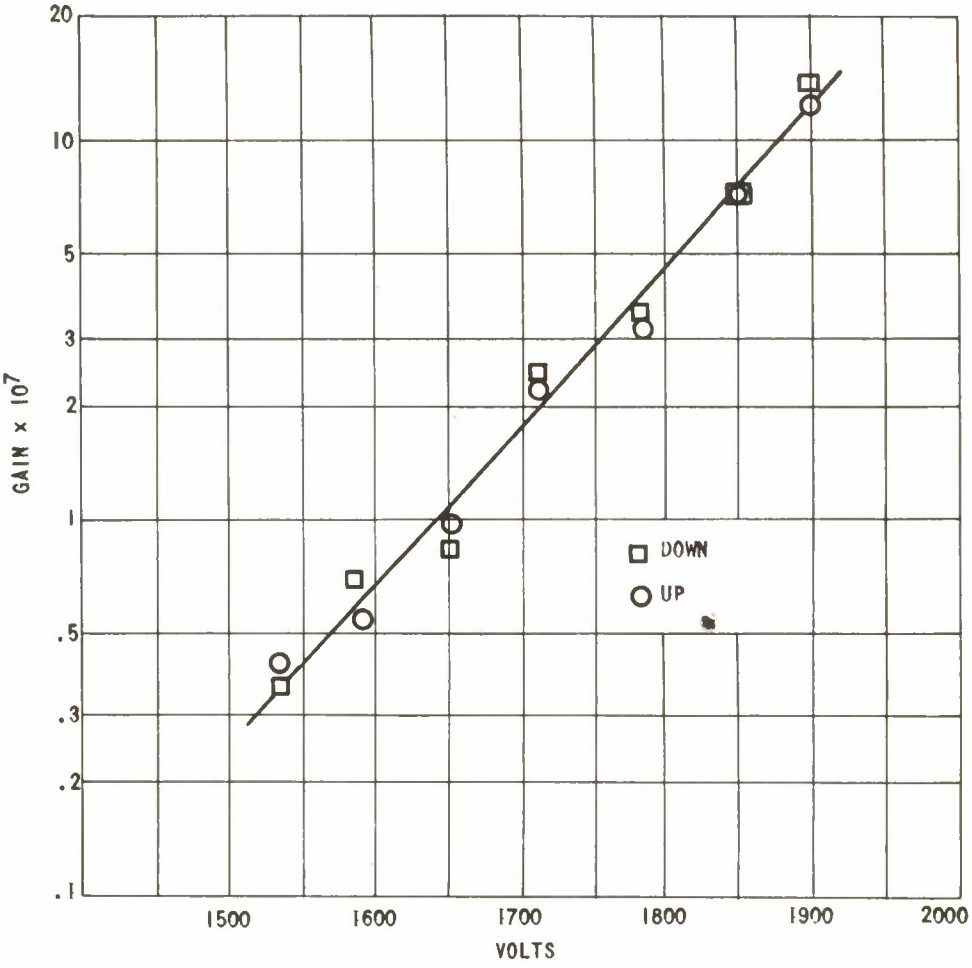


FIGURE 9.5. *Typical gain of M306 multiplier versus dynode strip voltage gradient.*

This is arranged so as to make the device free of sudden spontaneous changes. Also, the portion between the cathode and the first dynode is kept independent of the voltage-regulator circuit. This portion then acts as a diode-type SEMIRAD and allows one to obtain directly the dose rate as a function of time, which can be read on Recorder III.

To automatically lower the dynode voltage when radiation intensity is increasing and to raise it when intensity is decreasing, one puts a resistor of the same order of magnitude as the sum of the resistor values in the dynode stack in series with the dynode stack. A voltage approximately twice as high as the one required across the dynode stack is then applied across all resistors to obtain correct potentials on each dynode. The circuit now acts as a voltage divider and the voltage across the dynode stack drops when the multiplier current increases. We have to record both the voltage across the the dynode stack and the anode current as functions of time. Knowing the voltage across the dynode stack and the calibration of the radiation sensitivity (the current through the anode as a function of this voltage and the radiation dose rate), we can compute the dose rate as a function of time. In such a circuit, one should omit the condensers shown in Figures 9.1 and 9.2.

Neutron Detection. In the previous section, only gamma-sensitive instruments were considered. To make the electron-multiplier SEMIRAD sensitive to fast or slow neutrons, we coated the cathode with fissionable materials or with boron. The coating has to be made conductive by evaporation of a suitable metal. Successful methods have been reported in the literature for

measurement of single particles (References 21 and 22), and an arrangement suitable for measuring integral current without resolving it into pulses can be constructed.

A multiplier tube manufactured by CBS Laboratories (Stamford, Connecticut) can be used for the recording of variable high-neutron dose rates. Its photocathode is replaced by a coating of fissionable material and the tube is designed primarily to measure low fast-neutron rates by means of counting single fission events. When it is inserted in a circuit similar to one shown in Figure 9.1 or 9.2, and after removal of the bakelite base and potting of the assembly to prevent external ionization, this tube can be used directly for the recording of medium- or high-intensity neutron pulses.

It is very difficult to construct fast-neutron-sensitive electron-multiplier SEMIRAD using recoil protons from the hydrogenous insert at the cathode of a standard electron multiplier. The outgassing and baking of the multiplier tube, essential for its good performance, has to be accomplished at high temperatures and this ruins the inserted plastic. Such a system can be constructed by use of an electron multiplier that does not need baking and is called "Windowless Photo Detector M–306 Multiplier," manufactured by the Bendix Corporation, Cincinnati Division. Figure 9.5 shows the sensitivity of the device versus applied voltage. The rise time of the tube is less than 5×10^{-9} sec. To use the device for neutron detection, one has to replace the "entrance grid" with a piece of hydrogenous plastic made conductive by means of an evaporated coating.

Limitations of the Electron-Multiplier SEMIRAD. Experimenting with the electron-multiplier system, we found that its operation unfortunately depends in some cases on the total dose delivered to the instrument during the radiation pulse. One obtains true pulse shapes only if the total energy expended on the last dynode is low enough to prevent development of temperatures high enough to cause thermionic emission. Upon heating of the last dynode, emission may last for some time after the pulse has passed and result in an erroneous tail on the pulse recording.

The total energy delivered to the last dynode is given by

$$E = NV \ (ev) \tag{9.4}$$

where N is the total number of electrons delivered to the last dynode during the pulse, and V is the accelerating voltage to the last dynode. The usual photomultiplier tubes can be used only for pulses of a few microseconds duration. This restriction is caused mainly by the time-spread which the electrons suffer while traversing the tube. Several new developments, however, make it possible to use photomultiplier tubes for radiation pulses of much shorter duration. For example, with the RCA PM tube 70045A, transit times of less than $5 \cdot 10^{-10}$ sec can be obtained by successive acceleration and deceleration of electrons at each stage.

L. F. Wouters and coworkers developed an ultrafast photomultiplier with a high current output (Reference 54). The transit time per stage in this device is only $3 \cdot 10^{-10}$ sec with a spread of approximately 10^{-11} sec. An experimental 12-stage tube was built. The current output of this tube is more than two amperes. Devices of this kind may be used as a PM SEMIRAD without modification wherever the recording of short and weak radiation pulses is desired.

CHAPTER 10

MEASUREMENT OF FAST-NEUTRON FLUXES IN AN ENVIRONMENT OF FAST NEUTRONS AND GAMMA RAYS

General. When we wish to measure the contribution of fast neutrons only in a mixed fast-neutron-gamma environment, we can either use a fast-neutron-sensitive and gamma-insensitive device, or measure the gamma and the gamma-plus-neutron flux simultaneously and subtract the readings. This can easily be accomplished for total-dose measurement. To measure total fast-neutron dose during a radiation pulse, threshold dosimeters can be used wherein the total dose is proportional to the induced radioactivity in a suitable material. Also germanium or silicon diodes have been used successfully (References 23 and 48)—the total neutron dose being measured by the change of lifetime of the current carriers.

The above devices record the total neutron dose independently of both the rate of delivery and the simultaneous gamma radiation, but cannot be used to measure dose delivery rate as a function of time. For fast-neutron flux measurement in a mixed environment, a system has been used that consists of two scintillation phosphors, one hydrogenous and one hydrogen-free, with two photocells. The hydrogenous phosphor can be any fast organic scintillator (for example, toluene or TS–28M Shell Oil Co. (paint thinner) with popop) and the hydrogen-free phosphor can be hexafluorobenzene and popop (Reference 24).

Such a device suffers from two important setbacks: (1) when the neutron flux is low compared to the gamma flux, it is very difficult to get reasonably accurate neutron data, and (2) even a hydrogen-free phosphor responds to fast neutrons because of the recoil of atoms with $Z > 1$. The typical neutron sensitivity of such a device is ~ 10 percent. If two SEMIRADS are used where one is gamma-sensitive and the other gamma- and fast-neutron sensitive, and the difference between their readings is calculated, this difficulty can be eliminated to a high degree. Even if high Z recoils are produced in the wall of the neutron-insensitive instrument, the recoils are very unlikely to enter the chamber and produce secondary electrons, since the energy transfer between a fast neutron and an atom with the $Z > 1$ is low and the range of the recoil is very short. This method has often been successfully used where neutron and gamma fluxes were comparable. However, use of two independent SEMIRADS does not help eliminate the first difficulty mentioned above, so a more advanced system was designed.

Gamma-Insensitive Neutron SEMIRAD Triode. (Reference 53.) A device based on the SEMIRAD principle has been constructed and the principles are shown in Figure 10.1. Compton, photo, or pair electrons, produced by incident gamma rays in the surroundings of the instrument or in the body of the instrument itself, produce secondary electrons from the thin metallic film with which the three plates are coated on their vacuum side. The structure of the plate surfaces facing the vacuum are made identical, and therefore the yield of the secondary electrons, which depends only on the structure of the emitter surface, is the same in all directions. The voltages applied to the plates are higher than the voltage corresponding to the energy of the secondaries. The polarity of the voltages is such that the secondary-electron current reaching the central plate is the same as the outgoing current. Thus the net external current produced by the gamma radiation measured between this plate and ground vanishes. The primary electrons have a very high energy and cannot be influenced by the applied voltage. In the case of a monodirectional gamma flux, the central plate (hydronenous material) provides an attenuation for the gammas and the net current does not quite vanish, but in a practical case this attenuation can be made very small.

The two outer plates contain no hydrogen nor any material that would easily produce high-energy particles when reacting with neutrons. In the central plate, which is made of hydrogenous material on one side and nonreacting material on the other, recoil protons are produced, some of which escape into the vacuum on the side where the evaporated metallic layer does not absorb them. When crossing the interface, these protons produce secondary electrons that can leave the plate on one side only and thus produce an electric current proportional to the fast-neutron flux.

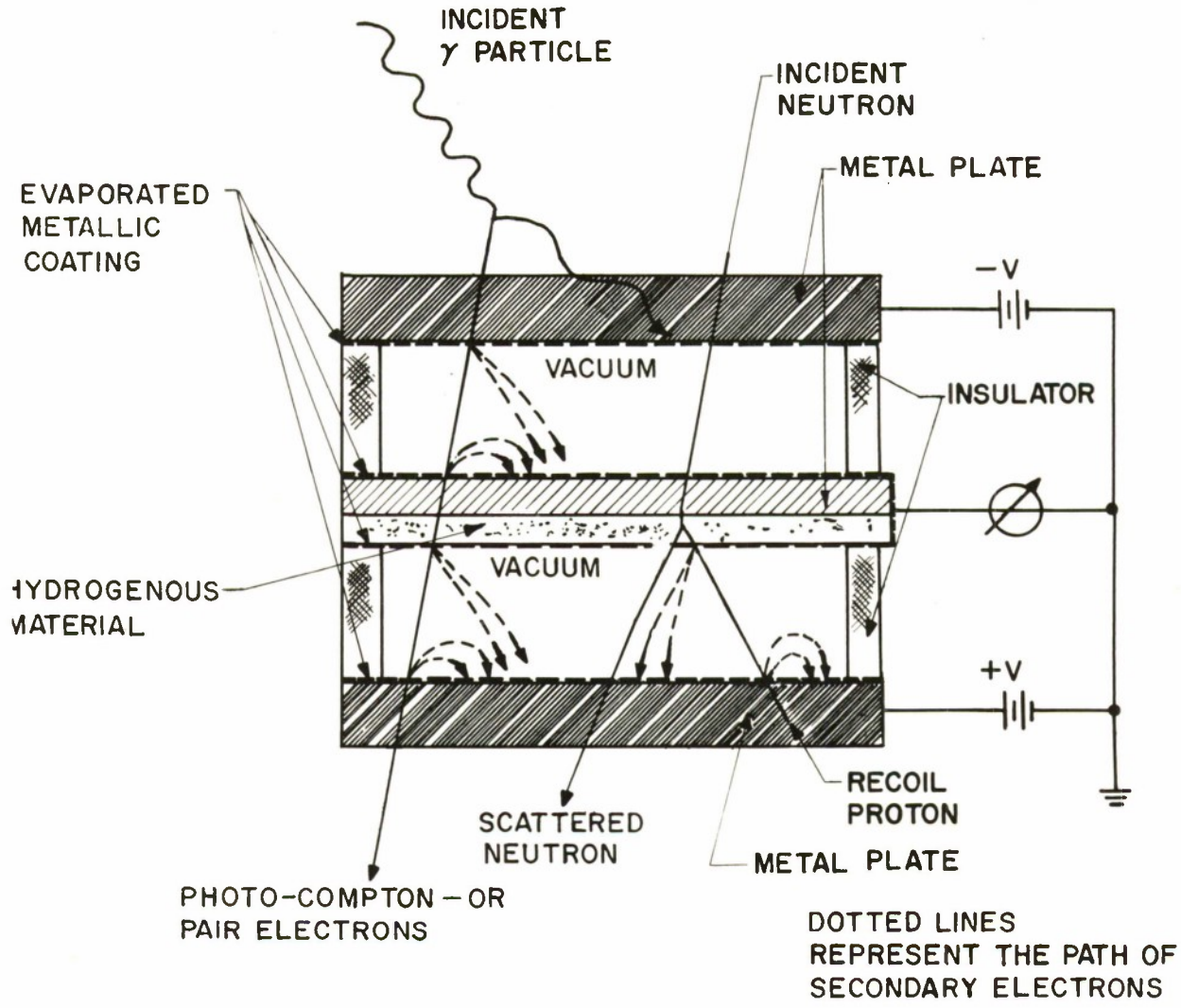


FIGURE 10.1. *Principle of operation of the gamma-insensitive fast-neutron device.*

This current is not compensated by another current, and can be measured by an external meter or displayed on an oscilloscope. Thus, the fast-neutron flux can be determined independently of the simultaneously present gamma environment. Obviously, the fast neutrons also produce recoils with $Z > 1$ in the exterior plates. As explained previously, however, the probability that they will cross into the vacuum is very small. Their contribution to the measured current can be made negligible even for high-neutron-scattering cross sections in the outer wall material.

Description of the Instrument and Its Construction. Figure 10.2 shows the actual construction of the instrument. The plates are circular and equal in area. The insulation between them is provided by alumina ceramic rings with Kovar flanges (metal-to-ceramic seals). The external plates are heliarc-welded to the flanges. The external plate facing away from the incoming radiation has two openings: one for a Vac Ion pump used to monitor the vacuum and to improve it if necessary, and the other for the copper tubing for the tip-off. The outer Kovar plates are lined on the inside with aluminum plates. The aluminum was buffed to a high polish and then coated with a 0.1 mg/cm^2 layer of evaporated gold.

The central plate assembly is wedged between the two heliarc-welded flanges and consists of 1-mm-thick glossy Mylar on the side away from the incoming radiation and of 1-mm-thick aluminum on the side facing the incoming radiation. For best results, the Mylar should be as thick as the range of the highest energy protons expected in

the environment. Again the sides facing the vacuum are coated with a 0.1 mg/cm² layer of gold that serves as the emitter for the secondary electrons and makes the Mylar surface conductive at the same time. The measured resistance of the gold layer was 0.1 ohm across the disc. The vacuum that could be obtained and permanently maintained in the system was 10^{-6} mm Hg after a prolonged application of the ion pump. This was made possible only by elimination of the moisture from the Mylar by heating it in a vacuum to 150° C before the evaporation with gold. After it was sealed, the assembly was placed in a thin-wall brass can with three hermetically sealed coaxial-cable connectors, each of which was electrically connected to one of the three plates. The can was then filled with an insulating plastic potting compound to a level slightly above the top plate to avoid the presence of air around the sensitive parts of the system. The presence of air would produce an unwanted ionization-chamber effect, whose signal would be superimposed over the secondary-electron signal and give erroneous readings. Solid-dielectric, 70-ohm, coaxial cable connected the can to a Keithley 610A electrometer for calibration. Two other cables supplied the necessary voltage to the outer plates (+300 volts, −300 volts). After proper termination of the signal cable and connection with the readout scope located outside the radiation area, the instrument can measure the neutron dose rate as a function of time.

Calibration and Performance of the System. To establish the X-ray sensitivity, or rather, insensitivity of the device, X-rays from a 250-kv machine were used. The fast-neutron calibration was made using Be(*D*, *n*) neutrons from a 2-Mev Van de Graaff accelerator. The signal current was measured with a Keithley 610A electrometer. The readings depended on the way the voltage was applied. For 1.7 rad/sec 250-kev X-rays (1.1-cm Cd filter) with polarity of −300 *V* at the side facing the radiation and +300 at the other, the sensitivity was approximately 3.10^{-14} a/rad/sec, and with reversed polarity, we obtained similar results. For equal polarity on the outside elec-

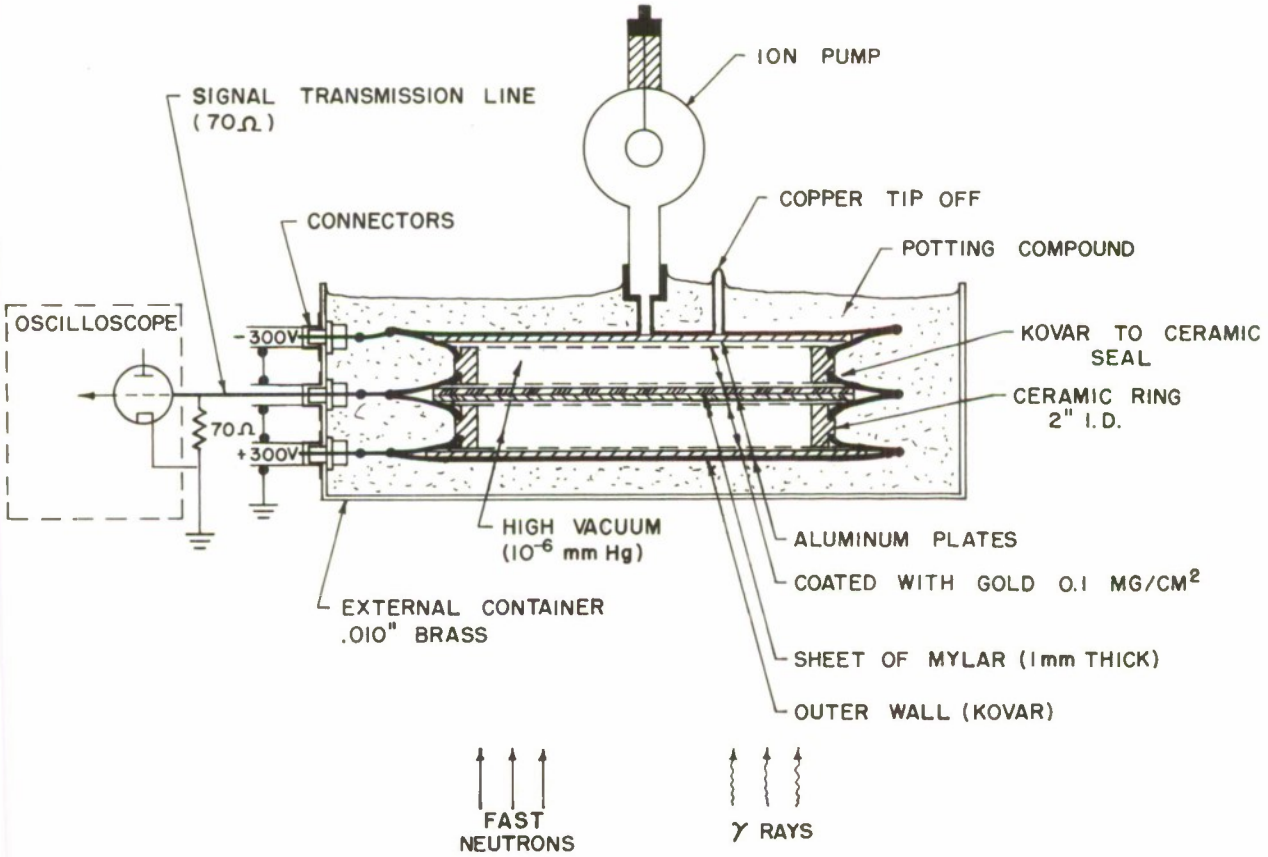


FIGURE 10.2. *Construction of the fast-neutron "triode."*

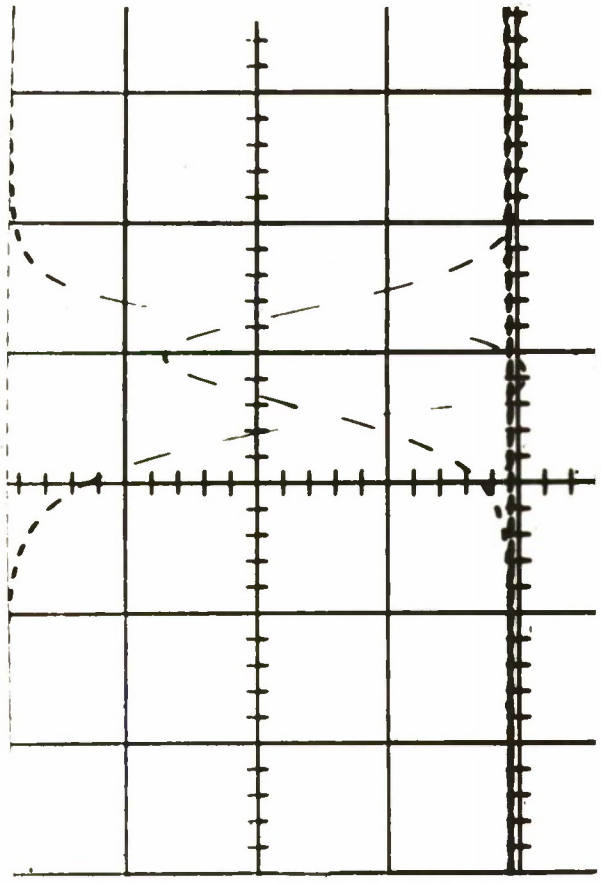


FIGURE 10.3. *Exposure (SPRF) of a "triode" for neutron rate as a function of time (positive pulse), and of a "diode" for gamma rate as function of time (negative pulse). Time scale: 50 μsec per division; Readout: 555 Tektronix scope; Sensitivity setting: diode—0.005 v/cm triode—0.05 v/cm; Distance from center of SPRF: diode—23 cm; triode—28 cm; total dose at the point of measurement: diode—2.01×10^3 rads (gammas) triode—1.68×10^4 rads (neutrons); peak dose rate for fast neutrons (Watt spectrum) for the triode: 3.53×10^8 rads/sec. Peak gamma dose rate (fission gammas) for the diode: 4.08×10^6 rads/sec.*

trodes, the system becomes, in the absence of neutrons, an X-ray detector, and its sensitivity was $6.4 \cdot 10^{-11}$ a/rad/sec. The fast neutrons yielded a sensitivity of $1.7 \cdot 10^{-11}$ a/rad/sec at the intensity of 0.3 rad/sec.

Figure 10.3 shows a typical application of the instrument to measure the neutron output of a fast reactor (SPRF, Albuquerque, New Mexico) as a function of time. The signal from the instrument followed the Godiva output. The peak rate at the point of exposure was $3.5 \cdot 10^8$ rad/sec (fission neutrons). Two separate instruments were exposed: (1) a neutron-sensitive gamma-insensitive "triode"; and (2) a gamma "diode." The resulting sensitivity obtained from these experiments for the triode is $5.6 \cdot 10^{-12}$ a/rad/sec.

Side Effects Induced by Radiation in the "Triode." Using the "triode" system, one can make a measurement which determines the influence of the cable and related effects caused by radiation on the calibration of the instrument and on the pulse recording. Let J_I through J_{IV} be the signal currents obtained with one and the same instrument in a constant radiation field with the following polarities on the outer plates:

J_I upper plate positive, bottom plate negative,
J_{II} upper plate negative, bottom plate positive,
J_{III} upper plate positive, bottom plate positive,
J_{IV} upper plate negative, bottom plate negative,

Further let i_1 through i_4 be the secondary electron currents between the plates so that

i_1 is the current from the top plate to the center plate,
i_2 is the current from the center plate to the top plate,
i_3 is the current from the center plate to the bottom plate,
i_4 is the current from the bottom plate to the center plate.

The following equations must be then satisfied:

$$\begin{aligned} J_I &= i_2 - i_4 \\ J_{II} &= -i_1 + i_3 \\ J_{III} &= i_2 + i_3 \\ J_{IV} &= -i_1 - i_4 \end{aligned} \qquad (10.1)$$

These equations apply regardless of how inaccurately the surface composition and the areas of the emitting surfaces are constructed. From 10.1 it follows that

$$J_I + J_{II} = J_{III} + J_{IV} \qquad (10.2)$$

After measured data for J_I through J_I are substituted, every deviation from the relation 10.2 must come from cable effects, traces of external ionization, polarization effects in the potting compound, and other side effects. We found that at dose rates of several rads per second encountered during X-ray and neutron calibration of the instruments, the side effects contribution was from zero to about 100 percent of the measurement, depending on the



FIGURE 10.4. *Assembled fast neutron SEMIRAD "Triode" (with ion pump attached to the top plates).*

quality of the experimental setup. We also noticed that these effects saturate at about 3×10^3 r/sec intensities and can, therefore, be neglected while working with very high intensities.

Devices similar to those described above were constructed with coatings of fissionable materials instead of hydrogenous foils, but we found it much more difficult to reproduce surface conditions (gold coating) on all plates because the uranium-coated surfaces were rough. To make the device sensitive to slow neutrons, one can use a boron coating on the neutron-sensitive part of the central plate (see Chapter 11). A photograph of a typical assembled fast-neutron SEMIRAD "triode" is shown in Figure 10.4.

The device is directional and the maximum sensitivity is obtained when the radiation enters perpendicularly from the side of the negatively charged electrode (for hydrogenous insert only). The insensitivity to gamma rays, however, is not dependent on the angle of the incident radiation. In the design of the device, one should consider the following points: (a) the sensitive area must be equal on all three plates, and the machining must be done with very low tolerances; (b) the central plate should be thin (about one mm) to prevent absorption of the gamma radiation in the central plate itself and thus produce asymmetry between the upper and the lower chamber; (c) the surface structures of all plates on the vacuum side should be equal (if a polished plastic coated with aluminum is used for the neutron-sensitive part, the other surfaces should be made of polished metal and also coated with the same thickness of aluminum); and (d) the distance between the plates should be equal and as small as the construction allows (about 5 mm) to minimize contribution of secondary electrons from the insulator separators that might result in the charging-up of the insulator. To avoid directionality of this type of SEMIRAD, two or even more such devices might be used simultaneously back to back, with common signal output.

CHAPTER 11

CONSTRUCTION OF SEMIRAD DIODES AND DIODE-TYPE DOSIMETERS

General. At the present time, instruments based on the SEMIRAD principle are being commercially produced in conjunction with U.S. Army, Navy, and Air Force contracts. Among the contractors are: Bendix Corporation, Cincinnati Division, which is working on "fountain-pen dosimeters" (Reference 25) using the SEMIRAD principle; Reuter and Stokes (Cleveland, Ohio), the EON Corp. (Brooklyn, N.Y.), Edgerton, Germeshausen & Grier, Inc. (Santa Barbara, California), and Nuclear Corporation of America (Denville, New Jersey), which are manufacturing SEMIRAD gamma and neutron diodes (Eon Tube Type 7316). Applications of SEMIRAD instruments are so different in individual cases, however, that many times the instruments have to be built by the experimenters themselves to suit their particular needs. For this reason, the following general instructions for designing and manufacturing SEMIRAD instruments are presented.

In general, one must stress the importance of the choice of the material from which the instrument, its case and shield are fabricated. The output of the instrument is proportional to the delivered dose in rads or to the delivered doserate in rads per seconds in this particular material. For this reason, it is more convenient to use low Z materials (aluminum or titanium) for the construction.

Construction of Gamma-ray Sensitive Diode. This device can be built with a standard envelope of any suitable steel electron tube as a body. We used a steel envelope of a 6L6 tube, which is 3 cm in diameter and 8 cm high. This envelope was lined inside with a pure aluminum layer 0.025 cm thick. A round disc of aluminum was inserted loosely at the end of the tube to prevent the gettering material at the end of the tube from distributing itself over the emitter surface during its firing. A rectangular piece of aluminum plate with one side equal to the length of the tube and the other to its circumference was then rolled in the form of a cylinder and held the round piece in place. The aluminum lining of the wall provides a well-known, reproducible, and constant secondary-electron emitter surface.

A stainless steel disc was then machined 0.08 cm thick with a diameter equal to the lip of the envelope. This disc had two holes, one in the center for the insulator and one off center into which a soft copper tubing was soldered. We used a Cerama Seal Inc. #52736/3 Alumina High-Temperature Terminal. This insulator was soldered in the stainless steel disc with soft solder, which proved to be a good vacuum seal; however, we could have applied brazing or welding with better success.

The central electrode was soldered on the short

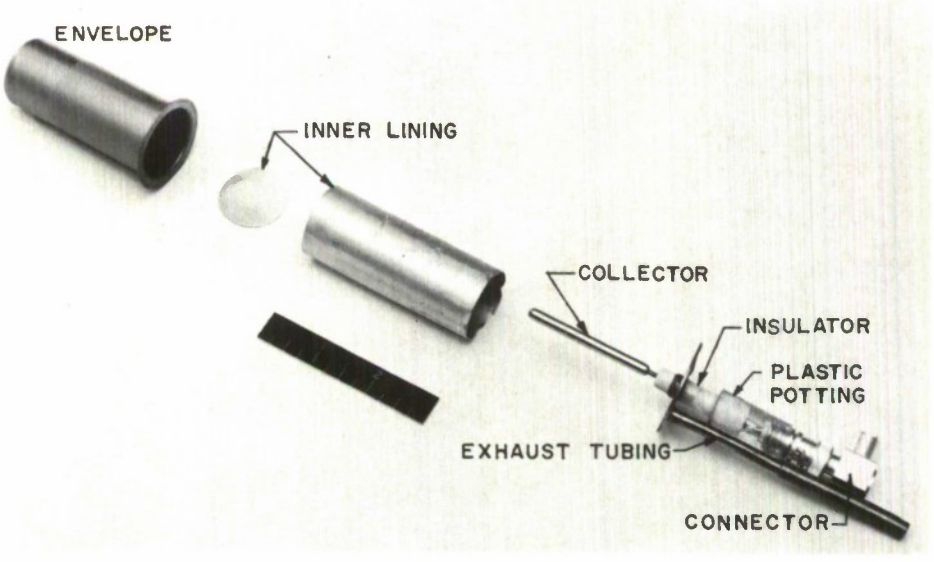


FIGURE 11.1. *Gamma-ray SEMIRAD diode disassembled.*

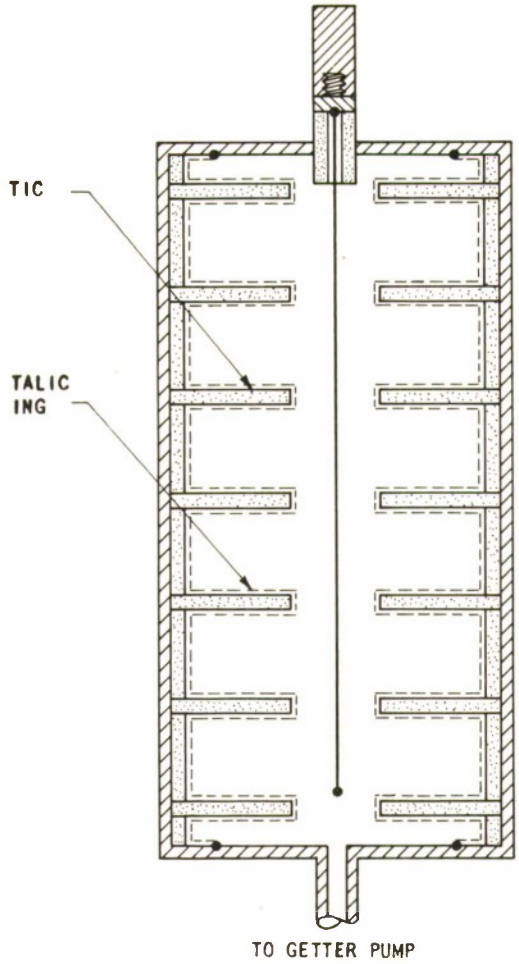


FIGURE 11.2. *High-sensitivity neutron-sensitive SEMIRAD diode with large emitter area.*

end of the central lead of the insulator. It was made from 0.48 cm stainless steel rod 5 cm long, rounded on top and polished. The 0.48 cm thickness was chosen to make the collection of all secondary electrons more likely (Figure 11.1). If a collector electrode with a very small diameter is used in a cylindrical geometry, some secondary electrons, which are emitted at a large angle to a line perpendicular to the emitter surface, miss the collector if the collecting voltage is not too high (Reference 45).

The stainless steel disc was heliare-welded to the envelope. Then the assembly was tested for leakage with a helium leak detector and evacuated through the soft copper pipe, and the getter fired. The tipping off was done by cutting off the copper tubing with a special tool. The seal thus obtained did not leak air.

Onto the exterior of the central electrode was soldered the connector Amphenol UG 1094/U, and the exposed part of the center lead was potted with Hysol #620 potting compound and "C" hardener (ratio 3:1). The instruments thus constructed had the sensitivity of $\sim 3.6 \times 10^{-10}$ a/rad/sec for Co^{60} gamma rays. This data may vary by 50 percent between individual instruments.

Figure 11.2 shows the cross section through another type of SEMIRAD diode. This device was constructed with ribs on the emitter to increase its area and therefore enhance the sensitivity.

Titanium SEMIRAD. A very reliable gamma diode was constructed using Titanium as the wall and collector material. The advantage of Titanium is that if it is thoroughly outgassed, a high vacuum can be maintained easily without a getter. The wall surface is also a well-defined secondary electron emitter. The construction of such a SEMIRAD is shown in Fignre 11.3. The insulator is made of alumina and is vacuum-soldered to the collector and the main body with nickel. All parts, including the ceramic, must be thoroughly outgassed before assembly and evacuation. All tubes have a reproducible sensitivity of 3×10^{-11} a/rad/sec measured with Cs^{137} gamma rays.

To use the tube for experiments where little or no electromagnetic effect is expected, we mount an NBS connector on the central electrode, fix a sleeve to extend the body on the ceramic side, and fill the space between the sleeve and the connector with a potting compound. For use in a strong electromagnetic environment, we must protect the tube against external ionization as well as against EM pickup. The tube is inserted in a hollow steel cylinder and Teflon spacers keep it concentric. The signal side leads to a modified General Radio Type 874 connector and the wall to a modified 10-kv amphenol connector. The inside is filled solidly with paraffin. The voltage and the signal ends are connected with a coaxial cable and the air spaces in the connectors are completely filled with silicon grease (Figure 11.3).

For very fast, high-intensity pulses the voltage is supplied from a paraffin-packed and EM-shielded low-inductance condenser bank, which is located close to the tube but possibly outside of the radiation field and is fed by a battery power supply (Figures 11.3, 11.4, and 11.5A). The sensitivity of the armed diode is reduced by the added shielding and is 1.44×10^{-11} a/rad/sec for Cs^{137} gammas when irradiated perpendicular to the axis of the instrument and 0.68×10^{-11} a/rad/sec when the gammas arrive parallel to the axis of the instrument through the potted high-voltage connector.

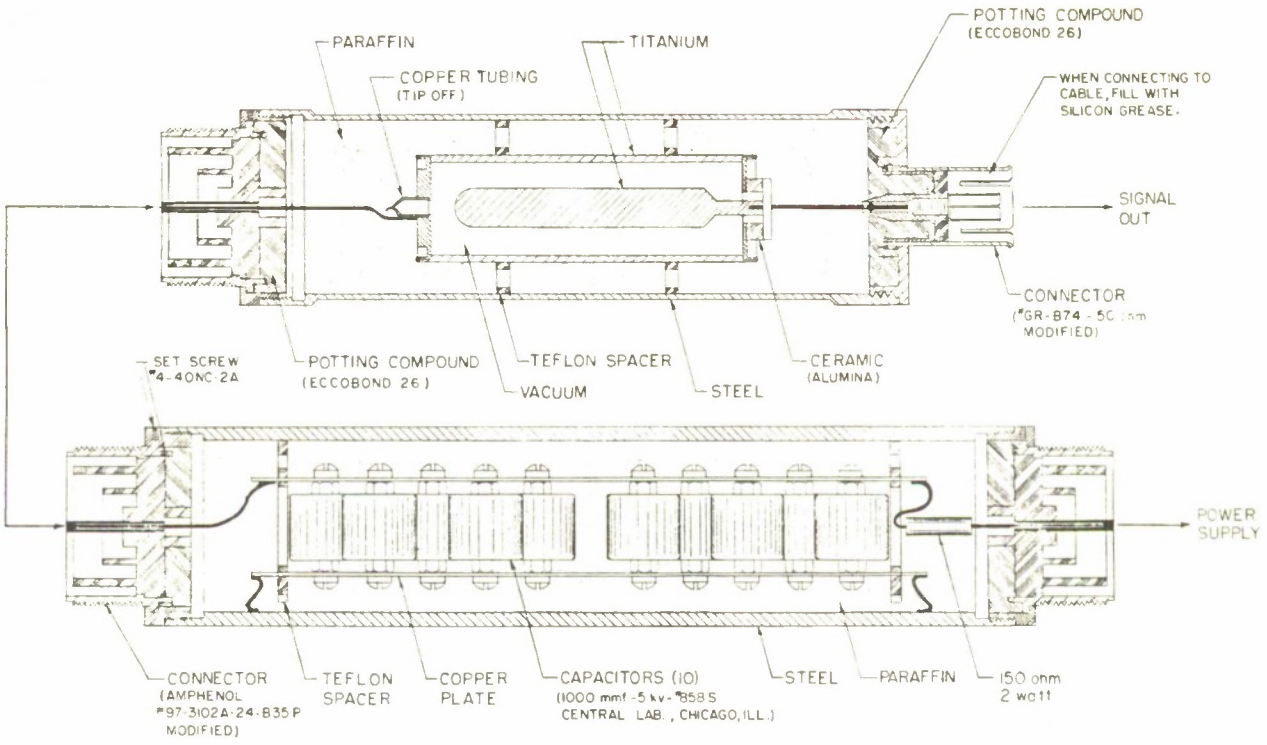


FIGURE 11.3. *Electromagnetically shielded SEMIRAD gamma diode with a condenser bank.*



FIGURE 11.4. *Shielded gamma diode (disassembled).*

An improved type of the titanium wall gamma sensitive instrument is shown in Figures 11.5B and 11.5C. The insulation between the chamber wall and the EM shield is made of shrink-tubing and, therefore, the bulk of the assembly is strongly reduced. The ratio of diameters between the emitter wall and the collector cylinder and the geometry of the brass piece which connects the collecting electrode with the output connector are chosen so that the whole tube has the characteristic impedance of 50 ohms. If the output is connected to the read-out oscilloscope by means of a 50-ohm coaxial cable,

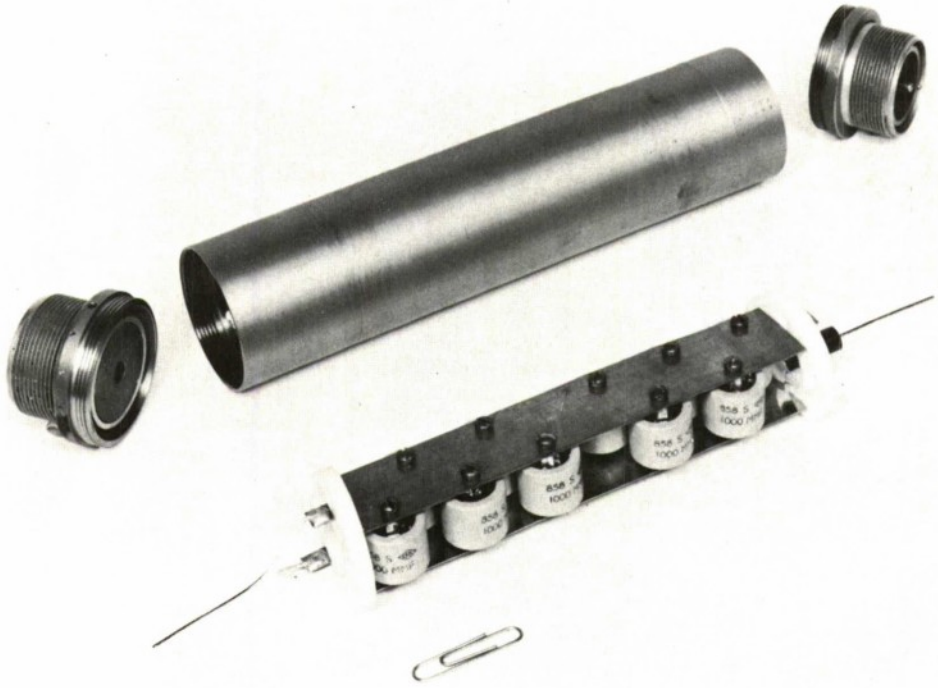


FIGURE 11.5A. *Low-inductance condenser bank (disassembled).*

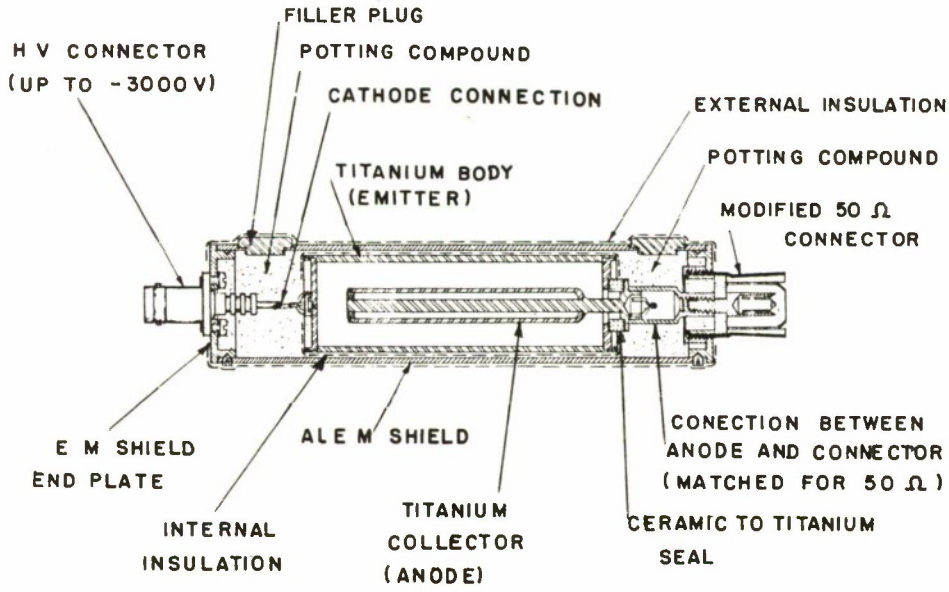


FIGURE 11.5B. *Assembly of the EON Tube 7316.*



FIGURE 11.5C. *Assembled EON Tube 7316, EM shield, and diode assembly.*

the instrument can be considered a part of the cable; with proper termination at the oscilloscope, a high time resolution can be obtained.

Substitute for a Gamma-sensitive SEMIRAD Diode. A simple substitute for a gamma-sensitive SEMIRAD diode can be obtained very easily. Any electron tube with a steel envelope can be used for this purpose. To build the instrument, the bakelite socket must be removed from the tube, and a check made to see if one of the leads coming through the glass base is internally connected to the steel envelope. If so, this lead has to be soldered to the exterior of the envelope. The remaining leads are then shorted together and connected to the central conductor of a coaxial cable, as shown in Figure 11.6. The entire bottom of the tube is then potted with a suitable compound to prevent the external ionization effect. The battery is applied between the grounded shield of the coaxial cable and the tube envelope and the instrument is ready for use.

In some cases this substitute may not give results as satisfactory as the SEMIRAD diodes that are especially constructed for this purpose because (a) their exposed internal insulator (glass base) is relatively large, (b) the secondary emitter surface (inner surface of the envelope) is not well defined, and (c) the geometry of the collector electrode (interior components of the tube shorted together) is complicated and unknown. For most experiments, for example the recording of the dose rate as a function of time in experiments concerning radiation damage on components, the SEMIRAD thus designed were never the less used successfully.

Figure 11.6A shows a most satisfactory recording of the SPRF pulse taken in the immediate proximity of the reactor (Sandia Godiva with a modified 6L6 tube). The reason for the relatively short half width of the pulse (~ 45 μs) is that a new fuel element was installed just before the experiment.

Construction of Neutron-Sensitive Diodes. The same components used in a gamma-sensitive diode can be used in a neutron-sensitive device for insulator, envelope, and collector. The emitter electrodes, however, must be made in a different way. The thickness of the hydrogenous material used for the wall lining should be greater than the range of the highest energy proton expected during the measurement and smaller than the mean free path of the lowest energy neutron. Figure 4.2B shows the ranges of protons as a function of their energies for plastic.

The plastic, as mentioned before, has to be coated with a layer of metal on both sides to make its surface conductive. The conductivity has to be low enough to prevent voltage buildup during the measurement of a high-intensity pulse, where high currents can be encountered. On the other hand, the coating should be thin enough so that the lower

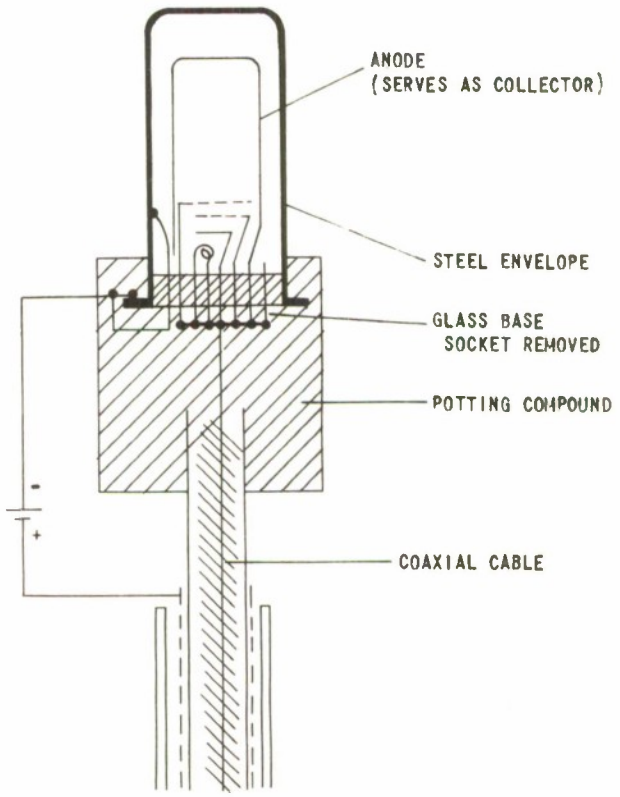


FIGURE 11.6. *Gamma-sensitive SEMIRAD diode made from an old 6L6 electron tube.*

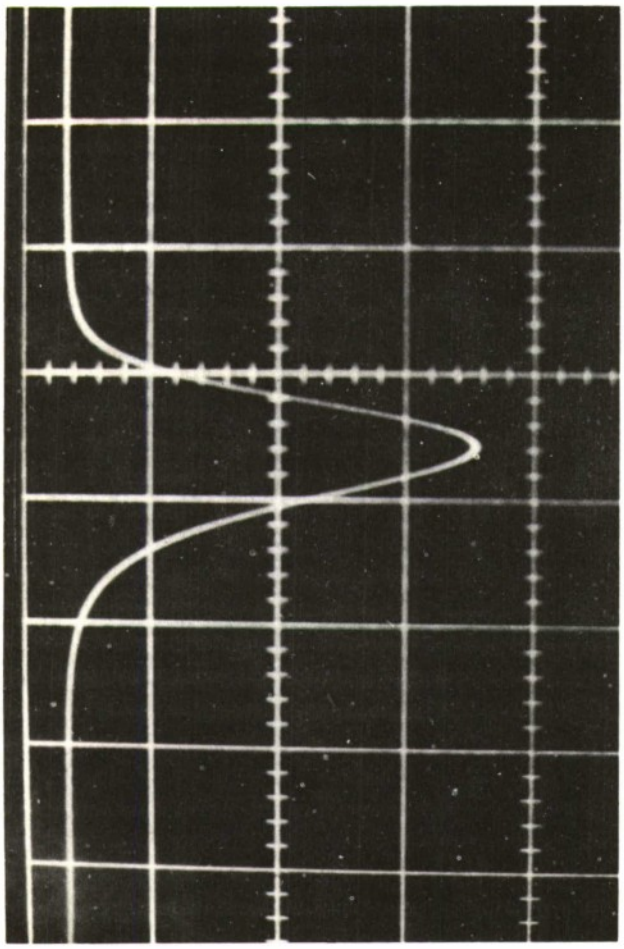


FIGURE 11.6A. *SPRF gamma pulse recorded with a modified 6L6 tube 20 cm from the center of the reactor. Time scale: 50 μs per division. Peak dose rate: ~ 3×10^7 rad/sec.*

energy recoil protons leaving the plastic are not absorbed or their energy seriously affected by the coating.

If I_{max} is the maximum expected secondary electron current through the instrument during a pulse measurement, and R the resistance between two opposite points on the coating, then the maximum voltage drop between the electrodes during the measurement will be:

$$\Delta V_{max} = I_{max} R \tag{11.1}$$

For reliable results ΔV_{max} should be smaller by an order of magnitude than the applied potential. In some of our laboratory devices we used mylar sheets coated with an aluminum layer on each side. The aluminum was evaporated onto the mylar in vacuum. The finished sheet had a transparency of 3.5 percent to visible light and a resistivity of 44 ohm-cms. Better results were obtained with gold, where a layer of 0.1 mg/cm^2 had a resistance of 0.3 Ω across a 5 cm disc. The sheet is then cut into rectangular pieces as long as the envelope, and about 1.3 cm wider than the circumference of the housing cylinder. The cutout piece is then rolled together and inserted in the cylinder. It is very important that the two edges parallel to the cylinder axis overlap because this provides electrical continuity between the inside and the outside aluminum coating, as shown in Figure 11.7. The contact between the metal envelope and the housing is made by the tension of the plastic against the outside wall.

Any deviations from cylindrical geometry caused by the application of the above technique are of no consequences for the performance of the instrument. To keep a check on the outgassing of the plastic, we must insert a titanium pump (see Chapter 2) or solder a small ion pump permanently to the instrument. In our laboratory instruments, permanent pressures of less than 10^{-4} mm Hg were obtained using the Vac Ion pump. Figure 11.8 shows an experimental model of a fast-neutron diode made as described above.

Construction of Neutron-sensitive Diodes Using Fissionable Materials and Boron. These instruments can be made by use of the same components as for the SEMIRAD with hydrogenous wall, except that the emitter lining has to be made different.

The fissionable material sensitive to fast neutrons is U^{238}. It is important not to use natural uranium, which is an isotope mixture, but one where the U^{238} isotope has been isolated by isotope separation. Such a material is expensive and difficult to obtain. The reason for the required purity is evident from the fast- and slow-neutron fission cross sections for U^{238} and U^{235}. The cross-section curve for U^{238} is shown in Figure 11.9 (Reference 44). For U^{235} the cross section is very high for slow neutrons (582 barns at 0.0253 ev) and it decreases for higher energies (about 1 barn at 10 Mev) (Reference 44, pages 330–336). Therefore, in practical application, to obtain a good insensitivity for slow neutrons, the concentration of U^{235} in U^{238} should be of the order of 1 part in 50,000. Using this material, the sensitivity of the instrument for thermal neutrons is approximately one percent of the fast-neutron sensitivity.

It is evident from the fission cross sections that the U^{235} isotope should be used as an emitter coating to measure slow neutrons. The requirement of high purity is not as critical as in the previous case and it is sufficient to use the U^{235} enriched isotope mix-

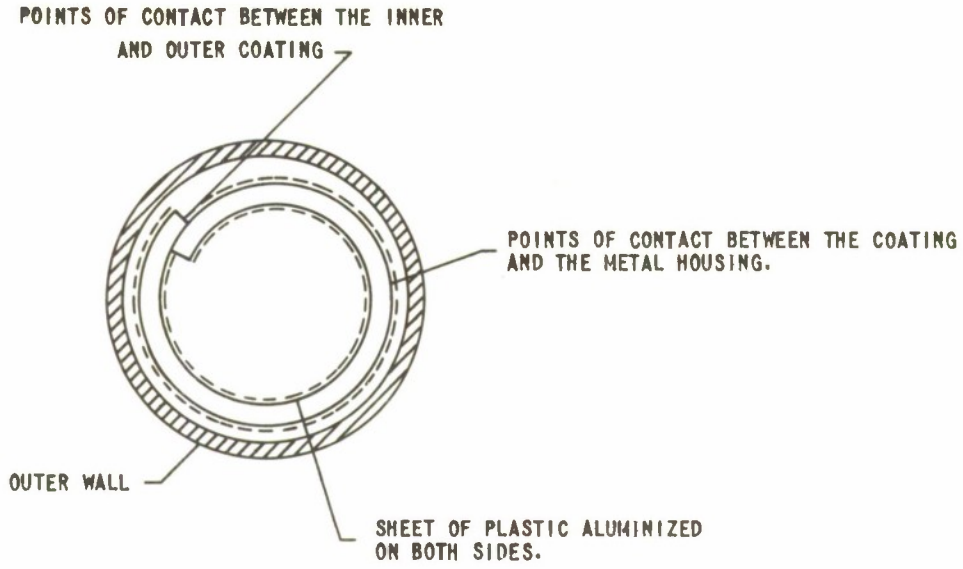


FIGURE 11.7. *Assembly of the flexible, metal-coated, plastic insert in the fast-neutron-sensitive diode.*

ture. In environments where very many fast neutrons and only very few slow neutrons are present, highly enriched or pure U^{235} should be used. To detect slow neutrons, a wall coating of the natural boron isotope mixture can be used. Here the nuclear reaction $B(n, \alpha)$ takes place, which has the cross section 575 barns for slow neutrons. The alpha particle produces secondary electrons whose current is then measured. The coatings of uranium and boron are made commercially by different companies, i.e., EON Corporation, Brooklyn, N.Y., Reuter and Stokes, Cleveland, Ohio, Westinghouse Corporation, Elmira, N.Y., and several others.

The coating is made by electroplating or by evaporation on metal foils. The coatings obtainable commercially are made to suit the requirements of neutron detectors based on the ionization chamber type. The uranium coating on a foil is not in metallic form but in the form of uranium oxide; therefore, the coating surfaces are not electrically conductive, as required in the SEMIRAD application, and they outgas in a vacuum.

To make the commercial coatings conductive, a transparent metal layer (gold or aluminum) should be evaporated on top of the coating in the same way as in the case of the hydrogenous SEMIRAD, and the foils should be fired in a vacuum oven to remove the absorbed gases. The remaining part of the processing is then the same as in the latter case. The thickness of the coating of neutron-sensitive materials should be chosen so that it equals approximately the range of the reaction product, with the highest energy expected in the reaction to obtain maximum sensitivity. For fissionable coatings made from U^{235} or U^{238}, the optimum thickness is about 2 mg/cm^2.

Construction of Gamma and Neutron Dosimeters Based on the SEMIRAD Principle. There is need for a tactical-delivered-dose meter which measures gamma and neutron doses, and does not saturate at high intensities. This is required, for example, for monitoring the exposure of personnel involved in pulsed radiation research or in cases of the exposure of persons and devices to the initial radiation from

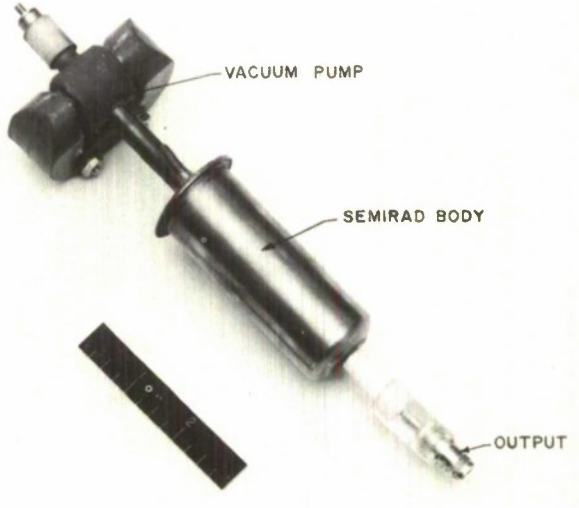


FIGURE 11.8. *Assembled fast-neutron-sensitive diode with an ion pump attached permanently to its body.*

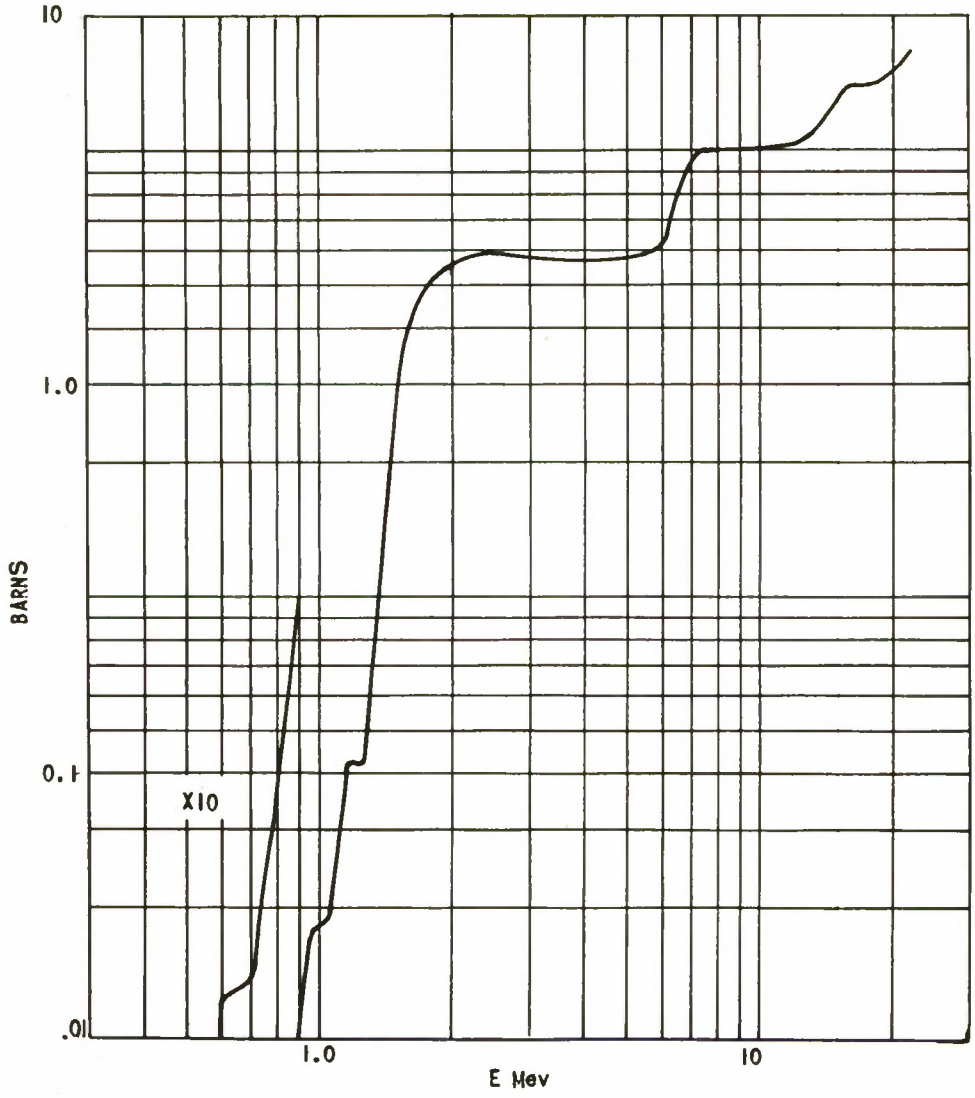


FIGURE 11.9. *Fission cross section as a function of neutron energy for* U^{238}.

an atomic weapon. A gamma-neutron film badge system cannot be considered tactical since it involves processing before the total dose data can be obtained.

The commonly used, very practical "fountain pen dosimeter," which works on the ion chamber principle, starts showing saturation at dose rates of about 10^7 rads/hr. Investigations were undertaken, however, to convert this type of instrument from an ion chamber to SEMIRAD operation. We simply drilled a hole in the body of a 200 mr IM–93 instrument with an hydrogenous wall, soldered a piece of tubing at the opening, and attached it to a vacuum pump. This converted instrument could not be successfully tipped off and kept under vacuum. It is constructed vacuum-tight, but the components used inside outgas very strongly.

While it was being pumped, successful calibrations on gamma rays and neutrons were made and the main observed change was a superior energy dependence, and much lower sensitivity. The sensitivity of a 200 mr ion chamber IM–93 was found to be approximately 500 rads for the whole scale, almost exactly what is required of a tactical instrument. The sensitivity was now dependent on the polarity applied to the collector.

Figure 4.1 shows a typical calibration of such an instrument. Measurements on Godiva II revealed that no saturation was observed up to 3×10^8 rads/sec in a mixed neutron-gamma environment.

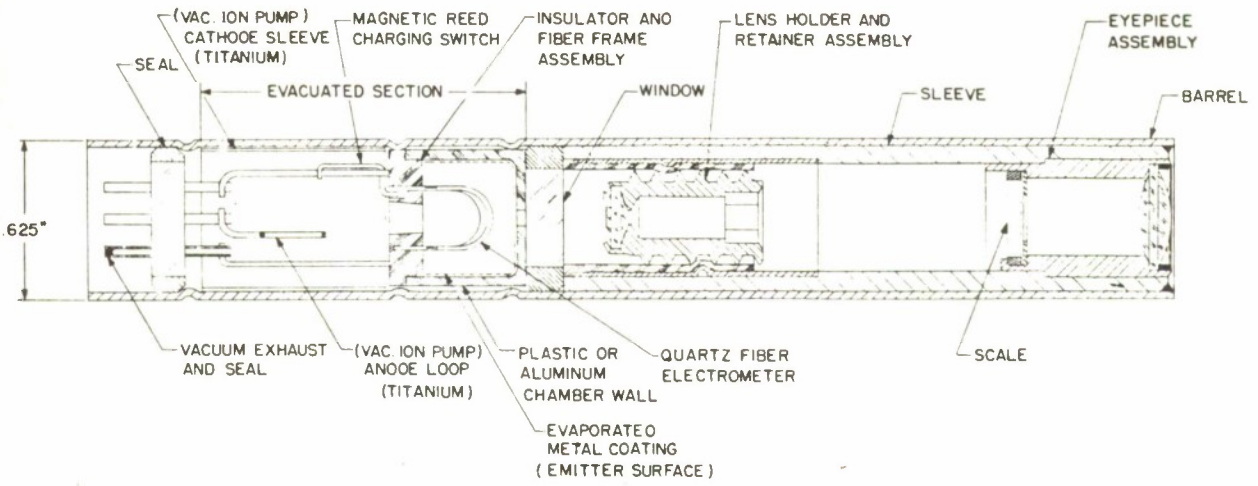


FIGURE 11.10. *Bendix total-dose meter for neutrons and gammas based on the SEMIRAD principle IM 185.*

The vacuum problem was solved by the Bendix Corporation, Cincinnati Division, under a U.S. Air Force Contract (Reference 25).

Figure 11.10 shows the engineering drawing of the SEMIRAD quartz-fibre dosimeters, and Figure 11.11 the photograph of an experimental model. It consists of an evacuated section which contains the charging apparatus, the chamber, the quartz-fibre electrometer, and the air-filled section with the optical system and the scale. The plastic required for the high-quality insulator and for the emitter wall does not outgas even at raised temperatures.

The charging of the quartz-fiber electrometer is accomplished by means of a magnetic switch (Reference 49) rather than by means of a bellows switch, as in ion chamber models. The present device has a permanently built-in, very small, titanium ion pump, located in the evacuated section so that in case the vacuum should become worse the instrument can be repaired quickly and simply. The charging of the instrument to approximately 150V before irradiation is done with a separate battery-operated charger.

During operation only the quartz-fiber electrometer assembly is charged: all other parts are on ground potential. Therefore, only the secondary electrons emitted from the aluminium coating of the



FIGURE 11.11. *Experimental SEMIRAD Quartz Fiber Dosimeter.*

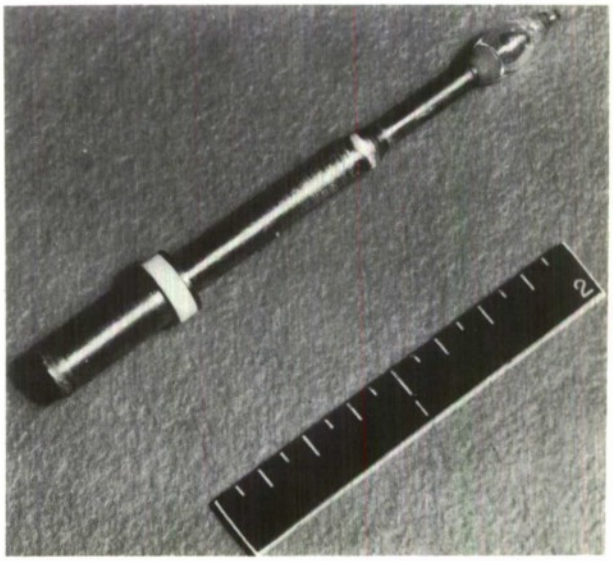


FIGURE 11.12. *Photograph of the MgO-RAD.*

chamber wall are collected and contribute to the readout, while the secondary electrons in the section containing the ion pump are ignored. Two versions of the instrument are under development: a neutron-gamma ray, and a gamma instrument.

High Yield Miniature SEMIRAD (MgO-RAD). The Techniques Branch of the U.S. Army Electronics Command laboratories, Fort Monmouth, New Jersey, developed a very small instrument, 1.8 cm in length and 0.6 cm in diameter, for recording of gamma pulses, particularly for use in experiments in the TREE (transient effects on electronic components) area (Reference 57). To compensate for the small emitter area of the instrument, the emitter wall is coated with a high secondary-electron-yield layer consisting of Magnesium Oxide and Magnesium Oxalate. As was mentioned in Chapter 4, such a coating presents serious problems because it is an insulator, but in some practical applications the device seems to perform dependably. Figure 11.12 shows a photograph of such a device. The typical sensitivity for gamma radiation of the MgO-RAD is $4 \cdot 10^{-8}$ amperes per rad per second.

Improved SEMIRAD with Guard Ring. An advanced type of neutron-gamma diode was recently constructed by the Nuclear Corporation of America for use by the U.S. Navy. After some modification, the same design was used by E.G.&G. for the United States Air Force.

Each unit has a built-in ion pump whose terminal is connected to the outside shield and grounded. The negative voltage of 4000 V applied to the wall of the instrument serves simultaneously to collect the secondary electrons and to operate the pump continuously while in use.

The pump magnet is sufficiently far away not to interfere with the collecting electrode. The insulator consists of two sections completely separated by grounded metallic guard ring as described in Chapter 7, page 48.

Such instruments were exposed successfully to intense mixed radiation without any shielding of the output connector. Their absolute calibration can be made very accurately, and the error observed at several consecutive Godiva pulse recordings was within the width of the oscilloscope trace.

CHAPTER 12

PULSED RADIATION RATE MEASUREMENTS WITH SEMIRAD

To acquaint the reader with some of the practical aspects of actual high-intensity measurements, we give examples of some of the experiments performed with SEMIRAD on a number of high-intensity pulsed-radiation sources.

Godiva II (References 26 and 42). Godiva II is a bare critical assembly of U^{235} located in Los Alamos Scientific Laboratories, Los Alamos, New Mexico. The assembly, which is subcritical before the burst, is made critical by insertion of an additional piece of U^{235} at the moment of burst. The heat released by the burst in the critical mass expands the surface, the surface-to-mass ratio increases, and its criticality ceases. The principle of operation and the theory of the device are discussed thoroughly in References 27 to 31.

The radiation in a Godiva II pulse has the following characteristics: the half-width of the pulse is about 80 μsec for an average burst, and varies little between individual bursts: the total neutron intensity in rads close to the assembly is about 10 times the gamma intensity; the neutron spectrum is similar to the Watt spectrum but slightly higher at low energies; and the total number of fissions for a typical burst is 1.2×10^{16}, which corresponds to a temperature rise in the critical assembly of 60° C.

The dose rates of gammas and neutrons were measured at different distances from Godiva II. Figure 12.1 shows the arrangement of the experiment. The high-dose-rate part of the experiment consisted of exposing SEMIRAD at very short distances from the reactor, and observing the output of the SEMIRAD on triggered oscilloscopes in the control room. Another part of the experiment, dealing with the spread in time of the neutron dose at distances of the order of one-third mean free path, was performed by exposing sensitive SEMIRAD outside the Kiva building in which Godiva II is housed at a distance of 100 meters (Figure 12.2). The signals from these sensitive SEMIRAD were also transmitted through coaxial cable to the control room and observed on oscilloscopes.

SEMIRAD Instrumentation. Two versions of SEMIRAD were used for this experiment—one of relatively low sensitivity for exposure within the Kiva, and another intended to have higher sensitivity for exposure at some distance from the Kiva.

The first instrument was a diode. Two aluminized polystyrene plates were used as emitters. They were connected electrically to the outside envelope. A centrally located wire electrode served as a collector. A titanium-wire vacuum pump was attached to permit renewal of the vacuum if necessary.

The second SEMIRAD consisted of a modified RCA 6810A photomultiplier vacuum tube in which the photoemissive surface was replaced by an aluminized polystyrene secondary-electron emitter (see Chapter 9). In order that the electrostatic field between the emitter and the focusing electrode might not be disturbed, and to permit the use of an equilibrium thickness of polystyrene, the envelope of the tube was made two centimeters longer than normal. The wiring used for the multi-

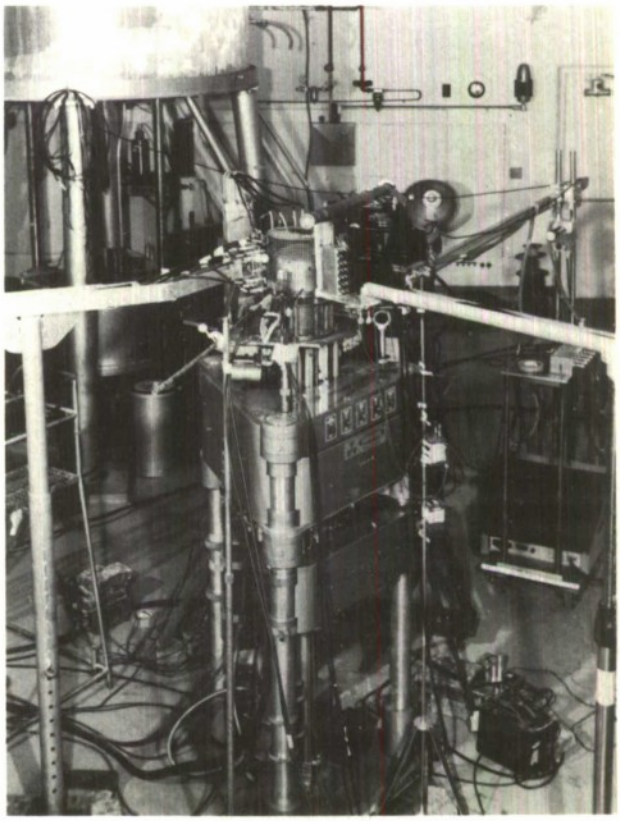


FIGURE 12.1. *The Godiva II reactor assembly.*

plier SEMIRAD was done directly on the leads as they emerged from the glass envelope. Paraffin potting was used to prevent ionized air from introducing unwanted signals.

Although the use of polystyrene within the vacuum prevented the use of cesium as an activating agent for the silver-magnesium electron-multiplying elements (because of the high-temperature treatment necessary to bake out excess cesium), the SEMIRAD did exhibit some electron multiplication. This was shown by exposing the SEMIRAD to unfiltered 250-kv X-rays at a dose rate of approximately 15.6 rads/sec and observing the anode current as a function of the voltage applied to the voltage divider resistor. The results of this test show that, for voltages ranging between 1600 volts and 2100 volts, the output signal is given by the following equations

$$I = KV^{7.8} \tag{12.1}$$

where I is the anode signal current (amperes),
K is a proportionality constant,
and V is the voltage applied to the voltage divider system.

The value of 7.8 found experimentally for the exponent of V is in good agreement with the approximate value of 7 suggested in Reference 32.

Because of the lack of cesium activation of the electron-multiplier dynodes, it was necessary to operate this SEMIRAD with very high interdynode voltages (160 volts per stage) to obtain the required high sensitivity. This high-voltage operation, coupled with the limited vacuum resulting from polystyrene outgassing, resulted in frequent internal-voltage breakdowns. As each breakdown released additional gas into the vacuum, it was necessary to operate the titanium getter; however, after a number of such operations, sufficient stability of the vacuum was achieved to permit successful operation of this instrument.

Electronics. Since the Kiva is connected to the control room by approximately 0.4 kilometers of coaxial cable, it was necessary to attach preamplifiers to each SEMIRAD to match impedance. An amplifier, shown in Figures 7.8 and 7.9, was used for this purpose. This amplifier was powered entirely by batteries and amplified the signals from the SEMIRAD with a gain of 10 while converting their impedance to 70 ohms to match the coaxial

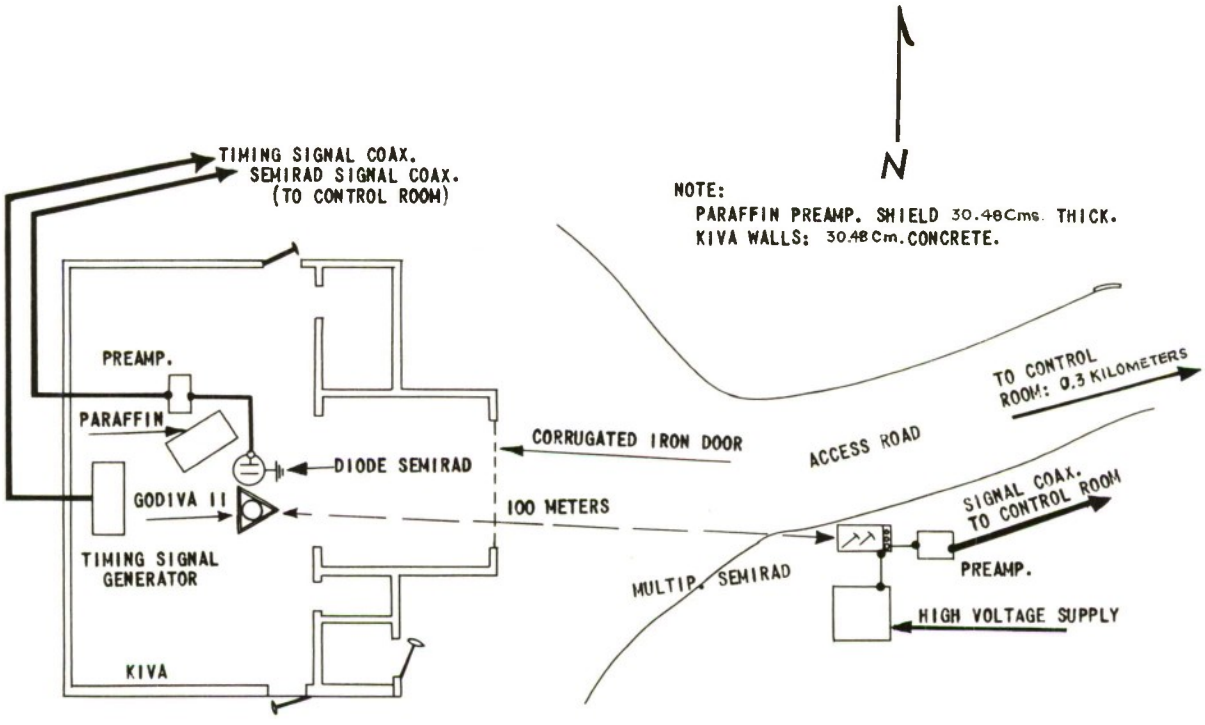


FIGURE 12.2. *Plan of the experimental setup used for the Godiva II experiment (not to scale).*

cable impedance. Since the rise time of the amplifier was 0.15 microsecond and the clipping time was 10,000 microseconds, SEMIRAD pulses of the Godiva bursts lasting about 100 microseconds were reproduced faithfully with less than one percent undershoot.

A novel system of varying the sensitivity of the detection system was used for this experiment. Since it was necessary to surround completely the high impedance leads of the amplifier with paraffin to avoid air-ionization effects, it was impossible to provide any switching system for varying the sensitivity of the system. Accordingly, the amplifier was made to have a fixed voltage gain, and variation of current sensitivity was obtained by inserting different load resistors encapsulated within coaxial cable connectors in the coaxial cable from the SEMIRAD to the amplifier, using 7 adaptors. These load resistors could be varied from 10^6 to 510 ohms, making current sensitivity variable by a factor of 2×10^3.

The SEMIRAD signals were observed and photographed in the control room as oscilloscope traces, using triggered sweeps. Triggering signals were obtained from a special scintillation detector operated by LASL. Although a time jitter of as much as 50 microseconds was observed to exist between the timing signal and the arrival of the peak of the burst, the signal was reliable enough to permit observation of the burst each time.

Dosimetry. Sulphur pellets were exposed with the diode SEMIRAD to provide a measure of the total fast-neutron dose received. This dose was based on information received from Mr. Sayeg, LASL, which suggests an effective cross section for the $S^{32}(n,p)P^{32}$ reaction of 227 millibarns for Godiva spectrum neutrons and for an effective threshold of 2.5 Mev. This dose was converted to rads by assuming, for Godiva spectrum neutrons, 0.66×10^8 sulphur n/cm^2 as equivalent to 1 rad (Reference 33).

For this experiment, the fast-neutron doses at distances of more than a few meters from Godiva were calculated by making the simple assumption that inverse-square-law attenuation is the sole mechanism of attenuation and by using the value of 430 rads as the dose at one meter for a standard burst. Obviously, this assumption is an oversimplification, but the degree of error may be lessened by the fact that back scattering of the neutrons from the Kiva walls make up for the attenuation of the neutrons in air.

Results. The results of this experiment were obtained from the photographs made of the triggered oscilloscope traces of the SEMIRAD response to each burst. In all cases, the results have been transformed to yield the dose rate as a function of time. This transformation was done by comparing the integral of the traces with the total fast-neutron dose received by the SEMIRAD as measured by sulphur pellets.

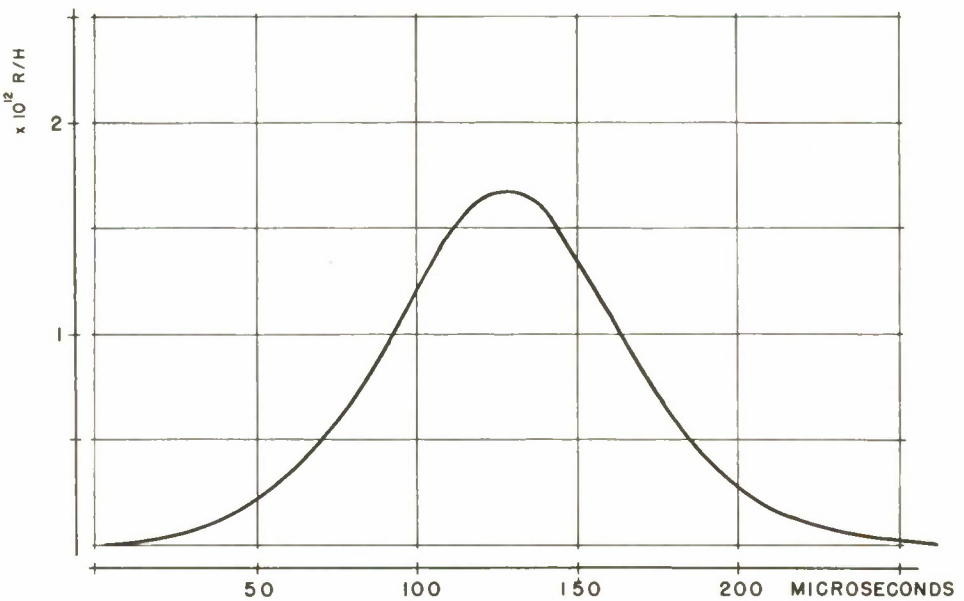


FIGURE 12.3. *Neutron radiation dose rate from Godiva II at 15 centimeters from the center of the assembly, measured by a fast-neutron-sensitive SEMIRAD diode.*

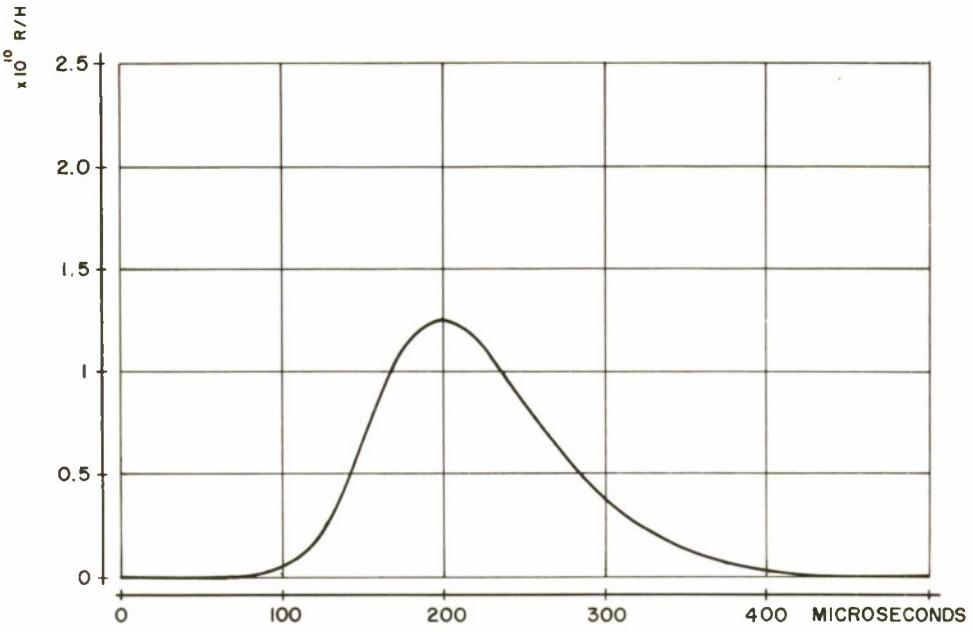


FIGURE 12.4. *Neutron radiation dose rate from Godiva II at one meter from the center of the assembly, measured by a fast-neutron-sensitive SEMIRAD diode.*

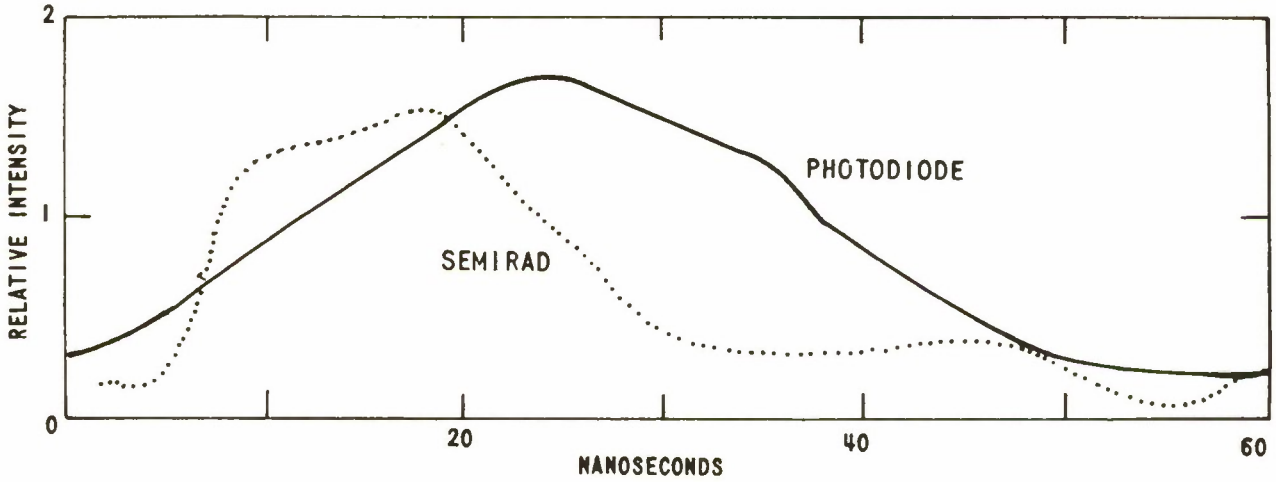


FIGURE 12.5. *Comparison of radiation pulse from 3 Mev flash X-ray unit. Total dose 10^4 rads.*

Figure 12.3 shows the fast-neutron dose rate as a function of time measured by the fast-neutron-sensitive diode SEMIRAD placed at a distance of 15 centimeters from the center of the critical assembly. Note that even though the peak dose rate was approximately 5.6×10^8 rads/sec, no flattening of the peak dose rate has occurred, and that the pulse is symmetrical in time.

Figure 12.4 shows the neutron delivery rate as a function of time at a distance of one meter from the critical assembly measured by the same SEMIRAD used to obtain Figure 12.3.

Since the radiation dose rate very near the Godiva II is directly proportional to the fission rate, a measurement of the dose rate may be considered a measurement of the fission rate. Figure 12.6 shows such a measurement as made by the SEMIRAD used in Figure 12.3 and compared with a fission-rate measurement made by Los Alamos using gamma-sensitive liquid scintillators at some distance from Godiva. Both of these curves have been normalized and have been shifted in time to have coincident maxima. Note the excellent agreement between the curves during the rise of the

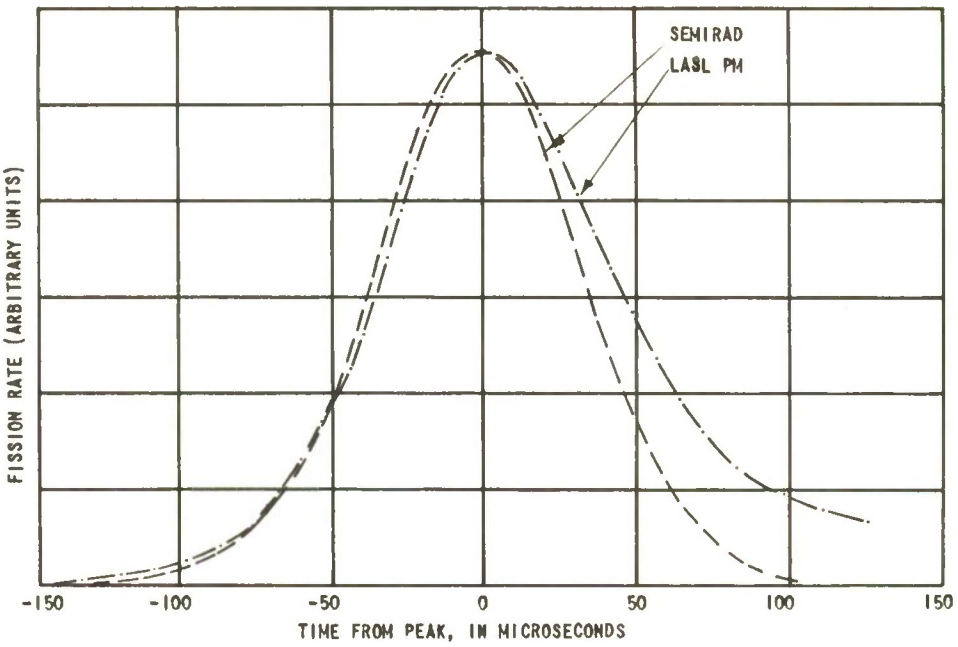


FIGURE 12.6. *Comparison of Godivu II fission rate as measured with neutron-sensitive SEMIRAD at 15 centimeters from the center of the assembly with the fission rate as measured by Los Alamos with gamma-sensitive scintillation detector.*

fission rate. Note also that the LASL measurement deviates from the SEMIRAD measurement past the peak rate.

Such a deviation was observed persistently when comparison between the light output of a scintillator and the SEMIRAD output was made. The deviation occurs for different kinds of scintillators and may be due to some kind of afterglow of the scintillator a short time after high-intensity irradiation. The burst record as shown by SEMIRAD agrees very well with the theory of a Godiva burst (References 28 and 34).

This is illustrated even more strongly by Figure 12.5. This measurement was made by G. Tochilin from N.R.D.L. San Francisco, Calif. The total dose of this pulse, approximately 10^4 rads, was used to calculate the peak dose rate of 4.2×10^{11} rads s^{-1} for the SEMIRAD recording and 3.2×10^{11} rads s^{-1} for the phosphor. The discrepancy between the shapes of the two curves opens the question which of them is closer to reality. Opinions vary, but there are certainly more possible explanations of how a pulse recording may appear too long than too short. Therefore, the SEMIRAD recording appears more credible than the other.

Triga (Reference 37). This is a pulsed reactor based on a uranium-zirconium-hydride fuel-moderator element owned and operated for General Atomics Division of General Dynamics Corporation by the John J. Hopkins Laboratory, Torrey Pines, California. Because the moderator is part of the fuel element, there is a negligible time delay between the temperature increase of the fuel and that of the moderator. The increase in moderator temperature increases the average energy of the thermalized neutrons. The fission cross section becomes smaller at the increased neutron energy, and the reactivity decreases, shutting down the reactor. In this way a pulsed operation is obtained. A more detailed description of the behavior of TRIGA is given in References 38, 39, and 40. The facility is located at the bottom of a well about 16 feet deep and 5 feet across. The well is filled with water, providing a radiation shield without obstructing the view of the core (Figure 12.7).

To measure the gamma and neutron dose rate as a function of time, we used two types of SEMIRAD. One was the same hydrogenous wall model (Figure 12.8) used later on KEWB; the other more sensitive type (Figure 11.2), had plastic ribs on the emitter and was rather large to provide greater sensitivity. Similar instruments but without plastic on the walls served for the gamma measurement.

The components were placed in a watertight container and lowered through the 4.9 meters of water to the top of the reactor core. Because of the de-

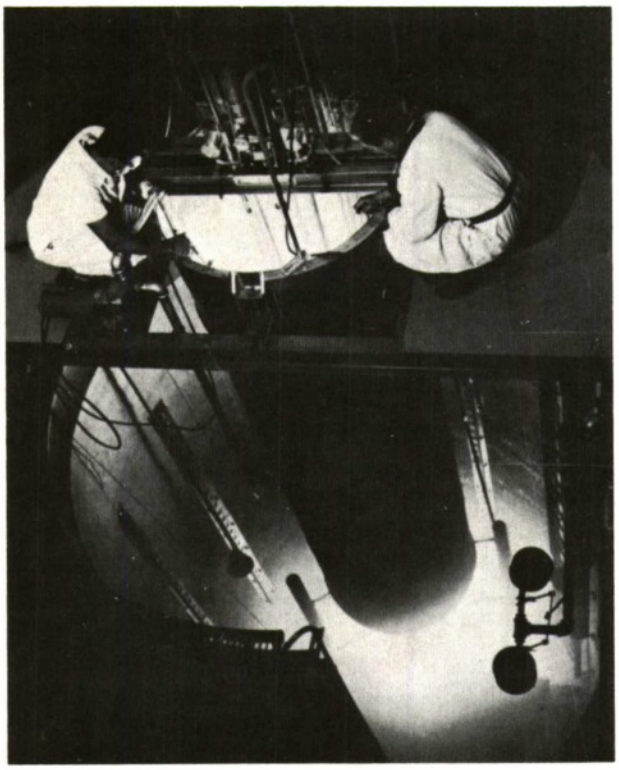


FIGURE 12.7. *Triga mark-f pulsing reactor General Dynamics, General Atomic Division.*

sign of the TRIGA and the size of the container, about two inches of water separated the core from bottom of the cylindrical container. The small SEMIRAD was located inside the container, and the large one was laid on its side a few centimeters from the component container. The large SEMIRAD was potted in epoxy resin to make its connections watertight. The epoxy thickness was about 0.635 cm high on the sides. The instruments were connected by means of 9-meter coaxial cables to the recording arrangement, located in a radiation-safe area immediately above the pool, and their signals were displayed on oscilloscopes.

Dosimeters were lowered to the core to measure total doses of the gamma radiation, sulphur neutrons, and thermal neutrons for a typical burst. This measurement was supplemented by dosimeters attached to the SEMIRAD walls for several bursts to obtain the total dose for dose-rate callibration purposes. Predicted values for the peak power and pulse duration at each burst were obtained from the operating personnel to assist in estimations of the radiation intensities.

A power-versus-time plot for a typical TRIGA pulse is shown in Figure 12.9. The peak power of all pulses was observed to have a spread of less than ± 10 percent. Gold-foil dosimetry substantiates this finding, and for the specific shots measured, shows 4.33×10^{11} thermal neutrons/cm^2 with a reproducibility of ± 8 percent. Because of the unknown amount of water between the core and the sulphur pellets, the sulphur neutron results varied by as much as a factor of 10. The maximum sulphur flux dose was 7.84×10^{11} neutrons/cm^2, which corresponds to a peak rate of 1.96×10^{13} neutrons/cm^2-sec. This measurement was taken as close to the core as possible, while a sulphur pellet taped to the SEMIRAD showed one tenth of this dose.

As in the KEWB experiments, the peak sulphur flux was obtained by assuming that the ratio of peak power to total energy release was the same as the ratio of peak sulphur flux rate to total flux. The total energy released per pulse was calculated by integrating the curve in Figure 12.10 which shows a typical SEMIRAD pulse, obtained with the use of a d-c oscilloscope amplifier. The gamma dose at the location of the highest neutron flux was found to be 2500 rads ± 20 percent per burst.

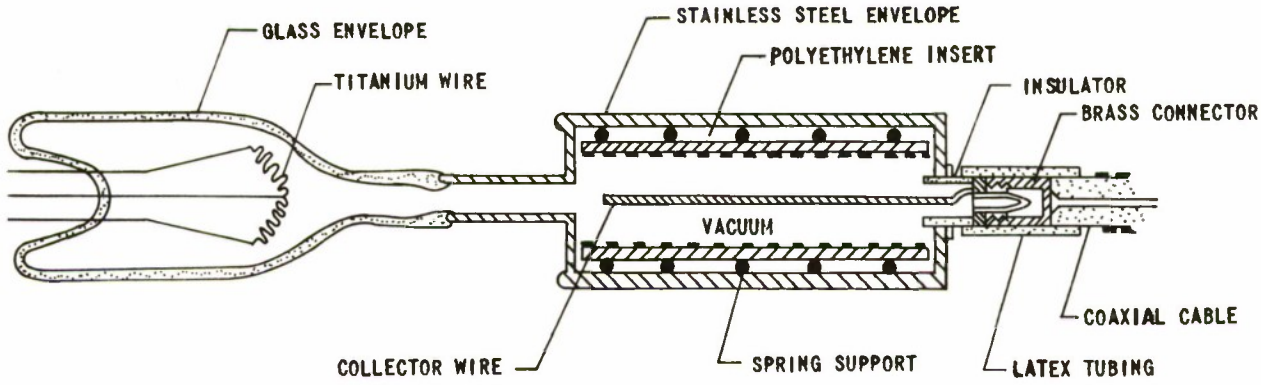


FIGURE 12.8. *Cross section of a fast-neutron SEMIRAD diode with a hydrogenous insert and a titanium getter-pump.*

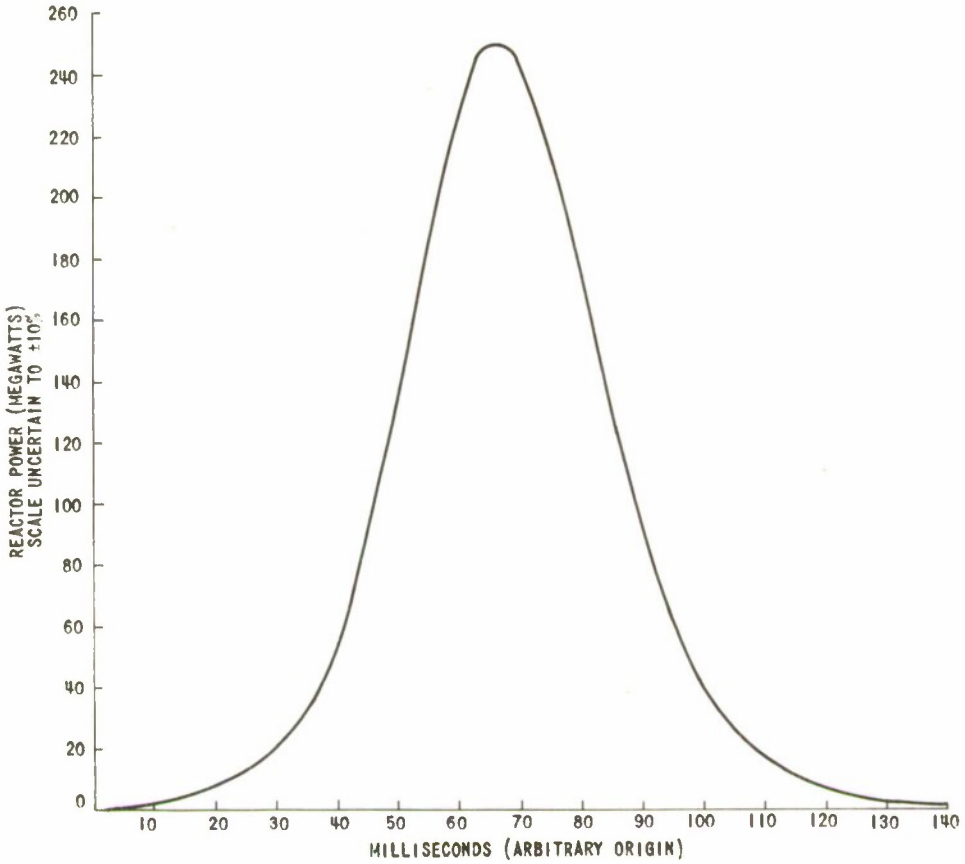


FIGURE 12.9. *Power-versus-time plot for a typical Triga pulse.*

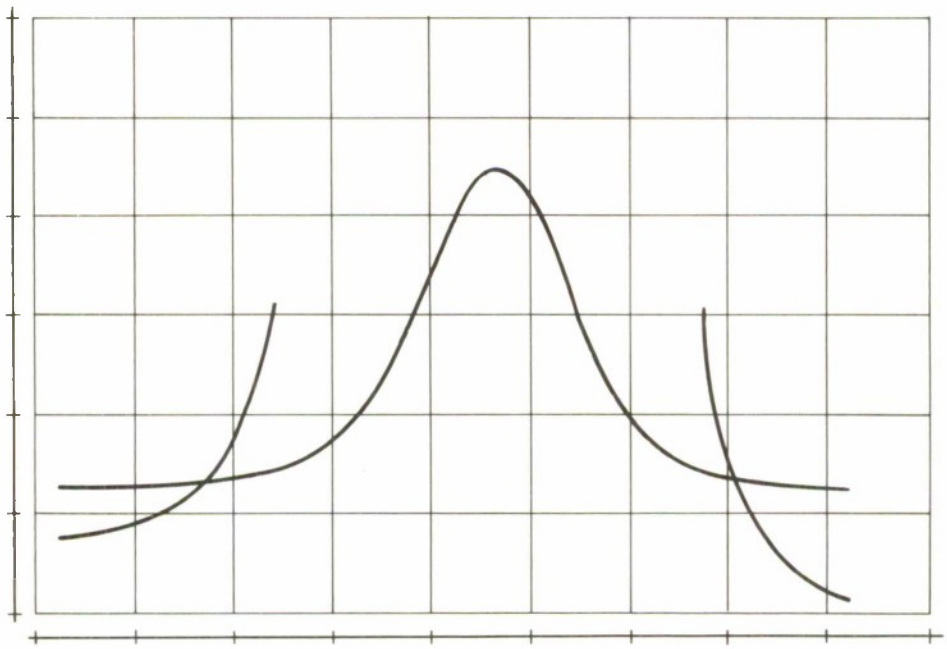


FIGURE 12.10. *The Triga pulse recorded with SEMIRAD.*

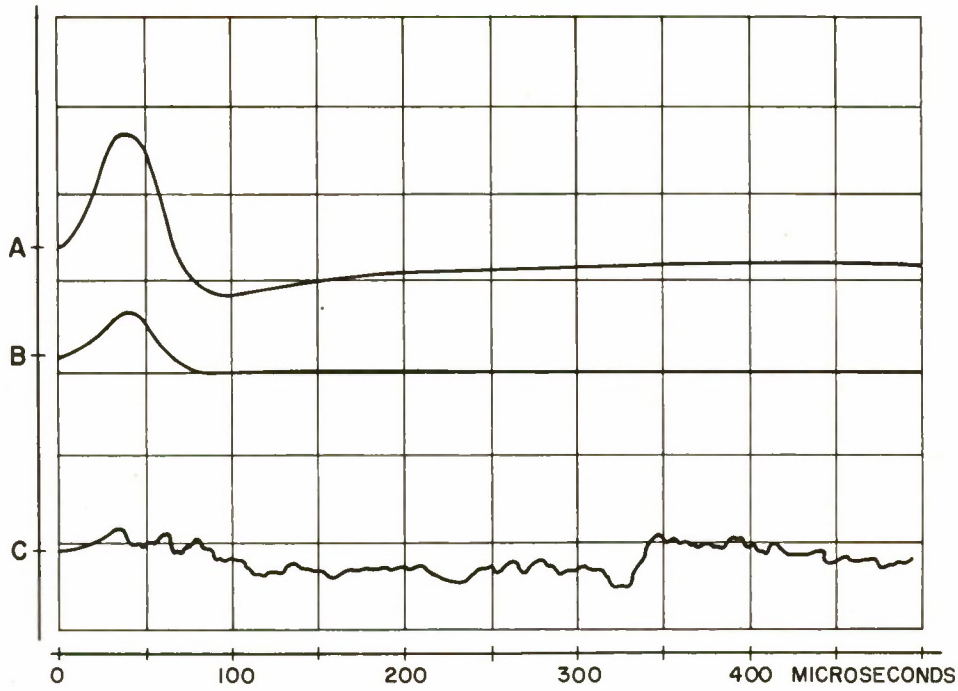


FIGURE 12.11. *Triga experiment: recorded pulses of:*
A: SEMIRAD
B: 100kΩ metal film resistor,
C: 0.01 μf ceramic capacitor
Sweep rate: 50 milliseconds/cm.

Figure 12.11 shows the SEMIRAD track of the Triga pulse used to correlate radiation effects of some electronic components when exposed to the TRIGA burst. In this measurement, the d-c amplifier on the scope was used. The amplifier had a limited low-frequency response and this caused the undershoot of the SEMIRAD trace.

KEWB (Reference 37). This device (Kinetic Experimental Water-Boiler reactor) is operated by Atomic International at Canoga Park, California, for the U.S. Atomic Energy Commission. The main purpose of the experiment performed on this reactor was to measure transient effects of electronic components during the KEWB radiation burst. The radiation data for a typical KEWB burst were as follows: Peak power, 457 megawatts; peak fast-neutron flux (sulphur flux); 6.9×10^{14} n/cm^2-sec; total energy (megawatt-seconds); 3.72; core sulphur neutron dose; 5.9×10^9 neutrons/cm^2; Outside thermal neutron dose (gold dose); $1.18 \cdot 10^{11}$ neutrons/cm^2.

Figure 12.12 is a cutaway view of the reactor and Figure 12.12A shows the reactor core. To record the fast-neutron dose rate as a function of time, hydrogenous SEMIRAD were used as shown in Figure 12.8. The components were taped between the SEMIRAD and its titanium getter. This package was pushed to the end of an aluminum tube that extended to the center of the reactor (Fig. 12.13). A stop tube was necessary to prevent the KEWB poison rod from damaging the SEMIRAD and components when this rod was thrust into the reactor after a burst.

The SEMIRAD signal was fed into a simple cathode-follower preamplifier, located immediately outside of the "glory hole" (aluminum tube opening) where the radiation intensity was not severe enough to influence the preamplifier components. The components being tested within the reactor were connected to bridge circuits, amplifiers, and the recording oscilloscopes by means of a 30-meter coaxial cable. These readout instruments were located in a safe area away from the reactor.

Whenever possible, the SEMIRAD signals were displayed on the same screen as the components' pulses. This arrangement made it possible to compare the component effects relative to the radiation pulses.

To trigger the sweep during the early part of the radiation burst, we used the output of the

facility's sensitive ionization-chamber detector. The slow rise of this pulse made it necessary to use the d-c mode of triggering. Because of the high sensitivity of the ionization chamber, however, very little of the initial rise was lost. Total dose data necessary for the dose-rate calibration of the recorded pulse were measured with sulphur pellets and gold foils attached to the SEMIRAD. Also, use was made of the assumption that

$$\frac{\text{peak power}}{\text{energy released}} = \frac{\text{peak flux rate}}{\text{total flux}}$$

Figure 12.14 shows a typical KEWB burst recorded by the hydrogenous SEMIRAD. Figure 12.15 shows what happened during a KEWB burst to an ion chamber, a coaxial cable whose end was not protected, and two other components.

LINAC (References 41 and 42). The experiment described is one in which SEMIRAD instruments were irradiated with short bursts of gamma radiation at the Linear Electron Accelerator (LINAC), General Dynamics Corporation, San Diego, California. The purpose of the experiment was to determine SEMIRAD response to radiation pulses of less than 10-μsec duration.

The Linear Accelerator is capable of producing pulses of electrons with 2 to 32.5 Mev energy and a pulse-width variable between 0.5 and about 14 μsec. The pulses can be delivered one at a time or with a repetition variable from 7.5 to 720 pps. The electrons emerge from the LINAC through a 0.635 cm titanium "window" at the end of the accelerator tube.

For this experiment, SEMIRAD were exposed to the electron beam and to neutron-gamma radiation from a uranium target placed in the electron beam. The neutrons produced in the uranium target were the result of photofission reactions, and can be assumed similar in their spectral distribution to fission-spectrum neutrons. The instantaneous beam current was monitored by a measurement of the current between the uranium target and ground. Figure 12.16 shows the setup for

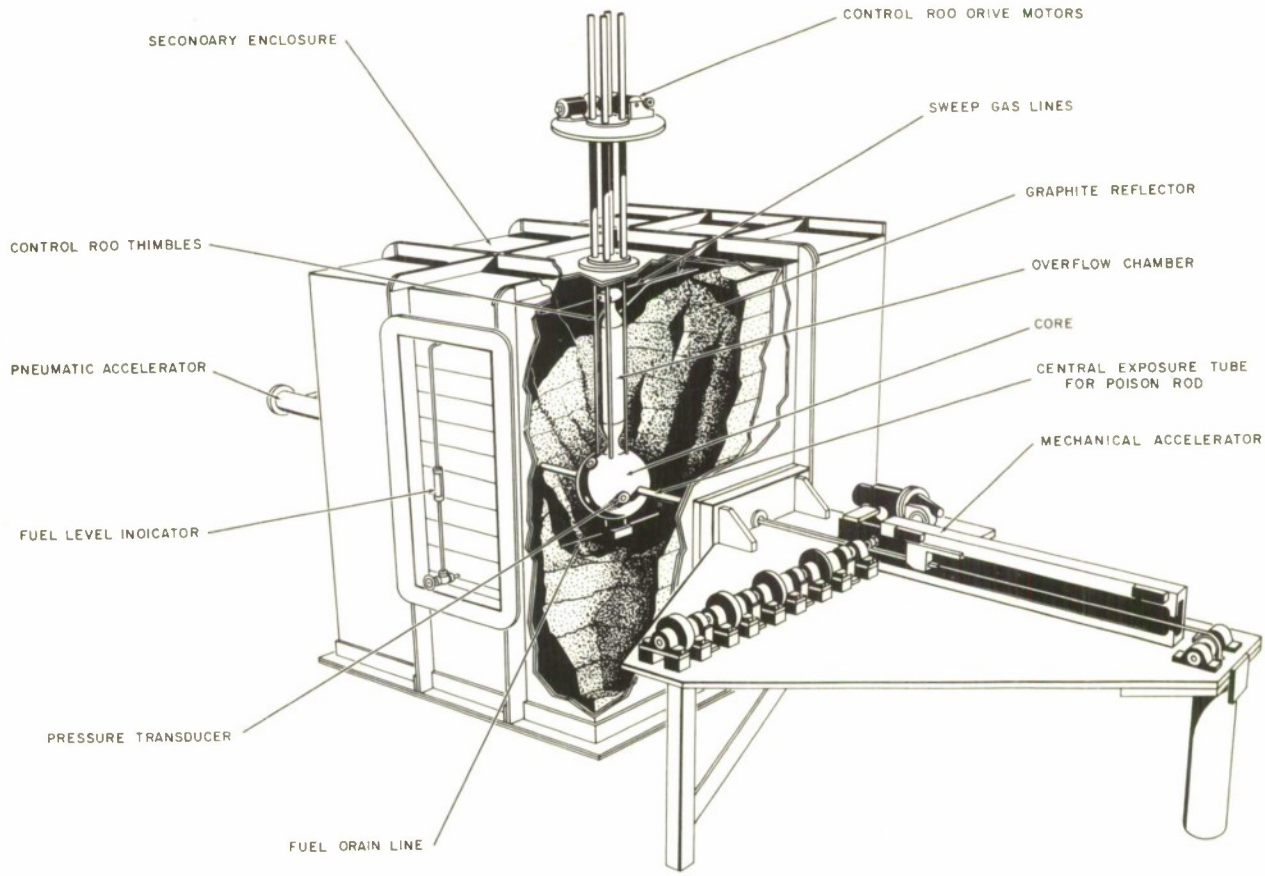


FIGURE 12.12. *Cutaway view of the KEWB reactor.*

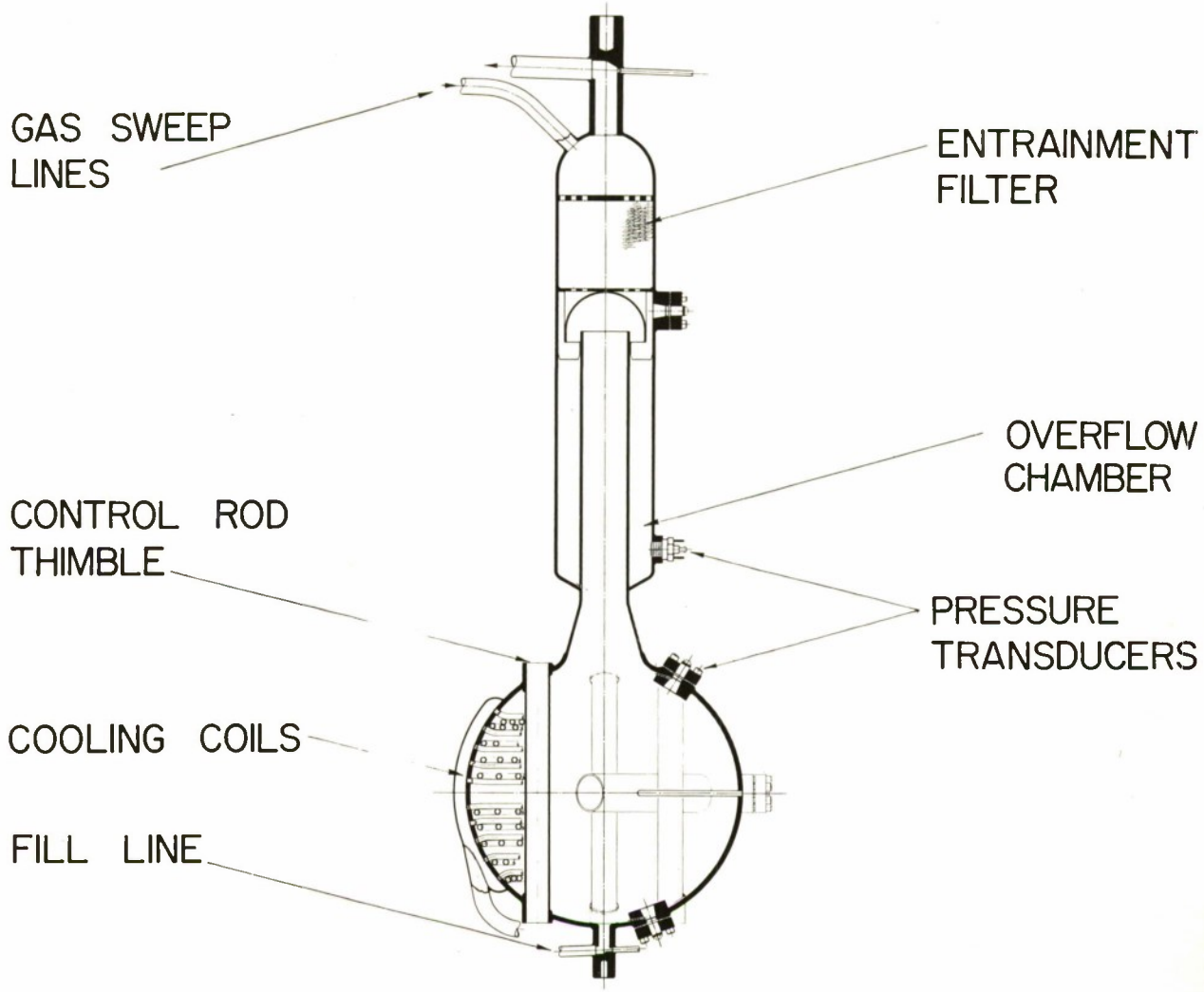


FIGURE 12.12A. *Core of the KEWB reactor.*

neutron-gamma irradiation of the SEMIRAD using the uranium target.

The SEMIRAD used in this experiment were the same used on TRIGA and KEWB (Figure 12.8). Since the polyethylene was coated with an evaporated layer of aluminum, both kinds of instruments (i.e., aluminum wall and polyethylene wall) had the same secondary-electron-emitting surface, whose dimensions were 6.5 cms in length and 2.0 cms in diameter (the total emitter area was 41 cm^2). The collecting electrode was a coaxial nickel wire attached to the ceramic insulator. A titanium getter-pump was attached to permit maintenance of a good vacuum.

Special care was taken to prevent air ionization from affecting the SEMIRAD measurements according to the description in Chapter 7. An aluminum tube, which acted as an effective electrostatic shield for the connector, was slipped over the latex tubing and then attached to the grounded braid of the coaxial cable.

The SEMIRAD used in this experiment were calibrated at low X-ray dose rates, using the USASRDL 250-kv X-ray machine. The calibration factors, which were obtained by using SEMIRAD as integrating dose-rate meters, varied somewhat from instrument to instrument. A typical calibration factor was about 0.72×10^{-10} a/rad/sec corresponding to about 1.8×10^{-12} coulombs/rad/cm^2.

The signals from the SEMIRAD were transmitted from the LINAC target room to the control room by means of a 100-ohm coaxial cable. For that

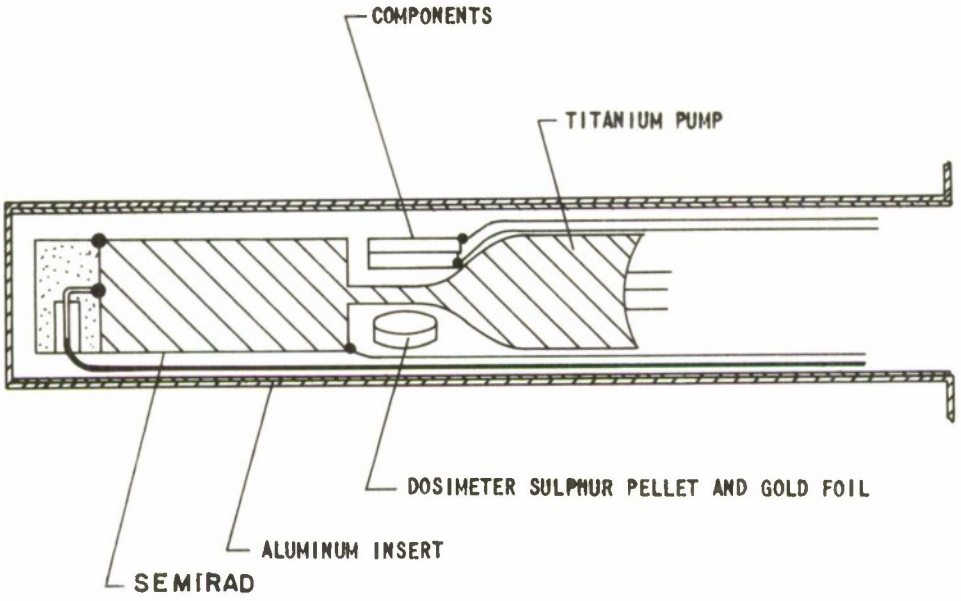


FIGURE 12.13. *Cutaway view of KEWB "glory hole," showing relative positions of SEMIRAD, dosimeters, and components under test.*

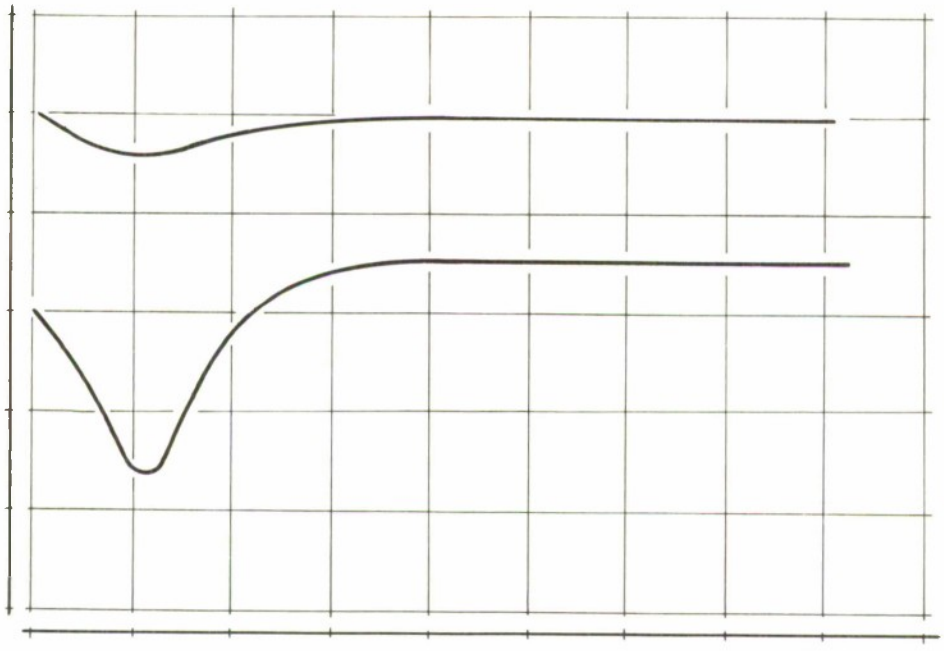


FIGURE 12.14. *KEWB fast-neutron pulse recorded with SEMIRAD.*

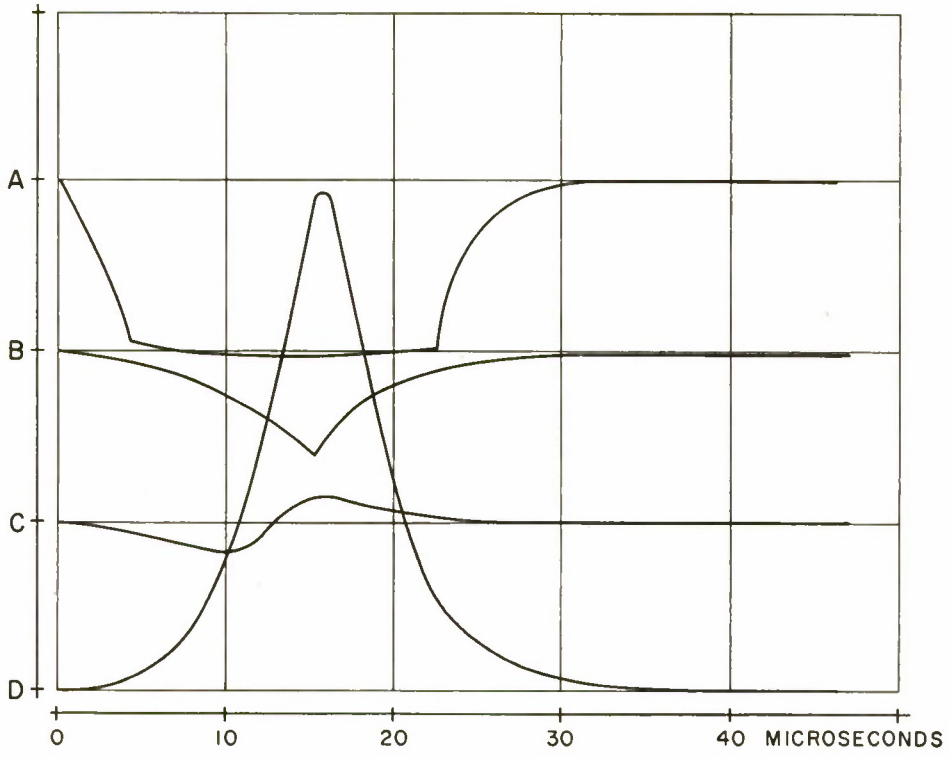


FIGURE 12.15. *KEWB experiment showing records of the pulse with:*
A: Ion chamber,
B: 100 kΩ carbon resistor,
C: 0.0047 μf ceramic capacitor,
D: Ungreased coax cable.
The Sweep rate is 10 milliseconds/cm.

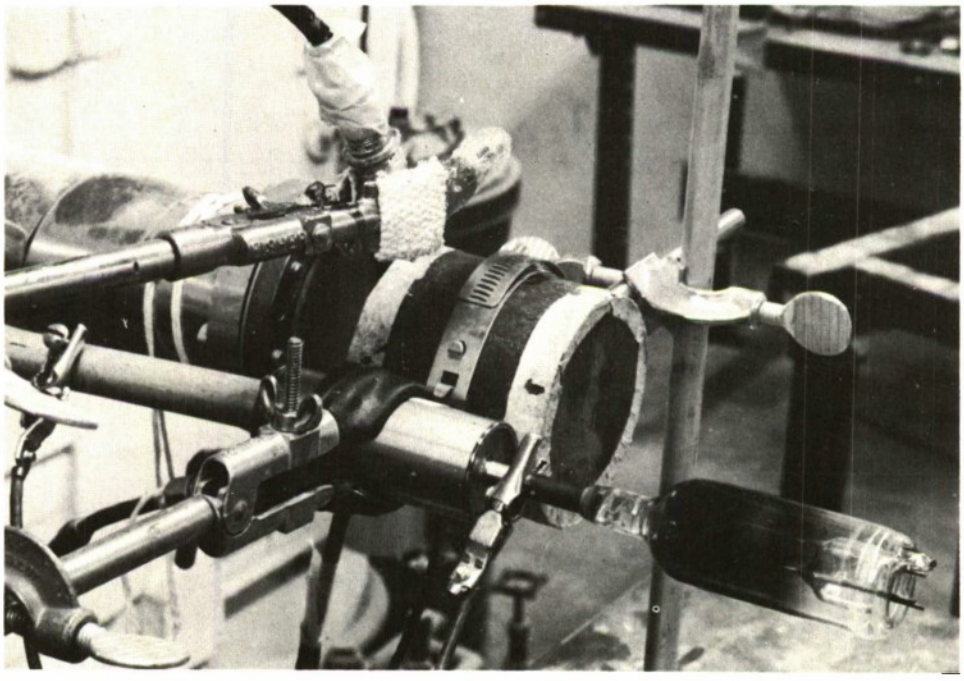


FIGURE 12.16. *Experimental setup for the LINAC measurements.*

part of the experiment in which a SEMIRAD was irradiated directly with the electron beam, the output current of the SEMIRAD was great enough to permit the use of a terminated 100-ohm coaxial cable as the load impedance, and the signal was transmitted over this cable without preamplification.

For that part of the experiment in which a SEMIRAD was irradiated with gamma and neutron radiation from the uranium target, however, the output of the SEMIRAD was too weak to permit direct transmission over a coaxial cable, and a fast preamplifier (Figure 7.8) was used to amplify the signal and to match the signal to the impedance of the coaxial line. Since the preamplifier should not be operated in an intense-radiation field, a six-foot length of RG–22B coaxial cable connected the SEMIRAD to the preamplifier input. The sensitivity of the preamplifier was set by a load resistor of 10 megohms placed in parallel with the 22-megohm resistor shown in Figure 7.8.

The results of this experiment are shown in Figures 12.17 and 12.18. Figure 12.17 shows the SEMIRAD response to direct-high-energy electron irradiation as compared to the LINAC beam current. Figure 12.18 shows the response of the SEMIRAD when exposed to the gamma and neutron radiation as compared to the beam current. In both cases, the sweep rate is one microsecond per division.

Sulphur-pellet measurements were made of the neutron dose above 2.5 Mev at the surface of, and 6.35 cms from, the uranium block. A total of 1000 pulses were used for this measurement. We assumed fission spectrum for the neutrons, and that the value of 6.6×10^7 sulphur neutrons/cm^2 was equivalent to one rad of fission neutrons. The value of the data obtained per pulse are shown below:

Surface of Block: 1.44×10^6 n/cm^2 2.5 Mev, 2.2×10^{-2} rads

6.4 cms from Block: 6.48×10^5 n/cm^2 2.5 Mev, 10^{-2} rads

The SEMIRAD response shown in Figure 12.18 for direct-electron irradiation demonstrates that the time resolution of this SEMIRAD was of the order of 0.1 μsec or less. We believe that the fine detail shown on the beam-current trace and not on the SEMIRAD trace is probably due to electrical noise, since the beam-current-collecting electrode was not electrostatically shielded.

Knowing the peak-electron-beam current (80 ma) and the peak current through the SEMIRAD

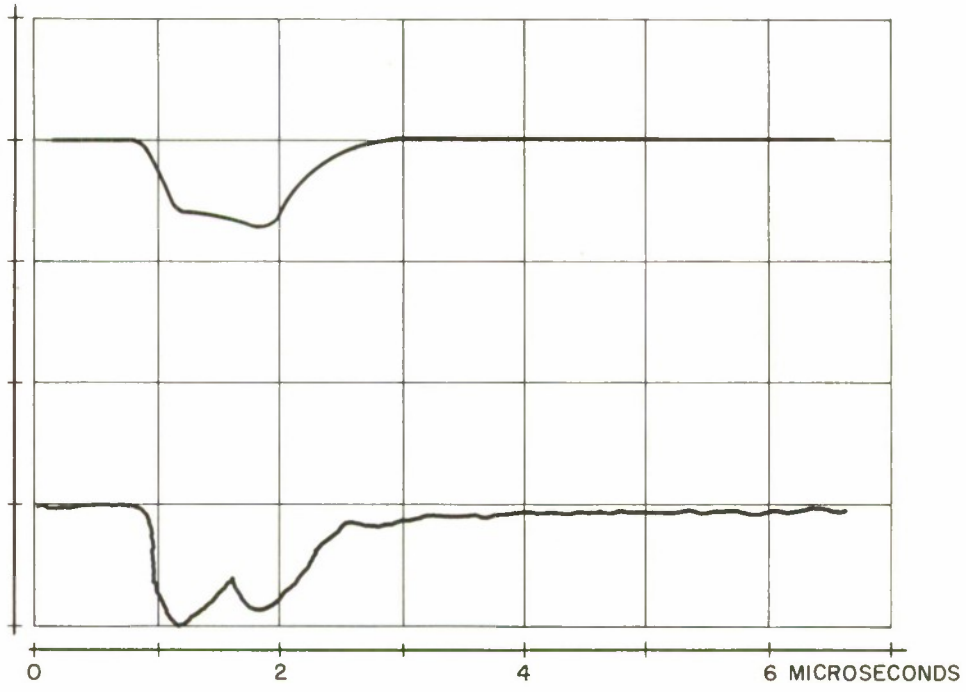


FIGURE 12.17. *Pulse of 27 Mev electrons at LINAC. Top: SEMIRAD current (negative signal). Bottom: LINAC beam current. Sweep rate: 1 μsec/cm.*

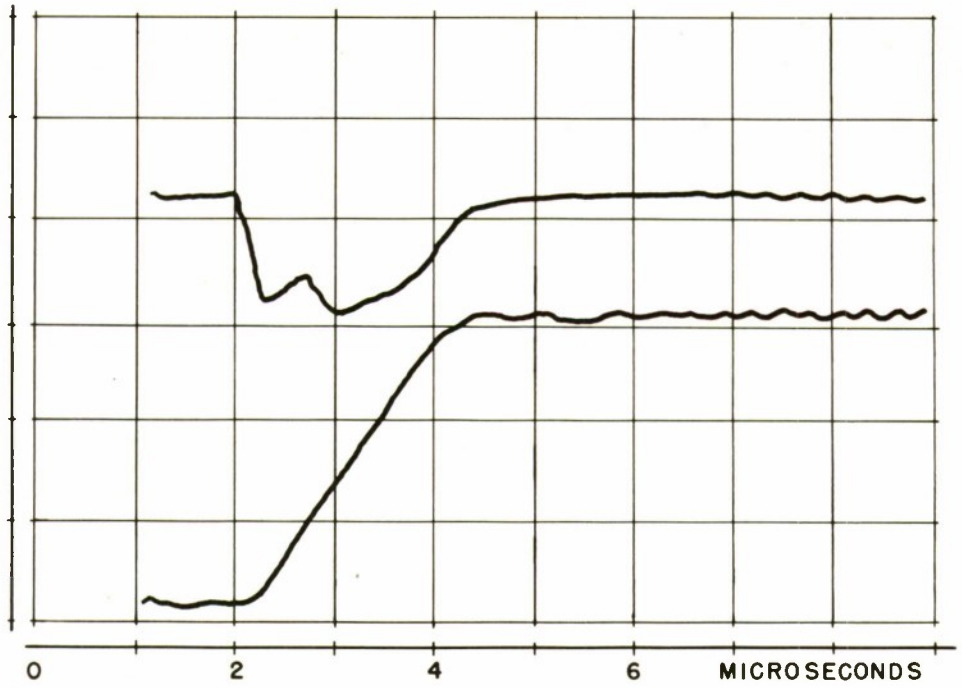


FIGURE 12.18. *Pulse of 27 Mev electrons at LINAC. Bottom: SEMIRAD current (integrated). Top: LINAC beam current. Sweep rate: 1 μsec/cm.*

(one volt developed across 100 ohms; 10 ma), and remembering that primary electrons make two passes through the emitter surface, we estimate the yield, Y, of secondary electrons for 27-Mev electron irradiation to be

$$Y = \frac{10 \times 10^{-3}}{80 \times 10^{-3}(2)} = 0.062 \frac{\text{secondary electrons}}{\text{primary electron}}$$

If we estimate the yield for primary particles produced by the X-ray calibration to be approximately one, we can estimate the equivalent instantaneous LINAC dose rate to be

$$\frac{I_s Y_{\text{cal}}}{K Y_{\text{LINAC}}} = 2.2 \times 10^{9} \text{ rads/sec}$$

Where I_s = peak SEMIRAD current (10^{-2} amp),
K = SEMIRAD calibration 0.72×10^{-10} a/rad/sec
Y_{cal} = secondary electron yield at calibration energy (~ 1),
Y_{LINAC} = secondary electron yield at LINAC energy (~ 0.062).

An independent method allows us to check the estimate of dose rate. If we assume that each electron, in passing through an absorber with a thickness of 1 g/cm^2, loses approximately 2-Mev energy, then the dose delivered to the material as a consequence of 1 electron/cm^2 irradiation is:

$$2 \times 1.6 \times 10^{-6} \text{ ergs/gram} = 3.2 \times 10^{-8} \text{ rads.}$$

Since the current from the LINAC was 80 ma, the electron flux was 5×10^{17} electrons/second. Therefore, the corresponding dose rate is

$$3.2 \times 10^{-8} \times 5 \times 10^{17} = 1.6 \times 10^{10} \text{ rads/sec}$$

or: 5.8×10^{13} rads/hr.

The difference between the value of 2.2×10^{9} rads/sec and the value of 1.6×10^{10} rads/sec is reasonable, if we consider the number of approximations present in each derivation. For the results shown in Figure 12.18, the SEMIRAD was connected to the fast preamplifier by means of 125 cms of RG–22/B coaxial cable. The signal was developed across the parallel combination of the 10-megohm load resistor and the 22-megohm resistor shown in Figure 7.8. This resistance, in combination with the 140-μf shunt capacitance of the coaxial cable, resulted in an effective integrating circuit. As a consequence, the trace shown

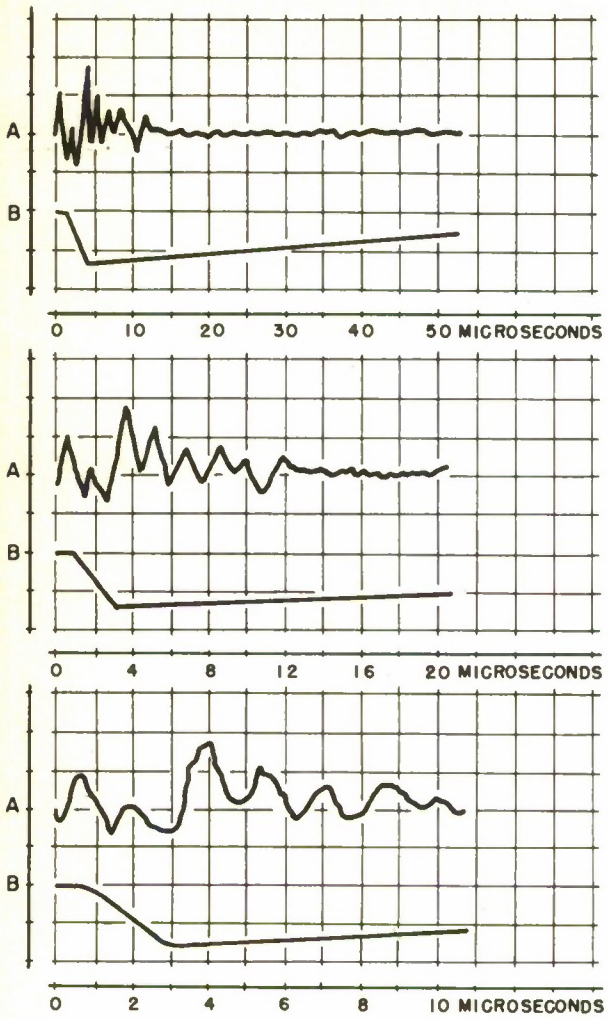


FIGURE 12.19. *LINAC experiments showing pulse recording of:*
(A) *100 kΩ metal film resistor,*
(B) *SEMIRAD dose signal (integrated)*
Sweep rates: (top to bottom),
5 microseconds/cm,
2 microseconds/cm,
1 microsecond/cm.

in Figure 12.18 represents total accumulated dose as a function of time, and not the dose rate as in previous experiments.

The total dose delivered to the SEMIRAD can be estimated from Figure 12.18. The deflection shown there represents a signal of 0.056 volt at the preamplifier input, and may be considered to be the voltage developed across the 140-$\mu\mu$f cable shunt capacitance. Since $Q = CV$, we may estimate the charge delivered by the SEMIRAD to the capacitor to be:

$$(140 \times 10^{-12})\,(0.056) = 7.9 \times 10^{-12} \text{ coulombs.}$$

Using the calibration factor found above of 1.8×10^{-12} coulombs/rad/cm^2, the 41 cm^2 area of the SEMIRAD, and a high-energy secondary-electron yield of 0.062, we find that the equivalent gamma dose is:

$$\frac{7.9 \times 10^{-12}}{(1.8 \times 10^{-12})\,(41\ (0.062))} = 1.6 \text{ rads}$$

Since the fast-neutron dose at 2.5 inches from the uranium block is approximately 10^{-2} rads per shot, we see that the gamma-neutron ratio for LINAC at 90° to the main beam is on the order of 100:1 for photofission neutrons.

Figure 12.19 shows an interesting effect on a 100-kilohm metal film resistor induced by the LINAC pulse as timed by the integral dose recording made with SEMIRAD.

Another pulse measurement was performed using the LINAC located in the White Sands Missile Base, White Sands, New Mexico. This machine produces a pulse of 8-Mev electrons. The pulse width can be changed between a fraction of a microsecond and 10 microseconds. The armed SEMIRAD diode was exposed to the maximum dose of electrons with enough shielding to prevent the electrons from hitting the collector electrode directly.

Figure 12.20 shows the recorded 10-μsec pulse (negative pulse) on a Tektronix 555 oscilloscope. Figure 12.21 shows the recording with a phosphor-phototube system on an E.G.&G. scope. There is a strong electromagnetic effect at the output of the accelerator and some of it is visible on the pulse recordings.

Pulsed X-rays. This device produces a very short high-intensity X-ray pulse during the discharge of a condenser bank over a specially designed X-ray tube. The low-inductance condenser bank, consisting of coils of coaxial line, is charged with high voltage in parallel, then switched into series, which increases the voltage, and then it is discharged. The maximum energies of the X-rays may vary between 100 and 600 kv, depending on the setting of the machine.

Figure 12.22 shows a recording of the pulse with a SEMIRAD diode (lower trace) and with a phosphor-photocell system (upper trace) on a dual beam oscilloscope. The pulse width is 0.2 μsec: The recording was made at AFWL Kirtland Air Force Base, Albuquerque, New Mexico. A very strong electro-

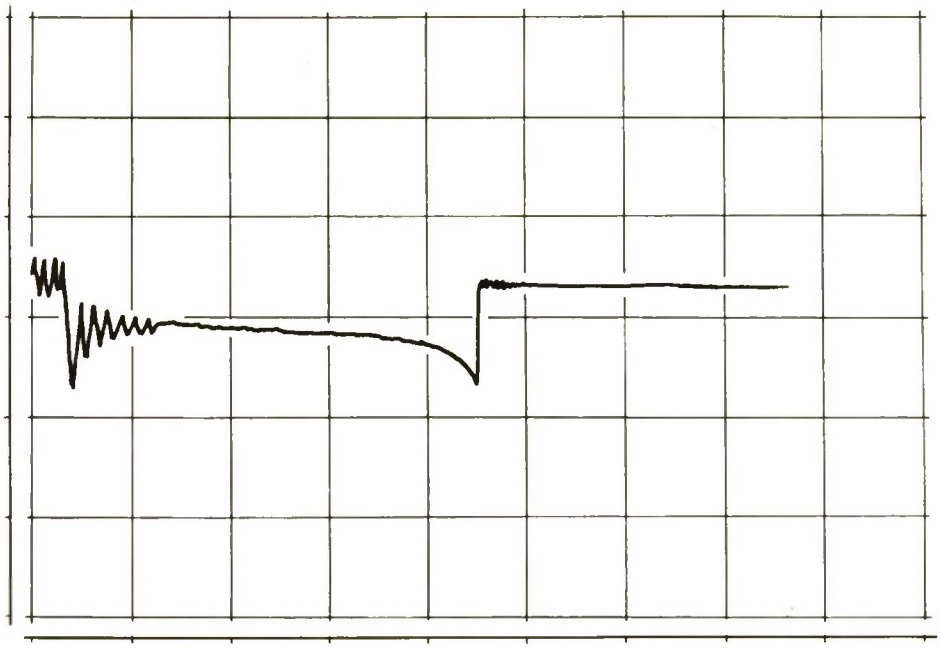


FIGURE 12.20. *10 μsec pulse from the White Sands Missile Base LINAC recorded with a gamma-diode SEMIRAD on Tektronic 555 scope.*

magnetic effect is present during the radiation pulse in the environment of such a pulsed X-ray machine. Therefore a very thorough electromagnetic shielding was necessary to bring the signal above background level.

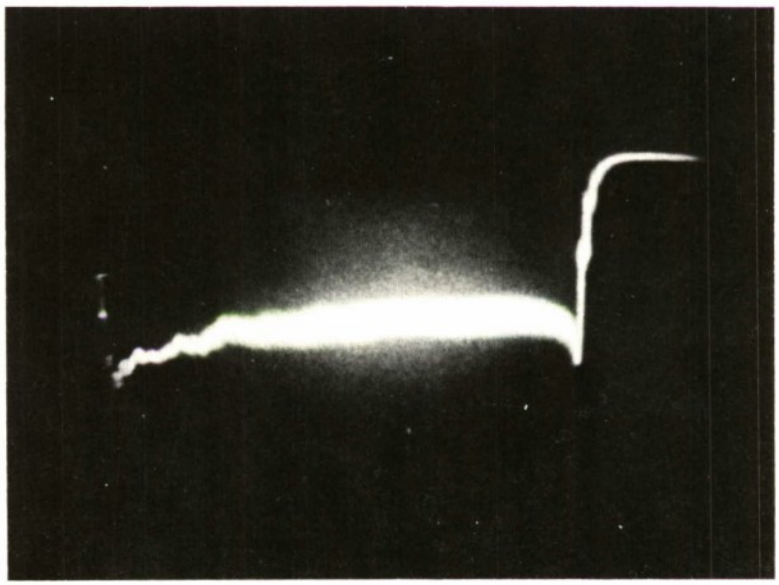


FIGURE 12.21. *10 μsec pulse from the White Sands Missile Base LINAC recorded with a phosphor-photo cell system on an E.G.&G. scope.*

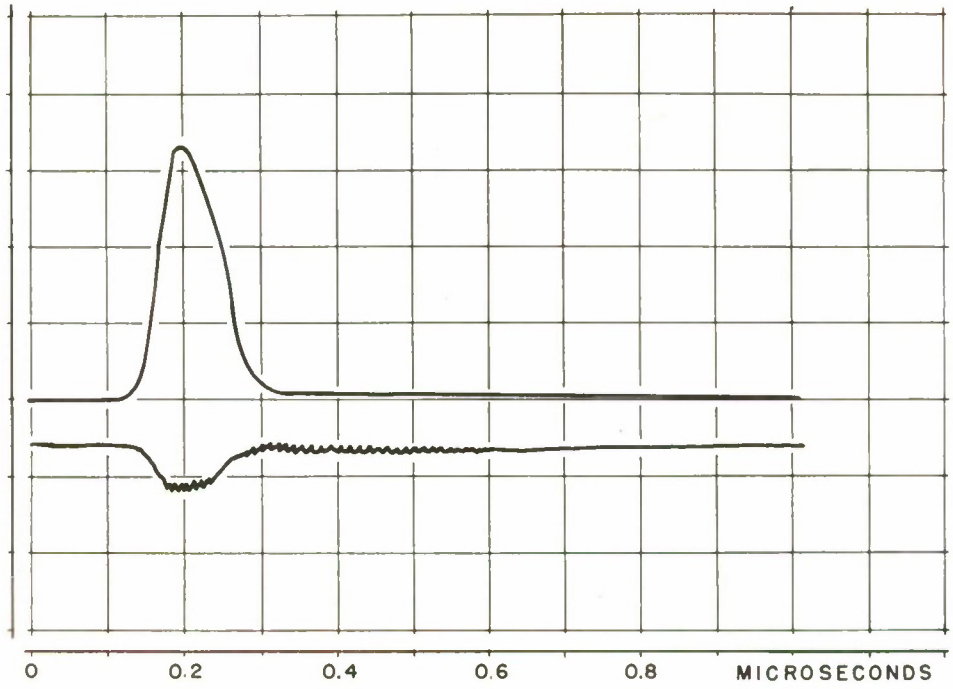


FIGURE 12.22. *Pulsed X-ray recording. Pulse width 0.2 μsec.*
Top: Phosphor photo-cell system
Bottom: gamma SEMIRAD diode

REFERENCES

1. N. Jensen, "Vapor Pressure of Plastic Materials," J. Appl. Phys. *27*, 12, pp. 1460–62, Dec. 1956.
2. I. Langmuir and K. T. Compton, "Electrical Discharges in Gases," Rev. Mod. Phys. *3* 2, April 1931, p. 191.
3. H. Kallmann, Progress Report # P.I.P., USAF Contract No. AF18(600)–1004, March 1955.
4. M. Stein, "Doserate Dependence of Dosimeters at Doserates Up to 2 Million r/hr," IRE Convention Record 1956, Part 8, Session 31.
5. B. J. Moyer, "Survey Methods for Fast and High-Energy Neutrons," Nucleonics, *10*, 5, May 1952, p. 14.
6. S. Kronenberg and H. M. Murphy, Jr., "Energy Spectrum of Protons Emitted from a Fast-Neutron-Irradiated Hydrogenous Material," Radiation Research *12*, 1960, pp. 728–735.
7. J. Fetkovich, "Derivation of the Electron Spectrum Inside of a Gamma Ray Irradiated Material," (to be published).
8. R. A. Shats, J. F. Marshall and M. H. Pomerantz, Phys. Rev., *102*, 3, p. 682.
9. H. Hendel and S. Kronenberg, "Electron Emission by Protons and Deuterons," (to be published).
10. Mironov and Nemenov, J. Exp. Theor. Phys., USSR 32,269, Feb. 1957.
11. E. J. Sternglass, "Theory of Secondary-Electron Emission by High-Speed Ions," Phys. Rev., *108*, 1, October 1957, pp. 1–12.
12. L. Miller and W. C. Porter, "Secondary-Electron Emission by Primary Electrons in the Energy Range of 20 kev to 1.3 Mev," Journ. Franklin Inst., *260*, July–Dec. 1955, p. 31.
13. J. G. Trump and R. J. Van de Graaff, "The Secondary Emission of Electrons by High-Energy Electrons," Phys. Rev., *75*, 1, Jan. 1949.
14. R. J. Van de Graaff, W. W. Buechner, and H. Feshbach, "Experiments on the Elastic Single Scattering of Electrons by Nuclei," Phys. Rev., *69*, 1946, pp. 452–459.
15. P. Kapitza, Phil. Mag., *45*, 989, 1923.
16. J. S. Allen, Phys. Rev., *55*, 336, 1939.
17. A. G. Hill et al., Phys. Rev., *55*, 463, 1939.
18. B. Aarset et al., J. Appl. Phys., *25*, 1365, 1954.
19. S. Kronenberg, K. Nilson, and M. Basso, "Emission of Secondary Electrons from Metals by 1-Mev Protons," Phys. Rev., *124*, 1709, Dec. 1961.
20. W. Widmaier, R. W. Engstrom and R. G. Stoudenheismer, "A New High-Gain Multiplier Phototube for Scintillation Mounting," IRE Transactions of the Professional Group on Nuclear Science, *NS*–3, 4, Nov. 1956.
21. W. E. Stein and R. B. Lachmann, Rev. Scient. Inst. *27*, 1049, 1956.
22. G. F. Erickson and S. G. Kaufmann, Rev. Scient. Inst. *27*, 107, 1956.
23. Summary Report on Experimental and Research Work in Neutron Dosimetry Phase 1, 31 March 1961, Battelle Memorial Institute, Signal Corps Contract No. DA36–039 SC–78924.
24. Los Alamos Technical Report No. LA–2375 Liquid Scintillation Radiation Rate Meters for Measurements of Gamma and Fast Neutron Rates in Mixed Radiation Fields.
25. Contractor's Progress Reports, Bendix Corporation, Cincinnati Div., U.S. Air Force Contract No. AF29(601)–4514.
26. S. Kronenberg and H. M. Murphy, Jr. "Godiva II Irradiation of SEMIRAD," 9 and 10 October 1958, Memorandum Report, USASRDL, 17 Dec. 1958.
27. L. Zipprich, "Godiva II, Its Availability and Suitability for Radiation-Effects Tests," Sandia Corp. Report SCR–76.
28. T. F. Wimett and J. D. Orndoff, "Applications of Godiva II Neutron Pulses," Peaceful Uses of Atomic Energy, Vol. 20, United Nations, 1958.
29. J. D. Orndoff, "Prompt Neutron Periods of Metal Critical Assemblies," Nuc. Sci. and Eng., 2, 4, 1957, pp. 450–460.
30. G. M. Frye, J. H. Gammel, and L. Rosen, "Energy Spectrum of Neutrons from Thermal Fission of U–235," LASL Report LA–1670, 1954.
31. B. E. Watt, "Energy Spectrum of Neutrons from Thermal Fission of U–235," Phys. Rev., *87*, 6, September 1952, pp. 1037–1041; also AECD–3073, February 1951.
32. W. J. Price, "Nuclear Radiation Detection," McGraw Hill Book Co., Inc., p. 183, New York, 1958.
33. J. A. Sayeg, E. R. Ballinger and P. S. Harris, "Dosimetry for the Godiva II Critical Assembly, Neutron Flux and Tissue Dose Measurements," LASL Report LA–2310, March 1959.
34. T. F. Wimett, "Time Behavior of Godiva Through Prompt Critical," LASL Report LA–2029, April 1956.

35. W. Whaling, "The Energy Loss of Charged Particles in Matter," Handbook der Physic, Ed. XXXIV., p. 193.
36. Kinsman, Simon, et al., Radiological Health Handbook, U.S. Dept. of Health, Education, and Welfare, Jan. 1957, PB 121784.
37. B. Markow, H. J. Degenhart, H. M. Murphy, Jr., and R. Sanna, "Effects of Mixed Neutron-Gamma Pulses on Electronic Components," USASRDL Internal Report 1959.
38. M. E. Ramley, J. W. Flora, et al., "Experimental Studies on the Kinetic Behavior of Water-Boiler Type Reactors," paper presented at the 2d International Conference on the Peaceful Uses of Atomic Energy, Geneva, Sept. 1958.
39. "Technical Foundations of TRIGA," 27 August 1958, GA-471, General Atomic Division of General Dynamics Corporation.
40. "An Inherently Safe Pulsed Reactor Based on the Uranium-Zirconium-Hydride Fuel-Moderator Element," 12 Feb. 1959, GA-620, General Atomic Division of General Dynamics Corporation.
41. S. Kronenberg and Harry M. Murphy, Jr., "Irradiation of SEMIRAD at the General Atomic Linear Accelerator (LINAC), 5 May 1959," USASRDL TR 2070.
42. "General Atomic Electron Linear Accelerator," 14 March 1958, GA-314, General Atomic Division of General Dynamics Corporation.
43. S. Kronenberg and Harry M. Murphy, Jr., "Evaluation of SEMIRAD for Dose-Rate-Independent Measurements of Fast Neutron and Gamma Radiations," USASRDL Memorandum Report, 10 Oct. 1958.
44. D. J. Hughes and R. B. Schwartz, "Neutron Cross Sections," pp. 330-338 2d Ed., BNL 325.
45. V. K. Zworykin and E. D. Wilson, "Photocells and their Application," John Wiley and Sons, New York.
46. L. Malter, "Thin-Film Field Emission," Phys. Rev. *50*, 48, 1936.
47. D. Dobischek, H. Jacobs and J. Freely, "The Mechanism of Self-Sustained Electron Emission From MgO," Phys. Rev. *91*, 804, 1953.
48. J. Mengali, et al., "The Use of P. N. Junctions in Silicon as Fast-Neutron Dosimeters," Proc. II Conf. on Nuclear Radiation Effects on Semiconductors, Materials and Circuits, Sept. 17-18, 1959.
49. U.S. Patent No. 2,687,480; F. R. Shonka, et al.
50. U.S. Patent No. 3,052,797; S. Kronenberg.
51. Evaluation of Military Radiac Equipment, Operation TEAPOT, May 1955, WT-1137, Project 6.1.1a.
52. Evaluation of Military Radiac Equipment, Operation PLUMBBOB, WT-1415, by Messrs. Cohen, Jachter, Ramm, Murphy.
53. "Measuring Fast Nentron Fluxes in Mixed Neutron—Gamma Fields," S. Kronenberg, Nucleonics, March 1963, p. 78.
54. L. F. Wouters, A. E. Villaire, V. E. Wheeler and K. Kalibjian, "A Fast, High Current Photomultiplier," I.R.E. Trans. NS-9, No. 4, 9, 1962.
55. J. W. Boag, and T. Wilson, "The Saturation Cnrve at High Ionization Intensity," British Jonrnal Applied Physics *3*, 222, 1952.
56. B. B. Rossi and H. H. Staub, "Ionization Chambers and Counters. Experimental Techniques," McGraw-Hill Book Co., Inc., 1949.
57. R. G. Saelens, "Tiny Gamma Detector for High-Intensity Radiation," Nucleonics, *20*, 60, 1962.
58. Hime Brownell, "Radiation Dosimetry," Academic Press Inc., Publishers, New York, 1956.

U.S. GOVERNMENT PRINTING OFFICE : 1966 OL—224-250